Describing the immune cell profile of ventricular cerebrospinal fluid (CSF) in paediatric brain infections

by

Kate Morris
MRRKAT014

Submitted to the University of Cape Town
In fulfilment of the requirements for the degree
MSc (Med) in Neuroscience

Supervisor:
A/Prof Ursula Rohlwink

Co-supervisor:
Prof Anthony Figaji

Department of Surgery
Faculty of Health Science
University of Cape Town
April 2024

DECLARATION

I, ……*Kate Morris*……, hereby declare that the work on which this dissertation/thesis is based is my original work (except where acknowledgements indicate otherwise) and that neither the whole work nor any part of it has been, is being, or is to be submitted for another degree in this or any other university.

This thesis/dissertation has been submitted to the Turnitin module (or equivalent similarity and originality checking software) and I confirm that my supervisor has seen my report and any concerns revealed by such have been resolved with my supervisor.

Signature: Signed by candidate

Date: ……30/07/2024…….

Acknowledgements

To A/Prof Ursula Rohlwink, my supervisor and guiding light throughout this process, thank you for your brilliant mentorship, patience, compassion and support that you have shown me over the last two years. It has been an incredible honour to undertake this study with you, and I have learnt so much from your phenomenal knowledge of the brain and the central nervous system. You have been, and will continue to be, an immense role model for me, and your dedication, work ethic and contributions as a neuroscientist have taught me a great deal. Thank you for believing in me and for trusting me along this unique journey.

Thank you to Prof Anthony Figaji, Head of Paediatric Neurosurgery and of our research team at Red Cross War Memorial Children's Hospital, for the opportunities you have given me and the many things I have learnt from you – about the brain but also about life in general – as part of your team. Your experience and wisdom have been a privilege to witness, and I thank you for your contributions to this study.

I would like to extend a huge thank you to all the neurosurgeons who have collected CSF samples for me over the last two years. This study would not be possible without all of you, and I am immensely grateful for the assistance you have so graciously granted me in my research.

To my colleague, mentor and friend, Gabriela Singh. You have been truly outstanding in teaching and nurturing me throughout my MSc. Thank you for the countless hours you have spent by my side in the lab, the hospital or at the flow cytometer, for being so patient with me and for being so willing to lend a hand or give advice when needed. All of this is so very appreciated. (And thank you to Simon for keeping us company in the lab!)

Thank you to Dr Tim Reid for your assistance and knowledge whenever the flow cytometer was misbehaving, and to Dr Jill Combrinck and Lisa Ungerer for your support and contribution to this study.

To Sarah Morris, thank you for our cherished weekly coffee dates, for being one of my biggest supporters and for being right beside me through the ups and downs of life since our Stellenbosch days.

Thank you very much to the neuroscience students in our team for your friendship and encouragement.

To my brother, Jack, thank you for keeping me smiling even during the stressful times, for checking in on me, for our many interesting chats and for our ice cream dates.

Last but certainly not least, to my parents, Sharon and Michael. Thank you for being with me every step of the way throughout this study and the completion of this thesis. Your love, support, encouragement and guidance throughout my life have gotten me to where I am today, and shaped me into who I am. Thank you for being the amazing role models that you are. This degree would not have been possible without you, and I dedicate this piece of work to the two of you.

Table of Contents

List of Tables

Chapter 2

Chapter 3

Chapter 5

Chapter 6

Appendix A

List of Figures

List of Abbreviations

ACSA – Astrocyte cell surface antigen
AFB – Acid-fast bacilli
APC – Antigen-presenting cell
APC-H7 – Allophycocyanin hillite 7
BB – Brilliant blue
BBB – Blood brain barrier
BDNF – Brain-derived neurotrophic factor
BUV – Brilliant ultraviolet blue
BV – Brilliant violet
C monocytes – Classical monocytes
CD – Cluster of differentiation marker
CD45RA – CD45 receptor antagonist
CNS – Central nervous system
CS & T – Cytometer setup & tracking
CSF – Cerebrospinal fluid
DC – Dendritic cell
DLBCL – diffuse large B-cell lymphoma
DMSO – dimethyl sulfoxide
EVD – External ventricular drain
FBS – Foetal bovine serum
FCM – Flow cytometry
FCS – Flow cytometry standard
FoxP3 – Forkhead box P3 (scurfin)
FSC – Forward scatter
GCS – Glasgow Coma Scale
GFAP – Glial fibrillary acidic protein
HCP – Hydrocephalus
HLA-DR – Human leukocyte antigen (DR isotype)
HSV – herpes simplex virus
ICP – Intracranial pressure
IFN – Interferon
IL – Interleukin
IL-1RA – Interleukin-1 receptor antagonist
IP-10 – Interferon-inducible protein-10
IQR – Interquartile range
LLOD – Lower limit of detection
LMICs – Low and middle income countries
MAIT – Mucosal associated invariant T cell
Max – Maximum

MCP – Monocyte chemoattractant protein
MFI – Median fluorescent intensity
MHC – Major Histocompatibility Complex
Min – Minimum
MIP – Macrophage inflammatory protein
MMPs – Matrix metalloproteinases
MS – Multiple Sclerosis
NC monocytes – Non-classical monocytes
NGF – Nerve growth factor
NHLS – National Health Laboratory Services
NIH – National institute of health
NIND – Non-inflammatory neurologic disease
NK – Natural killer
NT3 – Neurotrophin-3
NVU – Neurovascular unit
OI – Other infections
OIND – Other inflammatory neurologic disease
p – Percentile
ρ – Spearman correlation coefficient
p-value – Probability value
PAMP – Pathogen-associated molecular pattern
PE – Phycoerythrin
PE-CF – Phycoerythrin & cyanine-based fluorescent dye
PE-Cy5 – Phycoerythrin & cyanine dye Cy5 complex
PE-Cy7 – Phycoerythrin & cyanine dye Cy7 complex
PMN – Polymorphonucleocyte
PMT – Photomultiplier tube
PRR – Pattern recognition receptor
r – Pearson correlation coefficient
r^2 – coefficient of determination
RCWMCH – Red Cross War Memorial Children's Hospital
ROS – Reactive oxygen species
RPMI – Roswell Park Memorial Institute
SSC – Side scatter
Streptavidin PE
TB – Tuberculosis
TBM – Tuberculous Meningitis
TCR – T-cell receptor
TGF – Transforming growth factor
T_H1 – T-helper 1 cells
T_H2 – T-helper 2 cells

T_H17 – T-helper 17 cells
TLR – Toll-like receptor
TMEM119 – Transmembrane protein 119
TNF – tumour necrosis factor
T_{Reg} – Regulatory T cells
TST – Tuberculin skin test
UTD – Up to date
UViD – Ultraviolet-induced detection
VEGF – Vascular endothelial growth factor
VPS – Ventriculoperitoneal shunt
VZV – Varicella Zoster Virus
WHO – World Health Organisation

Abstract

Introduction: Paediatric central nervous system (CNS) infections are associated with high mortality rates and neurological disability in survivors due to brain injury caused by cerebral inflammation. Because the brain is difficult to study, the unique characteristics of the neuroinflammatory response are poorly understood. A better understanding of the immune response to these infections could lead to improved host-directed therapies. An important method to study this is the analysis of infected ventricular cerebrospinal fluid (CSF), but there is often a paucity of cells in CSF samples, especially in conditions like tuberculous meningitis (TBM), and these undergo rapid immune cell death after sampling. Consequently, the cell populations in CSF are not well described. Cryopreservation of CSF and flow cytometric analysis have improved the ability to study immune cells in CSF; therefore, these techniques were employed in this study.

Aims: This project aimed to 1) describe the cellular immunophenotype and inflammatory mediators in CSF samples from patients with common CNS infections through flow cytometric and Luminex® analysis respectively, and 2) explore changes in immune cells and analytes over time.

Methods: CSF samples were prospectively collected during clinically indicated procedures, the cell pellets and supernatant were cryopreserved. Flow cytometric analysis was performed after two weeks of storage at -80℃. Different populations of major peripheral immune cells ($CD45^+$: lymphocytes, monocytes and granulocytes) and CNS-derived immune cells (microglia ($CD45^-TMEM119^+$) and astrocytes ($CD45^-ACSA^+$) were examined along with their respective sub-groups. The sample supernatants were batch analysed for inflammatory biomarkers including interleukin (IL)-1β, IL-6, IL-8, IL-10, IL-1 receptor antagonist (IL-1Ra), tumour necrosis factor (TNF)-α, interferon (IFN)-γ, IFN-α, vascular endothelial growth factor (VEGF), monocyte chemoattractant protein 1 (MCP-1), macrophage inflammatory proteins (MIP)-1α and interferon-inducible protein 10 (IP-10) using Luminex® technology. Cell proportions and concentrations (using Flow-Count Fluorospheres) and cytokine concentrations were described in admission and serial samples.

Results: This study recruited 30 children with CNS infections (including tuberculous and other bacterial meningitis, shunt infections, and ventriculitis) in whom 61 samples were collected (30 admission, 31 serial samples). Microglia ($CD45^{-}TMEM119^{+}$) were the most abundant cell population on admission and over time. Lymphocytes ($CD45^{+}CD3^{+}$ and $CD45^{+}CD3^{-}$) were the most abundant peripheral immune cell, population above granulocytes ($CD45^{+}$) and monocytes ($CD45^{+}CD14^{+}$). Cytokines with the highest concentration included IL-1Ra, MCP-1 and IP-10. MCP-1 remained elevated over time whereas overall cytokine concentrations were highest on admission and decreased over time. Cytokine and cell data were influenced by the aetiology of the CNS infection (70% of the cohort comprised patients with TBM).

Conclusions: Brain-resident immune cells are important contributors to the neuroinflammatory response to CNS infection, particularly microglia, which are the most abundant immune cell present in the ventricular CSF of these patients. The techniques used in the study could be used at scale to characterise the unique characteristics of the neuroinflammatory response in different CNS infections and inflammatory conditions, which could lead to the development of novel immunomodulatory therapies. The role of microglia in inflammation as well as neurodevelopment is important to consider when studying children.

Chapter 1 – Introduction to CNS Infections

The central nervous system (CNS) encompasses much of what aids and enables our functioning as human beings. As such, infection and inflammation of the CNS are associated with notable morbidity and mortality and may result in severe neurological sequelae[1–3]. Such consequences are worse when children are affected because of the vulnerability of the developing brain[4]. Considerable effort is therefore being put into the causes, diagnosis, immunopathogenesis and treatment of these infections in the paediatric population.

CNS infections are responsible for a significant burden of disease globally, affecting millions of children and adults, most commonly in low- and middle-income countries (LMICs)[1,4,5]. The distribution of community-acquired CNS infections throughout the world is non-homogenous[2], given the many factors that can affect the epidemiology of CNS infections: the socio-economic characteristics of a population, the immune status of individuals, their geographic location, and the presence of comorbidities, among others[3,6].

Poverty, inadequate access to healthcare, overcrowding, and insufficient water and sanitation significantly increase the vulnerability of people in LMICs[1]. For patients in Sub-Saharan Africa, these risk factors are common; therefore, it is unsurprising that this region has the world's highest incidence of tuberculosis-related CNS disease and bacterial meningitis[1].

The range of causative pathogens is broad[7], including bacteria, fungi, viruses and parasites[1,5]. Meningitis, ventriculitis and encephalitis are some of the most commonly presenting CNS infections[8], each accompanied and driven by inflammation in the brain. Bacterial and tuberculous meningitis are the two most common serious paediatric CNS infections in our environment and are therefore worth special attention.

Bacterial meningitis

Bacterial meningitis is the result of acute inflammation of the meninges – the protective layers surrounding the brain, which include the pia, arachnoid and dura mater – and it is one of the most common CNS infections[9,10]. Among CNS infections of bacterial origin, acute bacterial meningitis is the most common manifestation[11]. Neonates and infants are most at risk due to their relatively immature immune system, with Agrawal *et al.* (2011) reporting that

up to 75% of all bacterial meningitis cases occur in children below the age of 5 – mostly in those under two months old[11].

The main bacteria responsible for such an infection are *Haemophilus influenzae type B, Streptococcus pneumoniae* and *Neisseria meningitidis*[9,10,12]. From colonization of bacteria in the nasopharyngeal region, invasion of the blood stream occurs through the mucosal membranes[13,14]. Through hematogenous dissemination (bacteraemia), the pathogen is able to reach and penetrate the blood-brain and/or blood-cerebrospinal fluid (CSF) barrier[15]. Another more direct route of entry into the CNS may be secondary to mastoiditis or sinusitis[11]. Extensive bacterial proliferation, inflammation, and influx of immune cells in the subarachnoid space can thus occur[14,15]. Some pathogens have specific characteristics that enhance their pathogenicity: *Streptococcus pneumoniae,* for example, causes neuroimmune suppression whereby host defences are inhibited and bacterial infection exacerbated[16].

Signs and symptoms of bacterial meningitis vary based on the age of the child[10,11]. Infants may present with fever, irritability, vomiting or seizures, whereas clinical features of slightly older children usually include fever, headache, vomiting, confusion, photophobia, or nausea, to name a few[10,14]. The gold standard diagnostic tool for bacterial meningitis is to perform a CSF culture after performing a lumbar puncture, with other CSF parameters such as raised protein, low glucose and polymorphonuclear pleocytosis being additional indicators of infection[9,12]. Based on the causative organism, a prompt antimicrobial treatment regimen should be implemented, with supportive and possibly adjunctive therapy, to try and eradicate this severe infection. Short-term and long-term neurological sequelae are common given the severity of bacterial meningitis and the nature of health care in LMICs[11]. Limited resources, delayed presentation to health facilities and inadequate access to care render patients vulnerable to short-term (focal neurological deficit, hydrocephalus, subdural effusion) and long-term (cognitive impairment, post-infectious epilepsy) complications[11]. In infants, 20% of surviving patients may develop serious long-term complications, with the mortality rate for bacterial meningitis being highest in neonates – and generally higher in LMICs[9].

Tuberculous meningitis

Dissemination of the *Mycobacterium tuberculosis* pathogen from the lung to the brain leads to the onset of ***tuberculous meningitis (TBM)***[17–19]. TBM is the most severe form of tuberculosis (TB)[20–22], presenting in 1–5% of individuals who have TB[23,24]. Compared to other forms of bacterial meningitis, it typically has longer symptom duration and more likely presents with neurological compromise[17]. Weight loss, failure to thrive, persistent cough, neck stiffness and fever are common presenting symptoms[17,21,25]. However, signs and symptoms of this infection may be vague in children[26]. The major risk factors for developing TBM are a compromised immune system (such as poor nutrition and co-infection with HIV) and young age (especially less than 5 years old)[23,27]. Disease history and manifestation differs between children and adults[28]. In children, severe morbidity and death occurs in 50% of those affected by TBM[21] and the significant correlation between poverty and the high incidence of TB means that LMICs are most affected by this infection[18].

The disease is associated with inflammatory exudate that develops in the basal cisterns of the brain, causing the disruption of CSF hydrodynamics – and therefore hydrocephalus (HCP) – to develop in up to 90% of TBM patients[21,29,30]. HCP is the accumulation of CSF in the brain, which results in an abnormal enlargement of the ventricular system[31–33]. This increased volume of fluid within the brain results in an increase in intracranial pressure (ICP)[20] and possible further neurological deficit[18]. The exudate also causes vasculitis of the basal vessels of the brain, which commonly results in cerebral infarction[34].

In a similar manner to diagnosing bacterial meningitis, performing a CSF culture to isolate acid-fast bacilli (AFB) is considered the gold standard for TBM diagnosis[17,24]. Identification of AFB in CSF is a good indicator of TB in the CNS, and culturing of *Mycobacterium tuberculosis* in CSF allows for drug sensitivity and resistance testing[24]. However both culture and identification are difficult, *Mycobacterium tuberculosis* is known to be paucibacillary, which may impact the results of CSF culture[24]. To this end, performing a PCR (GeneXpert or GeneXpert Ultra) test on CSF is often employed to increase the likelihood of making a diagnosis, but it has reduced sensitivity in CSF and a poor negative predictive value[35]. Given the difficulties in a definitive diagnosis of TBM, the international TBM consortium developed a research definition to aid int eh standardisation of TBM diagnosis across research studies.

This consensus statement is routinely used to determine definitive, probable or possible TBM and is based on a combination of patient history, CSF, radiological and clinical findings[36].

While the TBM CSF profile also shows decreased glucose and elevated protein values as is seen in bacterial meningitis, it is typically associated with lymphocytosis in the CSF[18,21,25]. A tuberculin skin test (TST) is also useful for disease diagnosis[24]. Imaging of the brain is helpful in making the diagnosis and monitoring the disease: there is a typical pattern of basal meningeal enhancement, hydrocephalus, and infarcts[25,30]. The admission CSF, clinical and radiological findings, a history of pulmonary TB and the results of diagnostics tests all form part of an international consensus criteria for determining definite, probable or possible TBM for research purposes[36]. In terms of treatment, the World Health Organisation (WHO) have outlined a four-drug treatment regimen for TBM[25], with advised adjunctive corticosteroids[18]. The recommended drug regimen consists of Rifampicin, Isoniazid, Ethambutol and Pyrazinamide, given orally for an intensive phase of all four drugs for the first two months, followed by a continuation phase of only Rifampicin and Isoniazid for ten months[37,38]. Prednisone is the recommended corticosteroid given daily for children with TBM[38]. There is no standardisation of the duration of treatment in adults or children. In our local context in children, a high intensity 6 month treatment regimen is standard of care. To treat acute HCP and control elevated ICP, it may be necessary to perform neurosurgical interventions including lumbar punctures and/or insertion of an external ventricular drain (EVD)[20], with potential subsequent insertion of a ventricular shunt to manage residual HCP[30].

CSF shunt infections

Hydrocephalus is a common condition in Africa, usually caused by CNS infections, prematurity-associated intracranial haemorrhage, spina bifida, head trauma, and brain tumours[39–41]. It is commonly treated by placement of ventriculoperitoneal CSF shunts[42–44]. The main aim of treatment for HCP is to successfully disseminate the built-up CSF to another area of the body where it may be absorbed into the blood (in the case of a shunt) or removal of CSF from the body (as with an EVD or lumbar puncture)[42–44]. Ventricular shunts have proven to be very successful in this regard[42–44], and these include ventriculoperitoneal, ventriculoatrial and ventriculopleural shunts – first described and used in 1955, 1952 and 1954 respectively[45]. A

common complication of the procedure, especially in the developing world context, is ***shunt infection***.

The literature shows considerable variation in reported failure rates of shunts, with a general failure rate of 3–15% in the first six months following shunt placement[46–48]. This infection is more common in children than adults – and more so in younger versus older children[49,50] – with other relevant risk factors being previous shunt revision(s) and aetiology of HCP[48,51]. The most common symptoms of a shunt infection include fever, vomiting and seizures, but there are a wide range of other possible presentations[50,52,53]. A definite diagnosis of shunt infection warrants a positive CSF culture[54], and coagulase-negative staphylococcus is the primary causative bacteria in such cases, followed by *Staphylococcus aureus* and the less-virulent *Staphylococcus epidermis*[47,49,55]. Diagnosis is challenging due to low positive CSF culture rates[56–58], with much variation between centres on the definition of shunt infection. Prominent clinical trials, including Mallucci *et al.*, have thus incorporated aspects from many studies in conducting a suitable definition for shunt infection diagnosis[54].

Shunt infections are challenging to treat and eradicate due to the ability of the causative bacteria to form a protective biofilm – an extracellular matrix structure surrounding the bacteria[59]. It enables the pathogen to resist being killed by immune cells and antibiotics[60]. Nonetheless, antibiotic therapy is administered in these cases, accompanied by removal of the shunt[61] and placement of an EVD[62]. A new shunt will be placed when the CSF is sterile[62]. Given the nature of this infection and its potential to circumvent antibiotic therapy, it may result in long-term morbidity and even death in paediatric patients[46].

Ventriculitis

Ventriculitis refers to a low-grade infection of the ventricular ependyma, which has a more gradual development compared to bacterial meningitis[63,64]. The most common precursors to the onset of ventriculitis are: head trauma resulting in a posttraumatic CSF leak; a burst brain abscess; progression of meningitis into the ventricles; or neurosurgical procedures[65–67]. The different bacterial species causing this infection depends on the disease aetiology[65,66], but gram-negative meningitis followed by *Staphylococcus* species are the most common infections associated with ventriculitis[64,65] and ventriculomeningitis[67]. Patients typically

present with altered mental status, fever, headache and clinical features of meningitis such as meningism, seizures, nuchal rigidity and photophobia[63,65,67,68]. Declining glucose levels and increasing protein in the CSF are common, similar to meningitis but with slower progression[64,65,68].

Ventriculitis also occurs commonly in children, with prompt and effective diagnosis and treatment having a large impact on the patient's prognosis[65]. Nosocomial ventriculitis contributes to significant morbidity and mortality[67], with microbiological tests proving useful with infection diagnosis[65]. Neuroimaging is also recommended given the typical ventriculitis 'picture' that such scans often depict, of ependymal enhancement and the presence of inflammatory debris within the ventricles[63]. Broad-spectrum antibiotics are typically given initially, which may be altered to more targeted antimicrobial agents as more clinical characteristics are revealed[67]. However, a study by Ochoa *et al.* (2022) has demonstrated the particular effectiveness of the neuroendoscopic lavage technique in ensuring CSF sterility in ventriculitis patients[63].

Vulnerability in Children

Children under 14 years old – and especially children younger than 5 years old – are more vulnerable to CNS infections, and demonstrate a higher incidence than adults[4,69]. The naïve nature of the peripheral immune system in children, which only reaches peak development and functionality during adolescence[4,70], is a major contributing factor. Not only are CNS infections more common, but their sequelae may also be worse in children because the CNS is still undergoing much development[70]. Because neurodevelopment is especially sensitive to environmental stimuli during the early postnatal stage, children are far more vulnerable to significant, long-term neurological sequelae and mortality[70].

For all of these reasons, it is imperative that CNS infections in children are diagnosed promptly to allow for early administration of targeted treatment and therefore improved prognosis[11,18]. However, many diagnostic methods currently used for CNS infections – such as microbiological and biochemical analysis of CSF – are costly, time-consuming and insufficiently sensitive or specific[18,71]. Early symptoms of a CNS infection may also be nonspecific, with the aetiology thereof being difficult to ascertain[24]. Additionally, in LMICs, the number of neurosurgeons is

disproportionate to the burden of disease and population sizes, and access to crucial medical resources and treatments may be limited[1]. These factors compound to result in a significant burden of disease in countries such as South Africa, with notable rates of severe morbidity and mortality in children.

It is important to note that despite it being clear that injury to the brain is caused by the ensuing cerebral inflammation, there is much about this inflammatory response that we do not understand. Because of the compartmentalization of the brain, understanding the systemic inflammatory response provides little additional insight into CNS pathophysiology. This is important because adjuvant host-directed therapies may be able to ameliorate the most harmful inflammatory effects. The next chapter summarizes our current understanding of the immunopathogenesis of CNS infections.

Chapter 2 – Immunopathogenesis of CNS Infections

2.1 Introduction to innate vs. adaptive immunity

The body faces numerous foreign microorganisms on a daily basis [72]. We are able to survive these encounters thanks to the body's immune system, which is constantly mediating potential immunological threats and invasions [72,73]. Many factors influence the effectiveness of the host's immune response. One's age – and thus the stage of immune development[4,70] – the state/strength of one's immune system and the pathogen load and virulence that the body is encountering [72] are but a few.

The immune response can be sub-classified into two components: the innate immune system and the adaptive immune system[73,74]. The *innate immune system* is a characteristically non-specific, rapid response to invading pathogens, and it is the host's initial line of defence [73,75]. Such a response depends on host cells recognizing molecular characteristics only associated with microbial pathogens, known as pathogen-associated molecular patterns (PAMPs)[73,74,76]. PAMPs are recognised via germ-line encoded pattern recognition receptors (PRRs)[4,74,76,77] found on key innate immune cells such as leukocytes and mononuclear phagocytes – including monocytes circulating in the blood and macrophages resident to tissue[75].

Recognition of a pathogen initiates intracellular signalling pathways and activates mechanisms of the innate response[75,76]. Activated PRRs subsequently trigger, among others, pathways involving the formation of an inflammasome, a membrane attack complex[77] or initiation of the complement cascade[75,78]. Crucially, PRRs also induce the release of inflammatory mediators, known as cytokines and chemokines, from the cell[74,75,79]. Such mediators enable additional innate immune cells to be recruited to the site of infection[75,79]. A cytokine milieu involving interleukin (IL)-6, IL-1β, tumour necrosis factor (TNF)-α and IL-12, typically governs the acute phase response to a pathogen, inducing both local and systemic effects – such as cell trafficking[75,78]. Chemokines are small polypeptide molecules also involved in the direction of cell trafficking and recruitment, as well as lymphocyte development and the generation of T-helper 1 (T_H1), 2 (T_H2) and 17 (T_H17) cell responses [75,78,80]. Through the tight-knit

interrelationship shared between cytokines and chemokines, the type and nature of immune response elicited by an infectious challenge can be determined[75,78].

Of most importance in the innate response are lymphoid-derived natural killer (NK) cells as well as polymorphonuclear and mononuclear leukocytes deriving from myeloid progenitors: monocytes (forming macrophages and dendritic cells), neutrophils and mast cells[4,75,81]. Table 2.1 provides an overview of cellular characteristics relating to these cells, and figure 2.1 demonstrates this lineage. While NK cells are classed as innate immune cells, figure 2.1 depicts that they have lymphoid origins which are typical of adaptive immune cells, setting them slightly apart from other innate cells[75]. By utilising these cells together with activated signalling pathways, cytokines and chemokines bring about local inflammation[79] as well as effector mechanisms such as opsonisation of the pathogen, phagocytosis, bacteriolysis and the synthesis of antimicrobial peptides[74,75]. The primary aim of these mechanisms, and of the immune system as a whole, is to destroy the invading pathogen and prevent its dissemination[72].

To this end, a crucial mechanism of the innate immune system is to activate and prime the *adaptive immune system*[73,74,76]. Key adaptive immune cells originate from lymphoid progenitors, including T cells (forming memory cells, cytotoxic T cells and helper T cells) and B cells (forming plasma cells and memory B cells)[81]. Table 2.1 provides an overview of cellular characteristics relating to these cells, and figure 2.1 demonstrates this lineage. In contrast to effector cells of the innate immune system, which are pre-programmed for their specific functions, cells involved in the adaptive response are naïve, and require presentation of a specific antigen to activate and specialize[74,82]. Phagocytic cells of the innate response – specifically dendritic cells and macrophages – can take up an antigen for a specific pathogen, process it and present peptides of that antigen to naïve adaptive immune cells[81]. Antigen presentation is possible due to complexes on the surfaces of these cells known as major histocompatibility complexes (MHCs)[74,76]. The interaction between innate and adaptive cells occurs after the migration of phagocytic cells to the site of secondary lymphoid tissue containing adaptive immune cells, namely lymph nodes[79].

Naïve T cells and B cells have T- and B-cell receptors respectively that recognise a particular cognate antigen[74,79,81]. During antigen presentation, PAMPs of the antigen's corresponding pathogen induce the release of co-stimulatory molecules from the antigen-presenting cell (APC)[74,82]. Therefore, binding of an antigen with its respective T-/B-cell receptor ultimately activates the T-/B-cell and results in clonal expansion thereof [74,76,81]. To indirectly control differentiation of these activated T-/B-cells, APCs release cytokines that further specify the functional fate of the adaptive immune cells[76,82]. Ultimately, mature adaptive effector cells with the identical receptor specificity as their naïve precursor cells are created, and the process of clonal selection prevents cells with self-receptors from joining the lymphocyte repertoire[76,78,79] . In this way, the innate immune system ensures that a relevant and specific adaptive immune response is launched based on the invading pathogen[76,82]. Thus, the innate component of the immune system is effective in mediating the initial infection, whereas the adaptive component is more capable of actually clearing the specific pathogen and infection [81]. This can be pathogen-specific.

These signalling pathways and intercellular communication strategies reflect the true intricacy and co-ordination required for an efficient and effective immune response. Although a child's immune system is able to respond dynamically to threat, it is still maturing[4,70]. From humble beginnings with precursor cells *in utero*[83], the immune system develops throughout infancy and childhood[4]. The physical defence barriers of the body – namely the epithelial (skin) and mucosal membranes – undergo age-related changes, with immune cell populations largely being in a naïve state and immune function believed to reach a peak from adolescence onwards[4]. As described by Rook *et al. (2015)*, many factors influence immune development and ultimately immune function, such as microorganism exposure, maternal behaviour during pregnancy, perinatal stress and genetics [84]. However, underpinning much of the age-specific honing of the developing immune system is one's exposure to environmental stimuli and microorganisms[4,84].

Microbial exposure contributes to the formation and biodiversity of the epithelial microbiotas of the body[84]. These microbiotas influence and drive development of the immune system, which in turn impacts the development and functioning of the brain[84]. Fine-tuning of immunoregulatory mechanisms by the immune system also occurs during infancy and

childhood and is similarly influenced by microbial exposure[84]. This suggests that children living in LMICs might have an advantage regarding the dynamic nature of their immune systems due to vast microbial exposure. However, this may be counter-balanced by the poverty, malnutrition and burdened healthcare systems often seen in these countries[1]. Considering these factors and the naïve nature of a child's immune system, children in LMICs – such as those included in this study – are more likely to develop infections and those infections are more likely to spread within the body[4]. Thus, infections of the CNS have a higher incidence in such children compared to children in more developed countries and compared to adults[4].

Table 2.1: Summary of Peripheral Innate & Adaptive Immune Cell Characteristics

Cell type	Origin	Surface markers
Monocytes	○ ≈10% of circulating leukocytes[85] ○ Derived from myeloid progenitors in bone marrow[86] ○ Hematopoietic cells[86]	⇒ Subsets classified through differential expression of CD14 & CD16[85–87]: • Classical: $CD14^{++}CD16^{-}$ • Intermediate: $CD14^{++}CD16^{+}$ • Non-classical: $CD14^{+}CD16^{++}$ ⇒ CD14 is a PRR in innate immunity & a co-receptor for several TLRs[88]
Neutrophils	○ Most abundant leukocyte of the innate immune system[89] ○ Capable of phagocytosis & degranulation[81]	⇒ Identified through CD16 & CD11b expression[89] ⇒ CD16 is a receptor for Igγ; involved in neutrophil transendothelial migration[89] ⇒ ↑ CD11b expression indicates activation by a pathogen/infection[90,91]
NK Cells	○ Constitute between 5 and 15% of peripheral mononuclear cells[92] ○ After activation: release cytokines & demonstrate cytotoxicity[92,93]	⇒ Defined as $CD56^{+}$ [92,93] and $CD3^{-}$ [92,94] ⇒ Subsets of NK cells further subdivided by relative expression of both CD56 & CD16[94,95] ⇒ CD56 functions as a pathogen recognition receptor[92]
$CD4^{+}$ T Cells	○ Conventional cell subset[96] ○ Cytokine-producing helper T lymphocytes[97,98] ○ Regulatory T cells (Tregs) are a subset[98]	⇒ Expression of CD45RA identifies naïve $CD4^{+}$ cells[97,98] ⇒ Tregs demonstrate $CD4^{+}CD25^{+}FoxP3^{+}$ phenotype[98,99] ⇒ CD4 regulates maturation & function of $CD4^{+}$ subset[100]

$CD8^+$ T Cells	○ Conventional cell subset[96] ○ Cytotoxic effector T lymphocytes[97,98] ○ Capable of suppressing viral replication[101] ○ Cytotoxicity enables killing of target cells[101]	⇒ Differential expression of CD27, C28 & CD45RA based on differentiation & maturation[101] ⇒ CD8 is a glycoprotein facilitating cellular adhesion; also functions as a cosignalling receptor[102]
$\gamma\delta$ T Cells	○ Possess cytolytic & cytotoxic functions[103,104] ○ When stimulated: secrete cytokines & proliferate[103,104] ○ Exact function remains unknown[104]; unconventional T-cell subset[105]	⇒ Mostly lack CD4 & CD8 surface markers[104] ⇒ $\gamma\delta$ receptors can recognise pathogens & damaged cells in absence of antigen presentation or MHC complexes[106]
MAIT Cells	○ Abundant in blood and tissues – esp. the liver[107], & lamina propria of intestinal mucosa[108] ○ Unconventional T-cell subset[105] ○ Anti-bacterial defence[109]	⇒ Co-expression of CD161 & Vα7.2 markers[105,107] ⇒ CD161 is a C-type lectin capable of acting as a costimulatory receptor in TCR stimulation[96] ⇒ Vα7.2 – an invariant TCR[107] ⇒ Double negative ($CD4^-CD8^-$) phenotype in blood[108]
B Cells	○ Develop from hematopoietic stem cells in bone marrow[81,99] ○ Crucial in humoral immunity[110] ○ Differentiate into plasma & memory cells – capable of antibody production & antigen presentation respectively[110]	⇒ Virtually all B-cell lineages are $CD19^+$ [111] ⇒ CD19 mediates intercellular signal transduction[111]

Abbreviations: CD: cluster of differentiation marker (CD^+ → expressed; CD^- → not expressed; for the case of CD^+ and CD^{++} in monocyte classification, CD^+ indicates a level ≈10-fold above the isotype control & CD^{++} indicates a level ≈100-fold above the isotype control[112]); *MAIT cells*: mucosal-associated invariant T cells; *MHC*: major histocompatibility complex; *NK cells*: natural killer cells; *PRR*: pattern recognition receptors; *TLR*: toll-like receptor

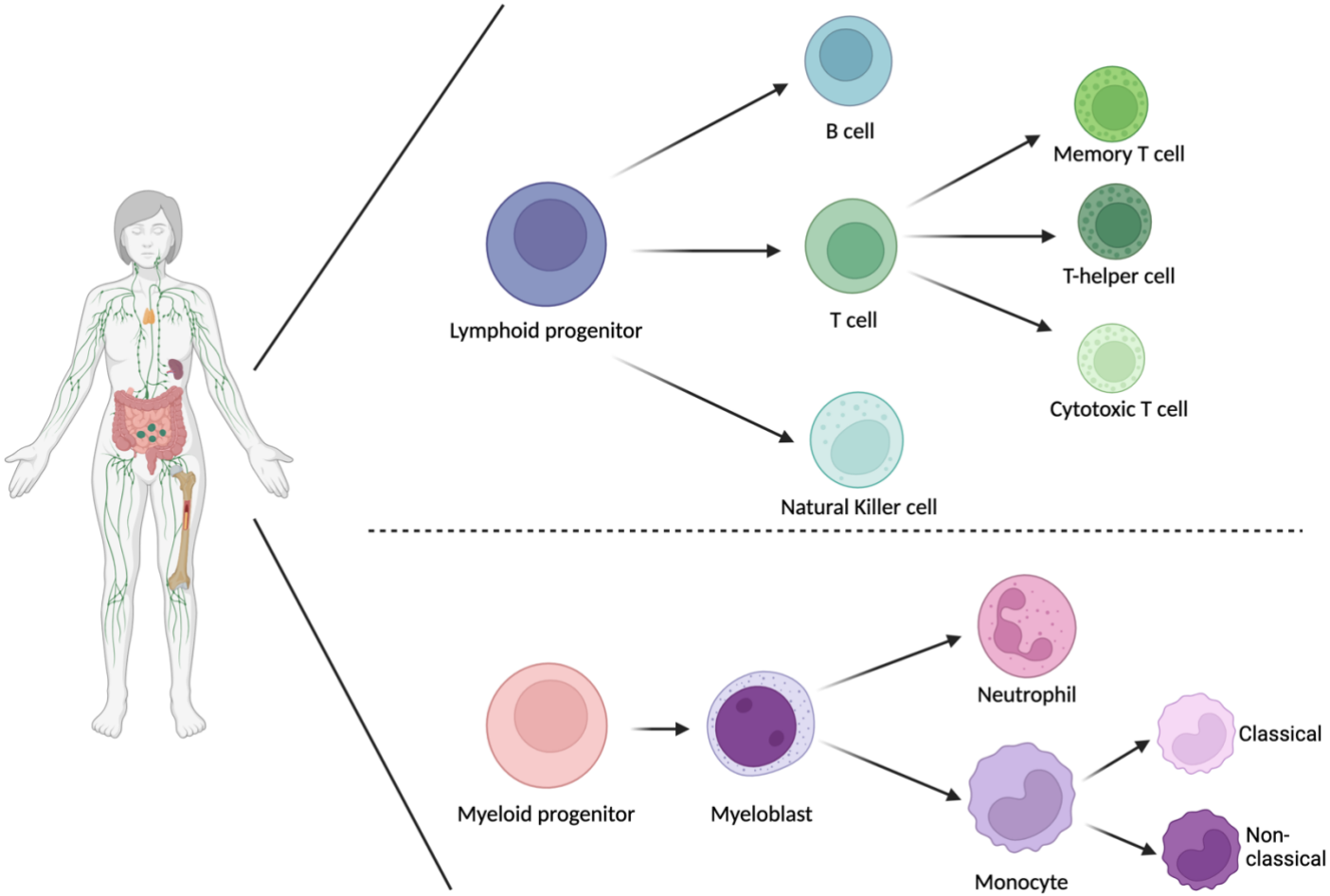

Figure 2.1. **Peripheral immune cell lineages considered in this study**. The *lymphoid lineage* includes B cells, Natural Killer cells and T cells – which in turn give rise to memory T cells, T-helper cells and cytotoxic T cells. The myeloid lineage ultimately includes neutrophils and monocytes. Created with BioRender.com

2.2 Immunity within the CNS in steady state conditions

Historically, the CNS was seen to be isolated from the systemic immune system and thought to lack an immune response[113,114]. This notion has since been revised, with further studies revealing robust immune response generation in the CNS [115]. However, it has been considered an immune-privileged site because of its unique separation from the periphery by the blood–brain barrier (BBB), the minimal presence of APCs in uninflamed brain parenchyma and the brain's seeming lack of lymphatics[113,114,116]. The BBB is vital in maintaining the integrity of the CNS, and consists of specialised endothelial cells joined together by adherens and tight junctions[116]. It is maintained by perivascular cells and astrocytic foot processes[113,117]. This barrier's selective permeability allows for strict control of molecular exchange between circulating blood and the CNS parenchyma, and is considered the first barrier of defence for the CNS[116,118]. Together with the blood–CSF barrier, the BBB therefore protects the CNS parenchyma, ventricular system and meninges surrounding the brain from blood-borne pathogens[113].

In essence, the CNS has been regarded as immune privileged due to the exclusive guarding by its innate immune responses and specific adaptive responses. However, this can be said for any organ in the body[116]. Incorporation of the blood–CSF barrier, the concept of a neurovascular unit (NVU), and the discovery of the glymphatic-like system in the brain has since allowed the concept of CNS immune privilege to evolve[113,115]. Under steady-state conditions, while the vascular endothelium of the BBB exerts tight control over cell trafficking, there are immune cells patrolling the CNS at potential sites of pathogen invasion[114,115]. This includes within CSF, at the choroid plexus, perivascular spaces, meninges and, ultimately, the brain parenchyma[114,115]. Such immune surveillance of the CNS is conducted by microglia (the brain's unique, tissue resident macrophage), as well as peripheral leukocytes – meningeal dendritic cells and perivascular macrophages [115,119,120]. While peripheral leukocytes originate from the bone marrow and circulate in the blood, microglia remain in the CNS and are not bone-marrow derived[119].

Microglia are the primary component of the brain's innate immune system[118], and are paramount to immune surveillance and homeostasis within the CNS [119]. These cells constitute up to 20% of the brain's cellular component[118], and are derived during early embryonic

development from myeloid progenitors – similar to macrophages[114,118]. As such, they serve as the initial cellular defence against invading pathogens in the brain parenchyma, and constantly sample the CNS extracellular space[119]. Astrocytes, a second type of resident CNS immune cell, have a more supportive role – providing structural support to neurons while contributing to their metabolism and synaptic plasticity[121]. However, these cells are believed to crucially contribute to the integrity of the BBB[121], and therefore also contribute to homeostasis within the CNS. Table 2.2 characterises these cells and their identifying surface markers, and figure 2.2 depicts these cells. Upon encountering a pathogen, both microglia and astrocytes become activated, and contribute to the innate immune response[122]. This process is discussed in detail later.

In conjunction with microglial and astrocytic activity, migration into the CNS of peripheral leukocytes – including T cells, macrophages, and dendritic cells (DCs) – allows for further surveillance under healthy conditions[114,119,123]. While their entry is tightly regulated by the BBB[115], access is mostly gained through the epithelial lining of the choroid plexus constituting the blood–CSF barrier, through the Virchow–Robin spaces and/or the postcapillary venules entering brain parenchyma[119]. Macrophages and DCs patrol the parenchyma and are stationed at common sites of pathogen entry[115]. In the event of pathogen confrontation, these cells present the corresponding antigen to the surveillant T cells, thereby activating them[118,119]. Studies have shown that the majority of the peripheral immune cells found in the CSF of healthy individuals are $CD4^+$ T cells, although some groups have disputed this[114,119].

Initial uncertainty regarding the immune properties of the CNS may have stemmed from the immunosuppressive nature of CNS cellular components, yielding the CNS immunologically quiescent[119]. Studies have reported that neuronal electrical activity can suppress the expression of MHC in microglia and astrocytes, which will affect the antigen-presenting capacity of these cells[119]. Neuronal neurotrophins, including nerve growth factor (NGF), brain-derived neurotrophic factor (BDNF) and neurotrophin-3 (NT3), were shown to dampen MHC 1 expression on microglia in brain slices, which would specifically affect interaction with $CD8^+$ T cells[119].

Resting microglia thus demonstrate a down-regulated immunophenotype[124]. Microglia and astrocytes themselves have been shown to release immunosuppressive mediators, with microglial IL-10 demonstrating autoregulatory dampening properties and astrocytic tumour growth factor (TGF)-β downregulating pro-inflammatory molecule release[119]. Upon activation by a pathogen, the immunophenotype of these cells changes from a quiescent to an activated state, with an efficient immune response being launched[70]. Considering its immune surveillance, the activation events triggering immune responses and its endogenous immunosuppressive mechanisms, CNS inflammation is under firm control.

Table 2.2: Cellular & surface characteristics of CNS-resident immune cells

Cell type	Origin/role	Surface characteristics
Astrocytes	○ Predominant glial cell type (≈ 50%)[125] ○ Maintain brain tissue homeostasis, vital in neuronal development[125,126] ○ Astrogliosis – activation of astrocytes in response to infection[127] ○ Cytotoxic or cytoprotective functions depending on activation phenotype[125]	⇒ ACSA serves as a determining, general marker for astrocytes[128] ⇒ GFAP is an intermediate filament in most CNS astrocytes[125,127] ⇒ GFAP provides mechanical support to astrocytes & the BBB[125] ⇒ Marker of reactive astrocytes (↑ GFAP levels)[127]
Microglia	○ Mesenchymal origin[129] ○ Resident macrophages of the CNS[129,130] ○ ≈ 10% of brain cell population[130] ○ Considered the primary resident immune cells of the CNS[129,131] ○ Principal source of cytokines in the brain[131]	⇒ TMEM119 is regarded as a standard marker specifically for microglia[130] ⇒ Under healthy conditions, express CD11b[129] ⇒ HLA-DR is expressed by activated microglia[129]

Abbreviations: ACSA: astrocyte cell surface antigen; *CD*: cluster of differentiation marker; *CNS*: central nervous system; *GFAP*: glial fibrillary acidic protein; *HLA-DR*: human leukocyte antigen-DR isotype; *TMEM119*: transmembrane protein 119

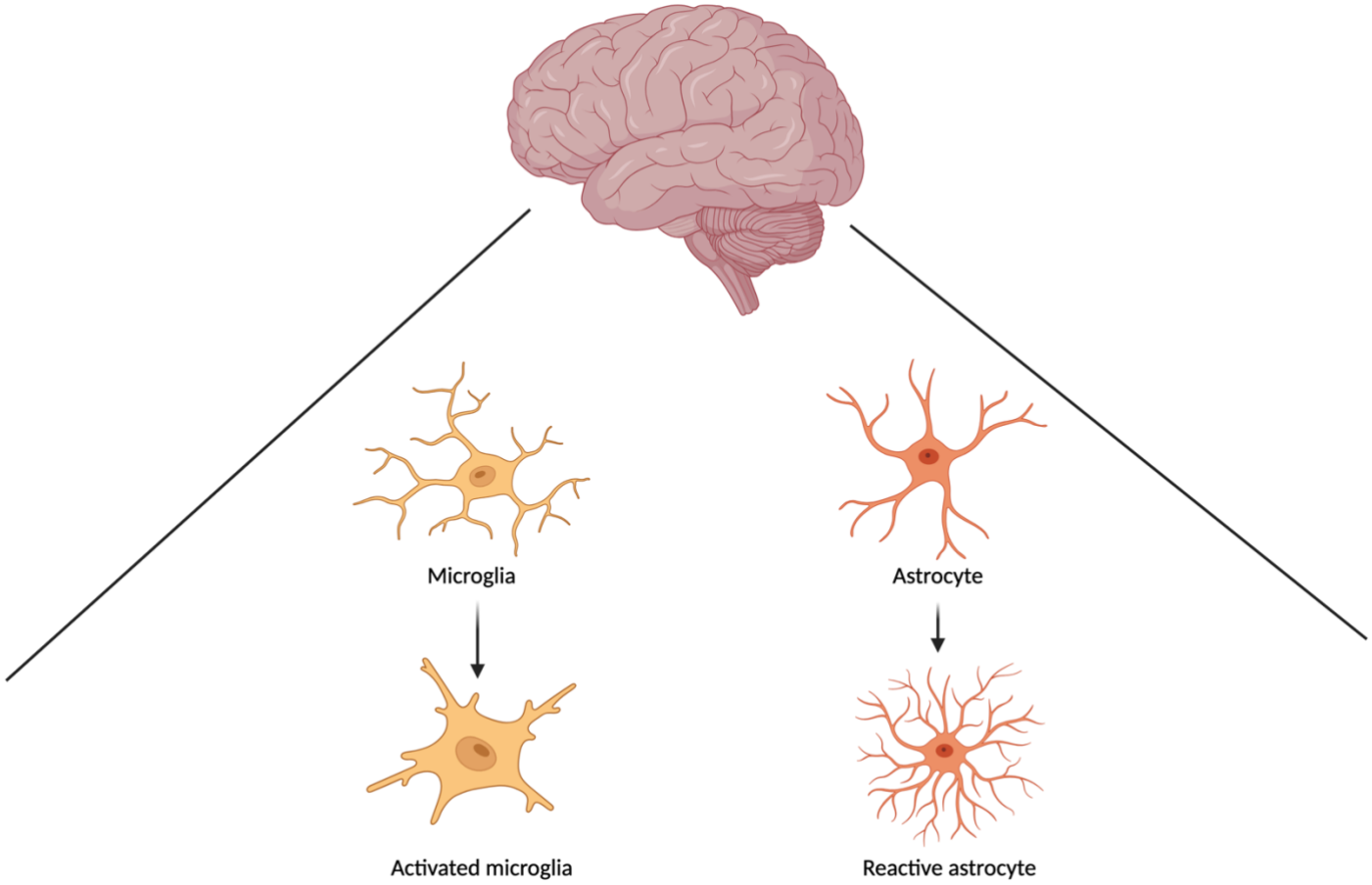

Figure 2.2. **Brain-derived immune cells.** The major brain-derived immune cells include microglia and astrocytes. Upon encountering and recognising a pathogen, both of these cell types become activated and participate in the immune response. Created with BioRender.com

2.3 Neuro-inflammatory response to pathogenic insult

For a pathogen to reach the CNS, ingestion/inhalation/inoculation of the microorganism first occurs, most commonly through the lungs, skin, or gut[113], followed by pathogenic replication and dissemination into blood circulation[113]. Entry into the CNS is only achieved via crossing of the unique BBB that shields the CNS from the periphery[116].

Should the pathogenic load be significant enough, breaching of the BBB may occur. As outlined by Lampron *et al.*, paracellular (between) and transcellular (through) transport mechanisms are commonly used by pathogens to cross the BBB's endothelium and enter the CNS[116]. Furthermore, weakening of tight junctions between endothelial cells by pathogens can impact the physical integrity of the BBB[116]. CNS-resident innate immune cells – namely microglia and astrocytes – detect pathogen-specific PAMPs via their PRRs – typically Toll-like receptors (TLRs)[115].

Microglia are vital innate responders to pathogens, while also shaping and protecting the environment of the developing brain by promoting angiogenesis, partaking in synaptic remodelling and influencing blood vessel patterning[130]. Given their derivation from myeloid precursor cells, microglia are phagocytic cells[121]. Similar to peripheral innate immune cells of this nature, microglia possess surface TLRs, enabling them to recognise a pathogen, endocytose and process its corresponding antigen, and present this to antigen-specific T lymphocytes[119,120]. Under these inflammatory conditions, microglia are activated[118] with an upregulation of MHC-II complexes on the microglial surface[120]. Antigen presentation is thus enhanced, specifically to $CD4^+$ T cells[120]. Morphological changes accompany microglial activation, shifting from a quiescent or ramified shape to an amoeboid shape[70]. Such activation results in one of two microglial phenotypes: M1, which is characteristically pro-inflammatory and neurotoxic, or M2, which is contrastingly neuroprotective and anti-inflammatory[80,118]. Microglia are therefore crucial in initiating the adaptive arm of the CNS immune response and mediating neuroinflammation[119].

Another type of resident glial cell demonstrating involvement in the neuroinflammatory response are astrocytes[122]. Astrocytes have been implicated in immune defence[121], expressing TLRs and therefore recognising, responding to and being activated by pathogens[116,122]. In

contrast to microglia, astrocytes do not express MHC-II under physiological conditions, but instead are induced to express this complex under inflammatory conditions[120,122]. However, both cell types are capable of acting as APCs under such conditions[120].

Both microglia and astrocytes release pro-inflammatory cytokines in response to their activation[116,122], including IL-1, IL-6, IL-12 and TNF-α [115,116]. Furthermore, the release of chemokines, free radicals and reactive oxygen species is also stimulated[115,116]. Due to these inflammatory mediators, specific local immune pathways are induced, with recruitment of both innate and adaptive peripheral immune cells to the CNS[115,116]. Recruited innate cells assist microglia and astrocytes by employing innate mechanisms of pathogen clearance – such as phagocytosis and degranulation[115]. Monocytes and neutrophils are among the initial innate cells recruited, followed by $\gamma\delta$ T cells and NK cells[120].

In contrast, adaptive naïve T cells recognise their corresponding antigen by encountering CNS-resident APCs – primarily microglia[120] – and recruited innate cells[132]. As in the rest of the body, this activates the T cells, resulting in clonal expansion, differentiation and cytokine release[132]. Ultimately, a T-cell mediated immune response is launched[115], with the specificity of that response depending on the cytokine milieu released[120]. CNS infections of a bacterial, fungal, viral or protozoan nature have demonstrated immune responses mediated primarily by helper $CD4^+$ T cells and cytotoxic $CD8^+$ T cells, both capable of interferon (IFN)-γ release[113]. Because of its induction of MHC-II expression on astrocytes[120], its promotion of macrophage activation, and its production of reactive oxygen intermediates, IFN-γ is regarded as a key cytokine in CNS inflammation[113]. $CD4^+$ T cells release cytokines capable of coordinating the adaptive immune response, whereas $CD8^+$ T cells conduct targeted cell killing[98]. Recruited B cells are capable of becoming APCs, as well as producing corresponding antibodies[110]. Thus, in conjunction with the innate response, the adaptive immune response will enhance pathogen clearance and resolution of neuroinflammation altogether.

While an immune response is warranted to fight a CNS infection and resolve neuroinflammation, excessive immune mechanisms can cause local cell damage within the brain[80,113]. Neuronal damage or death due to inflammatory processes may result in post-infectious neurological sequelae[113], which impact morbidity and mortality following CNS

infection. The CNS possesses immunoregulatory mechanisms aimed to limit immunopathology, including anti-inflammatory cytokines (e.g. IL-10 from T cells and IL-27 from microglia/macrophages), inhibitory receptors on T cells and the suppressive actions of Treg cells[113]. However, an exacerbated immune response may result in oedema, demyelination of neurons and ultimately reduced neuron functioning[80].

Inflammatory conditions induce the release of matrix metalloproteinases (MMPs) from all resident CNS cells[133]. MMPs break down BBB basement membrane constituents, compromising the BBB's physical integrity[133]. Oedema may result from a compromised BBB, since more permeability allows entry of more plasma proteins – and therefore more water – into the brain[134]. This brain swelling will contribute to raised intracranial pressure[20,134]. Impaired neuronal function and neuro-signalling may result due to excessive neuro-excitotoxicity[135]. Excess glutamate release secondary to inflammatory-induced ischaemic injury enables this neuro-excitotoxicity to develop[134,136,137]. Proteinaceous inflammatory exudate, which collects in the cisterns of the brain, impairs CSF flow dynamics and raises intracranial pressure (ICP)[20,134] – particularly in TBM[138]. This exudate can also cause vasculitis[20].

In the highly vulnerable environment of a child's developing brain, such neurological damage is potentially devastating[70]. Thus, post-infection long-term functioning in children may be more influenced by immunopathological consequences of neuroinflammation than in adults, with a greater impact on morbidity and mortality[70]. For this reason, a more comprehensive understanding of the immune response to brain infections, prompt diagnosis and targeted treatment of CNS infections is especially relevant in children. Early intervention and prevention of excessive neuroinflammation may help ameliorate the detrimental effects mentioned above, resulting in better outcomes. However, fundamental data on the inflammatory response at the site of disease is still lacking, particularly in the context of the developing brain. This project aims to contribute important pilot data to enhance our understanding and the identification in the future of potential novel avenues for immunomodulation and improved outcomes.

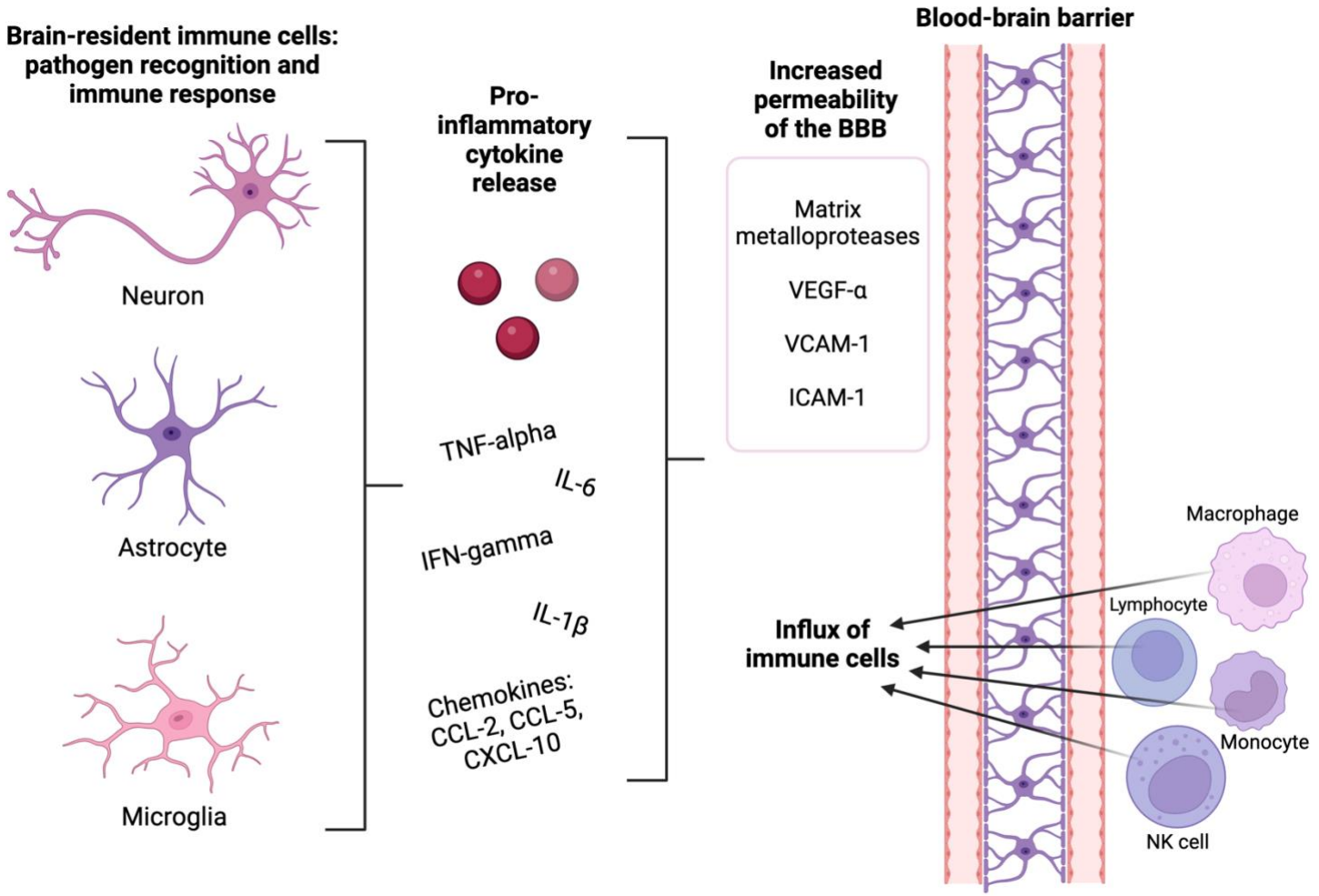

Figure 2.3. **Response of the brain to pathogenic insult.** Resident brain cells recognise the pathogen and initiate the immune response in the brain through release of pro-inflammatory cytokines. An increase in blood-brain barrier (BBB) permeability accompanied by the influx of immune cells into the brain. Created with BioRender.com

2.4 Markers of brain inflammation

Swift diagnosis of CNS disease is notoriously difficult, as is tracking disease progression and determining disease severity[138,139]. Radiological scans and clinical findings are typically utilised to quantify severity of disease[138], but there has been increasing interest and research into the role of cytokines and chemokines as CSF biomarkers, serving as an additional diagnostic tool[138,140]. These products can be measured as biomarkers/indicators of brain injury and inflammation[139], and could potentially help monitor drug efficacy during treatment[141].

Prominent immune-mediated inflammatory biomarkers include IL-1β, IL-6, IL-8, IL-10, IL-1 receptor antagonist (IL-1Ra), IL-12p40, TNF-α, IFN-γ, IFN-α, vascular endothelial growth factor (VEGF), monocyte chemoattractant protein 1 (MCP-1), macrophage inflammatory proteins 1 and 2 (MIP-1 and MIP-2) and interferon-inducible protein 10 (IP-10)[138,140,142]. Hallmark features of these biomarkers are provided in Table 2.3 below.

Table 2.3: Biomarker characteristics and functions during neuroinflammation

Biomarker	Characteristics & Role
IL-1β	⇒ Pro-inflammatory[140,142] – one of the most powerful[143] ⇒ Useful for tracking infection progression[140] ⇒ In a study López-Cortés *et al*., was most reliable marker – good sensitivity & specificity in differentiating bacterial vs. aseptic pleocytosis[144] ⇒ Protective in viral, bacterial & fungal infections[143] ⇒ Released by macrophages & activated monocytes[145,146]
IL-1Ra	⇒ Natural anti-inflammatory cytokine[147] ⇒ Inhibits IL-1 → increased vulnerability to infection[143] ⇒ However, also mediates inflammation & may limit extent of disease[148] ⇒ Upregulated during infection & inflammation[147] ⇒ Secreted by neutrophils, monocytes & macrophages[147,149]
IL-6	⇒ Pro- or anti-inflammatory cytokine depending on progression of inflammation[150,151] ⇒ Role in both innate & adaptive response[152] ⇒ ↑ levels in non-bacterial inflammation & nosocomial infection[153] ⇒ Levels correlated with CSF leukocyte cell counts[153] ⇒ Released by astrocytes[154], monocytes & alveolar macrophages[155]
IL-8	⇒ Pro-inflammatory chemokine[150] ⇒ Chemoattractant & activator of neutrophils[156] ⇒ Produced/released by microglia[156] & astrocytes[157,158]
IL-10	⇒ Anti-inflammatory, immunosuppressive cytokine[159] ⇒ Limits astrocytic & microglial immune responses[159] ⇒ Released by regulatory T cells[160–162]
TNF-α	⇒ Pleotropic pro-inflammatory cytokine[163] ⇒ Synthesized by microglia, astrocytes & neurons[164] ⇒ Role in leukocyte migration into the brain & glial activation[163] ⇒ Released by macrophages[165], monocytes, activated T cells[166], astrocytes[167]
IFN-γ	⇒ Pro-inflammatory cytokine[168] ⇒ Induces MHC-II expression on astrocytes[120] ⇒ Promotes macrophage activation & production of reactive oxygen intermediates[113] ⇒ Released by NK cells, DCs, activated T cells (mainly $CD4^+$) & B cells[169,170]

IFN-α	⇒ Released by glial cells & neurons[171], as well as by monocytes, macrophages, NK cells, DCs & T cells[172] ⇒ Major actions include proapoptotic, antiviral & antiproliferative[171] ⇒ ↑ levels in inflammation leads to cognitive dysfunction through ↓ dendritic arborization[173] ⇒ Upregulates inflammatory cytokines e.g. IL-1, -6 & TNF-α[173]
MCP-1	⇒ Synthesized by monocytes, microglia & astrocytes[174,175] ⇒ Direct innate & adaptive cell trafficking into CNS – such as monocytes, memory T cells & DCs [174,175] ⇒ Elevates reactive oxygen species (ROS) generation[174] ⇒ Potentially compromises integrity & permeability of BBB – promotes ECM protein degradation, induces pericyte injury, induced chemotaxis in monocytes & microglia, binds to neurons and inhibits GABA-mediated responses[176]
MIP	⇒ Pro-inflammatory chemokine[177] ⇒ Involved in neutrophil recruitment to the CNS[177] ⇒ T cell and macrophage activation & proliferation ⇒ Released by T & B cells, neutrophils, NK cells, monocytes, macrophages & DCs[178]
IP-10	⇒ Significant levels found in CSF in neuroinflammatory conditions[179] ⇒ Attracts T cells, NK cells & monocytes to CNS[180] ⇒ Released by leukocytes, monocytes, neutrophils, eosinophils, epithelial & endothelial cells[181,182] and astrocytes[183]
VEGF	⇒ Regulates brain vascularization during CNS development; indirect role in neuronal cell proliferation[184] ⇒ Both beneficial & pathological roles during neuroinflammation & injury[185] ⇒ ↑ levels during acute inflammation contributes to BBB breakdown[184–186] ⇒ Released by platelets & leukocytes[187]

Abbreviations: BBB: blood brain barrier; *CNS:* central nervous system*; CSF:* cerebrospinal fluid; *DCs*: dendritic cells; *IFN*: interferon; *IL*: interleukin; *IL-1Ra*: interleukin-1 receptor antagonist; *IP-10*: interferon-inducible protein 10; *MCP-1*: monocyte chemoattractant protein-1; *MHC-II*: major histocompatibility complex II; *MIP*: macrophage inflammatory protein; *NK cells*: natural killer cells; *ROS*: reactive oxygen species; *TNF*: tumour necrosis factor; *VEGF*: vascular endothelial growth factor

Chapter 3 – Analytical Techniques: Flow Cytometry

3.1 What is flow cytometry?

Flow cytometry is a powerful and efficient technique for cell analysis within body fluid samples[188,189]. It allows for the quantification of optical and fluorescent properties of single cells suspended in a fluid stream as they pass through a light source (e.g. a laser)[188–190], and is used to distinguish different cell types, to sort cells and to perform absolute cell counts[190,191]. Flow cytometry is based on the principle of light scatter and fluorescence emission when a laser beam strikes a passing cell[189], which will be expanded upon below. This technique has applications in many disciplines, such as immunology, virology, cancer biology and molecular biology[188].

In the context of infectious disease, flow cytometry has demonstrated effectiveness in studying the immune response and in immunophenotyping[188], and can be used to diagnose and monitor the progression of disease[190]. According to McKinnon (2019), immunophenotyping is the most common application of flow cytometry[188], which is the purpose of the technique for this project. Initially developed for the analysis of blood specimens, flow cytometry has been adapted to incorporate analysis of other body fluids[192], such as CSF. Though much technological advancement has been made within the last two decades, flow cytometers possess three primary components: fluidic, optic and electronic systems[188–190].

Fluidics

The purpose of the fluidics system is to direct the cells through the cytometer system to the laser intercept (i.e. interrogation point) for analysis[188,190]. Cells need to pass the laser in single file to ensure uniform, reproducible cell illumination, which is achieved by injecting the cells from the sample tube into a pressurised stream of sheath fluid[190,193]. A central sample stream forms within the sheath fluid stream due to differences in pressure between these two streams[189,193]. Sample pressure should always be greater than sheath fluid pressure[189]. This concept, known as hydrodynamic focusing, is what ensures that the cells pass the laser beam one by one[189,190]. Rate of cell injection into the laser beam may be altered faster or slower based on the experiment's analytical needs[189]. Slower injection rate allows for increased uniformity and thus increased accuracy of cellular illumination[189].

Optics

The optics system is comprised of excitation and collection optics[188,189]. The excitation component includes the lasers that emit light[188,189], whereas the collection component contains photodiodes and photomultiplier tubes (PMTs)[188]. Specific cell characteristics can be deduced through the cells' light-scattering capabilities and their fluorescence emission – if they are fluorescently tagged[190]. As the cells pass the laser, they scatter light that is collected parallel to the laser beam axis (forward scatter (FSC)) – and at a 90° angle (perpendicular) to the laser beam axis (side scatter (SSC))[189–191]. Emission of fluorescence is also collected perpendicular to the laser beam[190,191].

Cell size, granularity, shape, and internal characteristics affect the light scattering of cells[189], with FSC demonstrating proportionality to cell size and SSC demonstrating proportionality to a cell's internal complexity and granularity[189,191]. FSC is collected by FSC photodiodes[190], whereas SSC and fluorescence are collected and directed to PMTs by dichroic mirrors and filters[188,190]. These mirrors and filters ensure that different wavelengths of collected light are directed to the correct optical detectors[189].

Electronics

PMTs and photodiodes generate electrical signals that are relative to the magnitude of scattered laser light and fluorescence that they detect[189,190]. The electronic system of the flow cytometer is responsible for conversion of these signals into digital signals capable of being deciphered by a computer[188]. This is possible through amplification of the electric signal by an amplifier, creating an analog signal[189]. Analog to digital converters subsequently convert the signal into a digital one[189]. The computer will then process these digital signals into digital data, which can be represented/displayed via histograms or dot plots[189]. To differentiate cell population subsets, gating techniques are used[189].

3.2 Research thus far in CSF using flow cytometry

The efficacy of flow cytometry has been demonstrated in research concerning the immune system, making it a common analytical technique in clinical laboratories[188]. Work has expanded from analysis of blood specimens to other biofluids, including CSF. Van Acker *et al.* (2001) compared flow cytometric CSF analysis with the 'gold standard' microbiological and biochemical analyses[194]. They concluded that there was a reliable correlation between flow cytometric and gold-standard analyses in terms of CSF leukocyte and erythrocyte counts, although not for bacterial counts[194]. Twenty years later, another group, Dossou *et al.* (2022), compared the performance of more advanced flow cytometers with the gold standard in analysing biological fluids, including CSF[195]. Both CSF cell counts and bacterial counts showed an adequate correlation with gold-standard results[195]. These results point to the reliability and relevance of flow cytometry in clinical research. Upstream use of flow cytometry to microbiological analyses has been suggested to accelerate and enhance infection diagnosis[195].

In addition to these studies, a significant amount of work has assessed the capabilities of flow cytometry in detecting lymphoma and haematological malignancies, given the potential involvement of the CNS in these conditions. In 1998, Finn *et al.* examined the use of flow cytometry in detecting malignant lymphoma in CSF compared to conventional cytomorphological assessment[196]. Flow cytometry demonstrated sensitivity and effectiveness in detecting lymphoid clones within CSF samples and was suggested as an adjunctive analytical technique. Using CSF samples from patients with lymphoma or leukaemia with evidence of neurologic involvement, Roma *et al.* (2002) determined that flow cytometry could detect abnormal cell populations that weren't detected by conventional morphology alone[197]. Alvarez *et al.* (2012) depicted similar results in CSF from patients with diffuse large B-cell lymphoma[198]. Further, Nückel *et al.* (2006) found a 20% increase in detection rate of haematological malignancies involving CSF, when combining flow cytometry with conventional cytology[199]. Thus, this group also suggested flow cytometry as an additional diagnostic technique to cytology in such patients.

In conjunction with these studies, the use of flow cytometry for immunophenotyping purposes has gained more interest. Han *et al.* (2014) analysed paediatric and adult CSF samples from patients with a spectrum of neuroimmunological diseases[200]. By performing

flow cytometric immunophenotyping of these CSF samples, 14 different subsets of immune cells were isolated. Distinctions between intrathecal (CNS) versus systemic immunity were further described. CSF immunophenotyping depicts processes only relating to intrathecal immunity. This study thus proved that flow cytometric CSF analysis can be used to guide and monitor immunomodulatory treatment in patients with a neuroimmunological disease by monitoring biomarkers in the intrathecal environment[200].

CNS infections have not been exclusively analysed, and very rarely has this been done on ventricular CSF and in children. Table 3.1 below outlines data obtained from a selection of flow cytometry immunological studies, some of which are mentioned above.

Table 3.1: Summary of data from flow cytometry studies in CSF

Study	Method	Results	Study Conclusions
Van Acker *et al.* 2001[194]	• Correlate FCM cell counts with Fuchs-Rosenthal counting chamber, microbiology & biochemical data • 174 lumbar & 82 ventricular fresh CSF samples submitted to their laboratory (from Paediatrics, Haematology/Oncology, Emergency/ ICU, Neurology & Neurosurgery)	1. Good agreement between FCM & microbiology (counting chamber) for erythrocyte (r = 0.919) & leukocyte (r = 0.886) counts 2. Bacterial count less reliable (various sources of interference e.g. blood or cell debris in CSF)	⇒ Flow cytometer Sysmex UF-100 offers quick & reliable erythrocyte & leukocyte counts ⇒ FCM analysis is a useful additional tool for CSF examination (particularly in emergency setting)
Dossou *et al.* 2022[195]	• Compare FCM analysis to 'gold standard' microbiological cell counting, Gram stain & culture • 526 biological fluid samples submitted to their laboratory (of those, 125 = fresh ventricular CSF samples, mean age 58.91 years)	1. Sysmex UF4000 performed equivalently in CSF to standard methods for RBC (ρ = 0.9616) & leukocyte (r^2 = 0.91; P-value < 0.0001) counts 2. Cut-off point with max. sensitivity & negative predictability for bacteria detection in CSF is 17.2 bacteria/μL	⇒ Detection of bacteria in biological fluids with flow cytometer UF4000 prior to cytological/microbiological analysis could accelerate & improve diagnosis of infection

Finn *et al.* 1998[196]	• Comparison of FCM to conventional morphologic evaluation – testing detection of clonal lymphoid populations • 36 fresh CSF samples from malignant lymphoma patients	1. FCM analysis was successful in 27 CSF samples – lymphoma detected in 10 samples 2. FCM had sensitivity of 86% & specificity of 83%, positive predictive value of 67%	⇒ FCM is feasible detection method for malignant lymphoma in CSF ⇒ FCM could be used as an adjunct to conventional morphologic evaluation – rather than as a substitute
Roma *et al.* 2002[197]	• Immunophenotyping by FCM compared with morphologic examination • 53 fresh CSF samples from patients, ranging 6-76 years, with malignant lymphoma or leukaemia involving the CNS	1. Lymphoma/leukaemia detected in 21 samples: 12 by both techniques and 9 by FCM immunophenotyping alone	⇒ Cytologic examination of cell morphology in conjunction with FCM = 75% ↑ in detection rate in CSF vs. if utilise cytology alone ⇒ FCM is a useful adjunct to cytologic examination
Alvarez *et al.* 2006[198]	• FCM analysis compared with conventional cytology • 114 fresh lumbar CSF samples (prepared with Transfix®) from DLBCL patients at diagnosis or relapse, overall range 18-82 years	1. 14 samples were deemed positive for DLBCL through FCM analysis 2. 1 sample was deemed positive for DLBCL through cytology analysis	⇒ FCM yields significantly more positive results than conventional cytology ⇒ FCM therefore more sensitive in detecting DLBCL, but failed to be predictive of relapse

Nückel *et al.* 2012[199]	• Assessment of using conventional cytology vs. FCM for detecting CSF involvement in haematological malignancies • Fresh CSF samples from 45 patients with haematological malignancies	1. CSF involvement detected in 18 patients: 12 by both FCM & cytology; 3 by each technique on its own 2. Increase in detection by 20% to 600%	⇒ When coupled with conventional cytology, FCM improves detection of CSF involvement in patients with haematological malignancies
Han *et al.* 2014[200]	• FCM immunophenotyping of CSF & blood leukocytes – can reveal differences in inflammatory response & disease pathogenesis? • 221 fresh CSF samples including pediatric & adult patients presenting to NIH with neuroimmunological disease → MS, OIND, NIND subgroups	1. Significant difference in proportion & activation of blood vs. CSF immune cells 2. Observed prominent overlap of blood & CSF markers for different diagnostic subgroups 3. Poor yet statistically significant correlation of haemocytometer CSF counts between NIH laboratory & Han *et al.* laboratory (r = 0.4636; P-value < 0.001)	⇒ CSF immune cells represent a mixture of cells, some of which have been activated intrathecally and exit the CNS once they are no longer needed ⇒ Identified disease-specific immunophenotypes have potential to guide disease diagnosis, monitoring & provision of targeted immunomodulatory treatment

Abbreviations: CSF: cerebrospinal fluid; *DLBCL:* diffuse large B-cell lymphoma*; FCM*: flow cytometry; *MS:* multiple sclerosis; *NIND:* non-inflammatory neurologic disease; *NIH:* national institute of health; *OIND:* other inflammatory neurologic disease; r: Pearson correlation coefficient; r^2: coefficient of determination; ρ: Spearman correlation coefficient; P-value: probability value

3.3 Importance of flow cytometric work in CNS infections

As described above, flow cytometry has proven to be a sensitive tool to detect immune cells within CSF. Inflammation and infection in the CNS involves recruitment of peripheral immune cells, which can be detected in CSF samples from patients with infections. However, there is sometimes a paucity of cells in CSF samples, compounded by the rapid death of immune cells after CSF sampling[138]. In this regard, flow cytometry has advantageous characteristics including rapidity and the capability to evaluate multiple cell surface markers simultaneously[196,199]. Such evaluation of cell surface markers allows for effective immunophenotyping of different cell subsets in CSF samples. As demonstrated by Han *et al.* (2014), gating out of different cell subsets – and thus depicting an immunophenotype – is possible through flow cytometric CSF analysis[200]. This group highlighted the importance of improving the knowledge of the CNS immune response, considering the poor correlation between systemic and intrathecal biomarkers[200].

Better understanding the CNS immune response could have major implications for CNS disease diagnosis, monitoring and treatment, given the significance of early intervention and treatment in improving prognosis of CNS infections. Pragmatically though, the work is challenging, in part because it depends on patient presentation, and is thus subject to unpredictable timing and the nature of CSF samples.

This study had a novel opportunity and approach to this work with the new cryopreservation method devised and characterised in previous work from the group[201]. The demonstration of this method's efficacy when working with CSF has enhanced this study and immune cell and inflammatory biomarker results thereof. Neutrophils are more sensitive to cryopreservation, however, they are a minor cell population in paediatric TBM, and are detectable using the cryopreservation technique.

Additional research of value for this study from this unit is the documented variation in lumbar CSF versus ventricular CSF through biomarker[138,139] and transcriptomic work[29], at least in TBM. In particular, ventricular CSF appears to demonstrate a stronger signal of the cerebral response compared to lumbar CSF. This groundwork has guided and validated the particular

use of ventricular CSF for the purposes of this study. Additionally, the study benefited from being able to analyse more than one sample over time for most patients (71%). A single CSF sample or time point is insufficient to monitor the course of disease, and to investigate more deeply into why some patients may respond poorly to treatment. To our knowledge there are no data on the ventricular CSF immunophenotypes of specific CNS infections – such as those included in this study. The novelty of this study included looking at brain-derived cells, and a very large range of peripheral immune cells, and therefore this project aimed to generate pilot data on CNS infection immunophenotypes. This work is facilitated by the ability to conduct research on cryopreserved CSF, using a method established within our group. This adds to the currently available data by expanding the type and frequency of samples from the site of disease that can be analysed.

Chapter 4 – Aims & objectives

The primary aim of this research project was to describe the immune cell profile of ventricular CSF, and to examine biomarkers of inflammation in children with common CNS infections at our institution.

Objectives:

1. To describe subsets of peripheral and brain-derived immune cell populations in ventricular CSF using flow cytometry.
2. To describe downstream cytokines and chemokines (inflammatory mediators) in ventricular CSF using a Luminex® assay.

The secondary aims of this project were:

1. To describe the change in immune cell and inflammatory mediator concentrations over time in a sub-group of patients.
2. To explore the association between immune cells and inflammatory mediators.

Chapter 5 – Methods

5.1 Patient recruitment

Patients who were admitted to the neurosurgical ward at Red Cross War Memorial Children's Hospital (RCWMCH) for suspected meningitis, ventriculitis or shunt infection and who met the inclusion criteria for this study were identified by the student and supervisor. This was done with the input of collaborators from the clinical team. Informed consent was obtained from the patient's parents/guardians upon admission to RCWMCH. This was conducted in their language of choice – English, Afrikaans or Xhosa – with consent forms being made available in all three languages. Any concerns or questions from the parents either during the consent discussion or throughout the duration of the study were addressed by the principal investigator/supervisor.

Inclusion criteria: *TBM* inclusion criteria was based on an international uniform case definition for definite (CSF culture or GeneXpert confirmed) and probable TBM, which combined admission signs and symptoms, including symptoms potentially relating to pulmonary TB, findings on CSF cytology and chemistry, and imaging findings[36]. Patients with *other CNS infections* were included in this project if they had a reported ventricular CSF cell count of greater than 5 lymphocytes and/or polymorphonuclear leukocytes and were being treated at RCWMCH based on clinical suspicion of an infectious cause including meningitis, shunt infection or ventriculitis.

Exclusion criteria: Patients who were admitted to RCWMCH for a focal CNS infection (e.g. brain abscess), or who have an abdominal pseudocyst associated with their shunt, were not included in this study.

5.2 Study cohort & Sample collection

Ventricular CSF was collected during **clinically indicated neurosurgical procedures**. Such neurosurgical procedures typically included the insertion of an external ventricular drain (EVD), performance of a column test to assess the communicating nature of hydrocephalus–specifically in patients with TBM[20] – an EVD tap and/or the insertion of a ventriculoperitoneal shunt. These procedures were performed for clinical purposes only, and study samples were

collected from remnant CSF. Samples were prospectively collected at RCWMCH between July 2022 and November 2023. Given the absence of a flow cytometer on site at the hospital, it was necessary to cryopreserve all samples for batched analysis. Patients were treated as per standard of care as described in the literature review.

5.3 Sample processing

Collected CSF samples were subjected to a cryopreservation protocol developed in this research unit[201]. Immediately after collection, the CSF was centrifuged at 300 x g for 5 minutes with the break off. The supernatant was aspirated, and the remaining cell pellet cryopreserved. The cell pellet was resuspended in 500μl of cold Roswell Park Memorial Institute (RPMI) medium (Cytiva, HyClone™, Utah), followed by dropwise administration of 500μl of cryo-solution – consisting of 7% dimethyl sulfoxide (DMSO) (Tocris Bioscience™, United Kingdom) and 93% heat-inactivated foetal bovine serum (FBS) (Thermo Fisher Scientific™, United States of America). The cell suspension was subsequently transferred to a cryovial and stored in a Mr Frosty™ container in a -80℃ freezer for 2 weeks. Three 100μL aliquots of the CSF supernatant were stored in a -80℃ freezer, and were batch analysed for biomarkers of neuroinflammation using Luminex® technology (R&D Systems™, United States of America). An overview of sample processing is shown in figure 5.1, and Luminex® analysis is described in section 5.4.3.

Within 2 weeks of cryopreservation (our previous work demonstrated a decline in cell number after longer duration of cryopreservation)[201], the cells were partially thawed in a 37℃ water bath through gentle agitation of the cryovial until an ice block remained. Thereafter, 1mL of warmed RPMI was added to the partially thawed cells, and the cell suspension was transferred to a 15mL Falcon tube containing 1ml of warmed RPMI. The cryovial was washed with a further 1mL of warmed RPMI, which was also added to the Falcon tube. The sample was centrifuged at 4℃ (300 x g for 5 minutes) with the break turned off, and supernatant aspirated off. The remaining cell pellet was then resuspended in an antibody cocktail (50μL) and incubated for 30 minutes, covered in foil, in a 5℃ fridge. The breakdown of this antibody cocktail is provided in Appendix A. Following incubation, a wash step took place involving administration of 300μL of flow staining buffer (R&D Systems™) to the cell suspension and

centrifuging at 300 x g for 5 minutes. Supernatant was then aspirated off, the cells were fixed with the addition of 500μL of transcription factor (TF) fix/perm buffer, covered in foil and incubated for 20 minutes in a 5℃ fridge. The cells were washed with 300 µl of TF perm/wash buffer and centrifuged at 510 x g for 5 minutes. The supernatant was aspirated off and the cell pellet was resuspended in 50μL of TF perm/wash buffer. The cells were then stained for intracellular markers, GFAP and FoxP3. A volume of 1.25μl of each antibody was added to the suspension and incubated for 30 minutes, covered in foil, in a 4℃ fridge. After incubation, a wash step was performed by adding 300μL of TF perm/wash buffer to the sample, which was then centrifuged (510 x g for 5 minutes) once more. After this, any remaining TF perm/wash buffer was aspirated off. The cell pellet was then resuspended in 50μL of flow staining buffer, and the cell suspension transferred to a microtiter tube. This tube was then placed within a 5mL flow tube, at which point the sample was ready for flow cytometric analysis. Cells were acquired and analysed on a BD FACSymphony™ A5 Cell Analyzer.

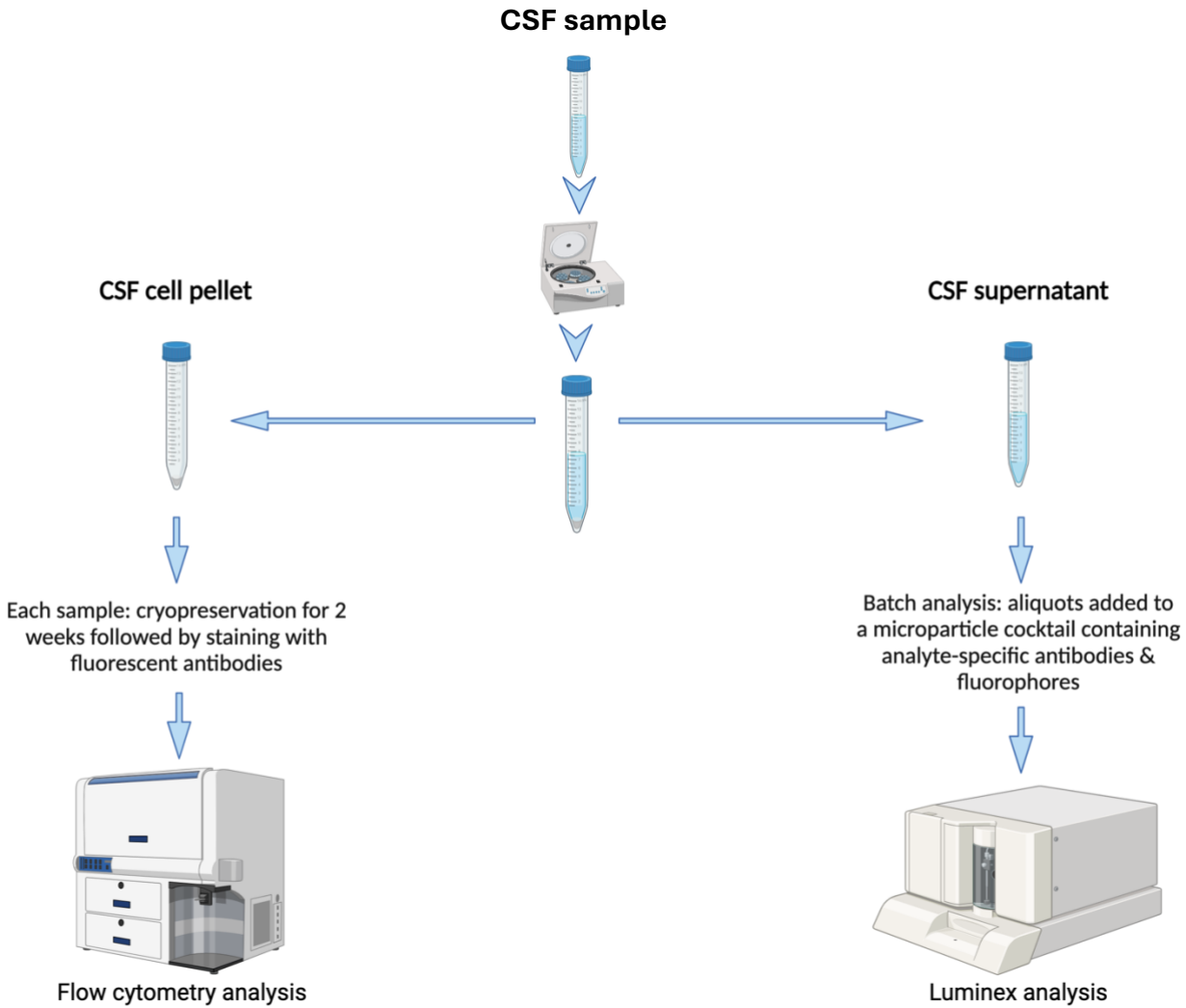

Figure 5.1. **Overview of sample processing for a ventricular CSF sample.** Once centrifuged, the CSF cell pellet was cryopreserved for 2 weeks at -80°C, followed by staining with fluorescent antibodies and analysis on the flow cytometer. The supernatant of the sample was stored in aliquots at -80°C, and batch analysed using Luminex® technology. Created with BioRender.com

5.4 Sample analysis

5.4.1 Flow cytometry

As alluded to in section 5.3 above, cells from CSF samples were stained with a 21-colour antibody panel. Table 5.1 describes these markers, their conjugated fluorochromes and their respective detection by the flow cytometer's lasers. Supplementary table A.2 provides a detailed account of the antibodies used. Samples were acquired on a BD FACSymphony™ A5 Cell Analyzer, and populations of interest were identified and gated using fluorescence-minus-one controls. The BD FACSymphony™ A5 Cell Analyzer used in this study had five lasers, namely Red, Ultra-Violet (UV), Violet, Blue and Yellow-Green, with a 30-colour configuration. This study could therefore use a 21-colour antibody panel. Major cell types relevant to the infections in this study were identified through distinct cluster of differentiation (CD) lineage markers (Table 2.1 & 2.2). Their respective immunophenotypes are defined in table 5.2.

Prior to commencement of patient recruitment and sample collection, the application setup on the flow cytometer specific to this study was optimized and standardized using ventricular CSF. This entailed determining optimal titres for each antibody of the 21-marker antibody panel (given in supplementary table A.1), to ensure that fluorescent intensity values acquired for all subsequent samples in this study were consistent. Moreover, Sphero™ Rainbow Calibration Particles (catalogue no. 559123) were run under optimized instrument settings to establish a set of target values. These application settings were then appropriately named and saved on the cytometer's computer for future use with the study samples.

Table 5.1: Overview of specificity & detection of fluorochrome-conjugated antibodies

Specificity	Marker	Fluorochrome	Filter	Laser
Early differentiation	CD45	BUV395	379/28	UV 355nm
Live/dead	Viability	UViD	450/50	UV 355nm
T-helper cells	CD4	BUV563	580/20	UV 355nm
Cytotoxic T cells	CD8	BUV615	610/20	UV 355nm
NK cells	CD56	BUV661	670/20	UV 355nm
Monocytes & neutrophils	CD11b	BUV737	735/30	UV 355nm
γδ T cells	γδTCR	BV421	450/50	V 405nm
B cells	CD19	BV480	525/50	V 405nm
Monocytes	CD14	BV605	610/20	V 405nm
Naïve T cells	CD45RA	BV650	670/30	V 405nm
MAIT cells	Vα7.2	BV711	710/40	V 405nm
Activation	HLA-DR	BV786	780/60	V 405nm
Microglia	TMEM119	AF488	530/30	B 488nm
Treg cells	CD25	BB700	710/50	B 488nm
Astrocyte activation	GFAP	PE	586/15	YG 561nm
Central memory T cells	CD27	PE-CF594	610/20	YG 561nm
MAIT cells	CD161	PE-Cy5	710/50	YG 561nm
Monocytes, neutrophils & NK cells	CD16	PE-Cy7	780/60	YG 561nm
Astrocytes	ACSA	APC	670/30	R 638nm
Treg cells	FoxP3	R718	730/45	R 638nm
T cells	CD3	APC-H7	780/60	R 638nm

Abbreviations: ACSA: astrocyte cell surface antigen*; AF*: Alexa Fluor®; *APC*: allophycocyanin; *APC-H7*: allophycocyanin hillite 7; *BB*: brilliant blue; *BUV*: brilliant ultraviolet; *BV*: brilliant violet; *CD:* cluster of differentiation; *CD45RA*: CD45 receptor antagonist; *FoxP3:* forkhead box P3 or scurfin; *GFAP*: glial fibrillary acidic protein; *HLA-DR*: human leukocyte antigen-DR isotype; *MAIT cell*: mucosal-associated invariant T cell; *NK* cell: natural killer cell; *PE*: phycoerythrin; *PE-CF:* phycoerythrin & cyanine-based fluorescent dye; *PE-Cy5*: phycoerythrin & cyanine dye Cy5 complex; *PE-Cy7*: phycoerythrin & cyanine dye Cy7 complex; *TCR*: T-cell receptor; *TMEM119*: transmembrane protein 119; *Treg*: T regulatory cells; *UViD*: ultraviolet-induced detection. An extra 10% of volume for each antibody was added when making the antibody cocktail, to account for any pipetting errors.

Because CSF samples were cryopreserved for 2 weeks and then analysed, flow cytometric analysis was ongoing throughout this study. At the beginning of each session at the flow cytometer, the cytometer's performance was assessed through running Cytometer Setup (CS) and Tracking (T) beads (lot no. 31881/28853) – which are performed daily. The optimized application settings were then applied to the experiment, after which the Rainbow Calibration Particles were acquired. Mean Fluorescence Intensity (MFI) ranges of 10% above and below the Rainbow target values from the previous flow cytometry session were calculated, and voltages adjusted if necessary to ensure that the bead peaks were within this range. A total of 10 000 events of Rainbow beads were then recorded. This was done to account for any day-to-day variations within the cytometer – including changes to laser alignment and instrument maintenance. After Rainbow bead peaks were recorded, single stained BD™ Compensation beads (catalogue no. BD/552843) were run and recorded for 10 000 events each. A compensation matrix could then be calculated and was applied to the experiment.

In a sub-group of samples, prior to acquiring the sample, 100μL of Beckman Coulter Flow-Count Fluorospheres (lot no. 7548273) were added to the sample to enable determination of absolute cell counts. The reverse pipetting technique was used for this, to ensure maximum accuracy. The sample was then gently vortexed, before running on the flow cytometer. If necessary, slight adjustments were made to forward scatter and/or side scatter, before recording the events. The entire cell suspension of the sample was then acquired. Once all samples were acquired, flow cytometry standard (FCS) files for the experiment were exported to Datshare until needed for further analysis. The Flow-Count Fluorospheres were only run in a sub-group of patients due to unavailability of stock at the start of the project.

After samples were run, exported flow cytometry standard (FCS) files were analysed using FlowJo software (version 10.9.0), a program designed to enable the analysis of flow cytometric data. Cell populations were gated in FlowJo according to the gating strategy depicted in figure 5.2. Data on cells included *cell proportions*, and for the sub-group of samples which included Flow-Count Fluorospheres *absolute cell numbers* were also calculable.

Table 5.2: Defined surface phenotypes of relevant immune cell populations

Cell populations	**Surface phenotype**
Leukocytes	$CD45^+$
Granulocytes	$CD45^+$
• Neutrophils	$CD11b^+$ $CD16^+$
Lymphocytes	$CD45^+$
• T cells	$CD3^+$
⇒ $\gamma\delta$ T cells	$CD3^+$ $\gamma\delta TCR^+$
⇒ MAIT cells	$CD3^+$ $V\alpha7.2^+CD161^+$
⇒ Non-MAIT cells	
○ T-helper cells	$CD3^+$ $CD4^+$
○ Cytotoxic T cells	$CD3^+$ $CD8^+$
○ T regulatory cells (Tregs)	$CD25^+$ $FoxP3^+$
○ Non-Tregs	$CD25^+$ $FoxP3^-$
▪ Naïve	$CD45RA^+$ $CD27^+$
▪ Central memory	$CD45RA^-$ $CD27^+$
▪ Effector memory	$CD45RA^-$ $CD27^-$
▪ Exhausted	$CD45RA^{++}$ $CD27^-$
▪ Terminal	$CD45RA^+$ $CD27^-$
• B cells	$CD3^-$ $CD19^+$
⇒ Activated B cells	$CD19^+$ HLA-DR^+
NK cells	$CD16^+$ $CD56^+$
Monocytes	$CD45^+$
• Classical	$CD14^+$ $CD16^-$
• Non-classical	$CD14^+$ $CD16^+$
CNS-resident cells	
• Microglia	$CD45^-$ $TMEM119^+$
⇒ Activated microglia	$CD45^-$ HLA-DR^+
⇒ $CD45^+$ microglia	$CD45^+$ $TMEM119^+$ HLA-$DR^{+/-}$
• Astrocytes	$CD45^-$ $ACSA^+$
⇒ Reactive astrocytes	$ACSA^+$ $GFAP^+$

Abbreviations: ACSA: astrocyte cell surface antigen; *CD*: cluster of differentiation; *CD45RA*: CD45 receptor antagonist; *GFAP*: glial fibrillary acidic protein; *HLA-DR*: human leukocyte antigen-DR isotype; *MAIT cell*: mucosal-associated invariant T cell; *NK* cell: natural killer cell; *TMEM119*: transmembrane protein 119

5.4.2 Gating of immune cell populations in FlowJo

Figure 5.2 below depicts the gating strategy used on all sample files once exported to FlowJo. To begin with, the 'time' gate was used to select for uniform fluorescence (Fig. 5.2A), with forward-scatter area (FSC-A) and forward-scatter height (FSC-H) used to identify single cells (Fig. 5.2B). Viable cells were selected for using dye exclusion (Fig. 5.2C), from which leukocytes (granulocytes, monocytes & lymphocytes) were identified through $CD45^+$ expression vs. CD45- populations (Fig. 5.2D). Microglia were gated from the $CD45^-TMEM119^+$ population (Fig. 5.2F.1), with astrocytes ($CD45^-ACSA^+$) and reactive astrocytes ($ACSA^+GFAP^+$) (Fig. 5.2G) being identified from non-microglial cells (Fig. 5.2F.2). From the monocytic population in Fig. 5.2D, $CD45^+CD14^+$ and $CD45^+CD14^-$ populations were identified and gated (Fig. 5.2E). The $CD45^+CD14^+$ cell group gave rise to non-classical ($CD14^+$ $CD16^+$) and classical ($CD14^+$ $CD16^-$) monocytes (Fig. 5.2I), whereas the $CD45^+CD14^-$ group gave rise to $CD45^+TMEM119^+$ microglia (Fig. 5.2J). The granulocytic population in Fig. 5.2D enabled the sub-group of neutrophils ($CD16^+CD11b^+$) to be identified (Fig. 5.2H); we did not stain to identify the remaining granulocyte populations. From the lymphocytic population in Fig. 5.2D, the $CD3^+$ and $CD3^-$ populations were elucidated (Fig. 5.2K). $\gamma\delta^-$ T cells identified from the $CD3^+$ population (Fig. 5.2L) enabled further identification of non-MAIT ($CD3^+$ $V\alpha7.2^-$ $CD161^-$), MAIT ($CD3^+$ $V\alpha7.2^+$ $CD161^+$), $CD161^+$ $V\alpha7.2^-$ cells and $V\alpha7.2^+$ $CD161^-$ cells (Fig. 5.2M). From the non-MAIT population, helper T cells ($CD3^+CD4^+$) and cytotoxic T cells ($CD3^+CD8^+$) were ultimately identified and gated (Fig. 5.2N). Regulatory T cells (Tregs) ($CD25^+$ $FoxP3^+$) and non-Tregs ($CD25^+$ $FoxP3^-$) were yielded from both $CD4^+$ and $CD8^+$ populations (Fig. 5.2O & Fig. 5.2P, respectively). $CD4^+$ and $CD8^+$ non-Treg populations resulted in the following sub-groups of cells in Fig. 5.2U & Fig. 5.2T, respectively: exhausted T cells ($CD45RA^{++}$ $CD27^-$), effector memory T cells ($CD45RA^-$ $CD27^-$), central memory T cells ($CD45RA^-$ $CD27^+$), naïve T cells ($CD45RA^+$ $CD27^+$) and terminal T cells ($CD45RA^+$ $CD27^-$). From the CD3- population, sub-populations of B cells ($CD3^-$ $CD19^+$) and non-B cells ($CD3^-$ $CD19^-$) were elucidated (fig. 5.2R). From the B cells, activated B cells ($CD19^+$ $HLA\text{-}DR^+$) were identified (fig. 5.2Q), and from the non-B cells, NK cells ($CD16^+$ $CD56^+$) were identified (fig. 5.2S). For samples containing Beckman Coulter Flow-Count Fluorospheres (lot no. 7548273), figure 5.3 demonstrates the plot in which these beads were gated.

Figure 5.2. (below). **Gating strategy for elucidation of immune cell populations in FlowJo based on cell surface markers.**

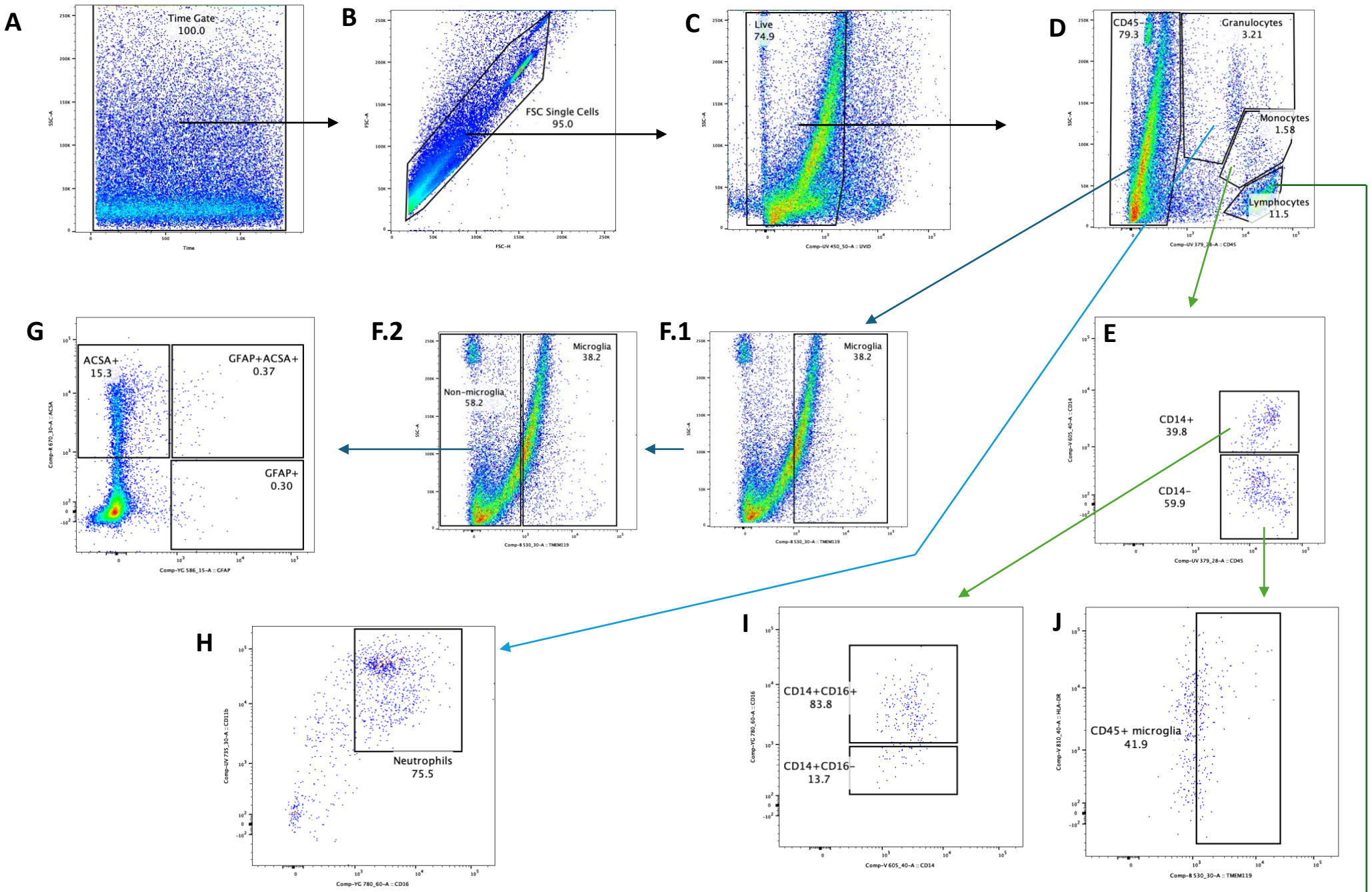
A
Time Gate
100.0
B
FSC Single Cells
95.0
C
Live
74.9
D
CD45−
79.3
Granulocytes
3.21
Monocytes
1.58
Lymphocytes
11.5
E
CD14+
39.8
CD14−
59.9
F.1
Microglia
38.2
F.2
Microglia
38.2
Non−microglia
58.2
G
ACSA+
15.3
GFAP+ACSA+
0.37
GFAP+
0.30
H
Neutrophils
75.5
I
CD14+CD16+
83.8
CD14+CD16−
13.7
J
CD45+ microglia
41.9

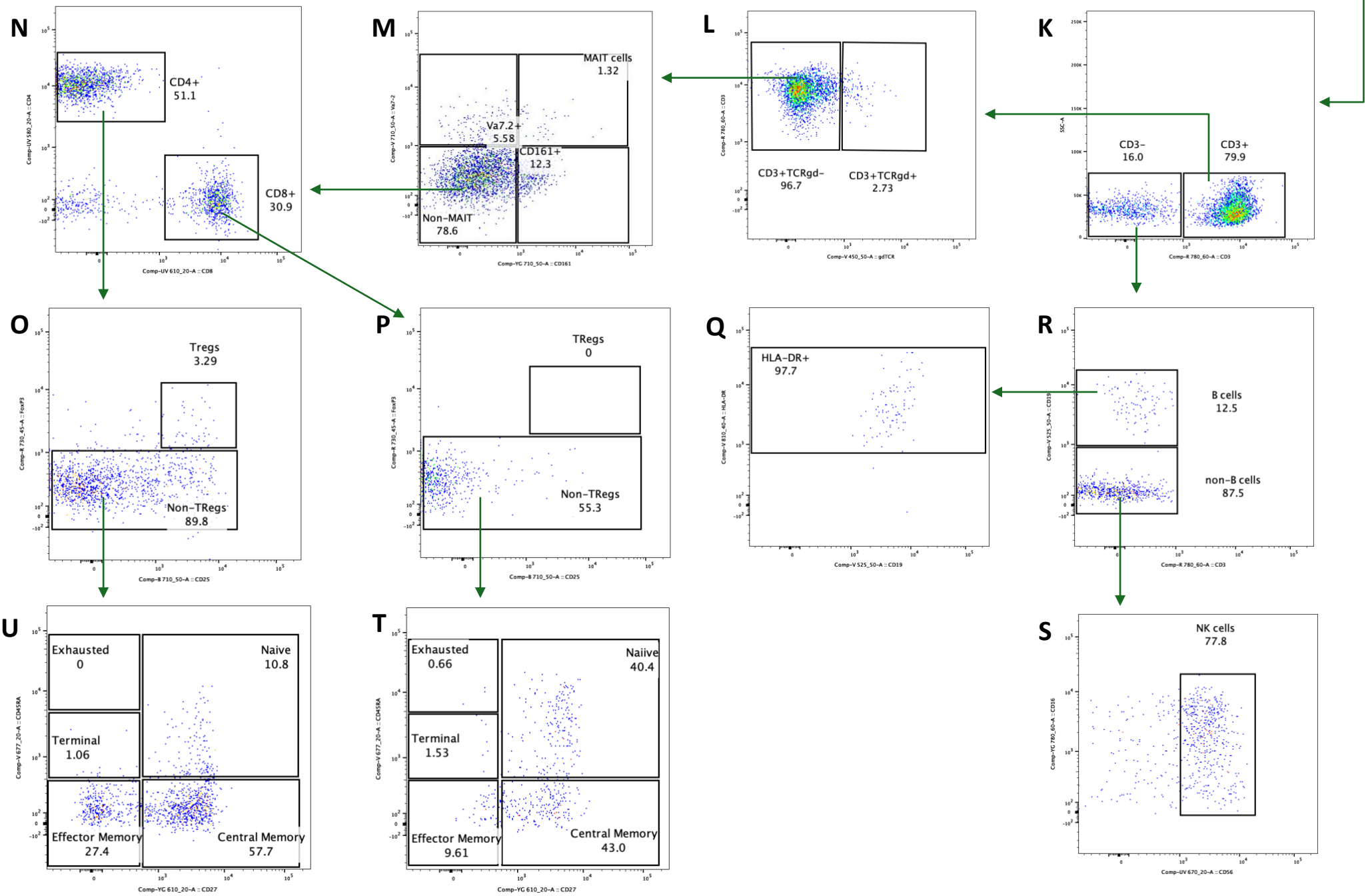
N
CD4+
51.1
CD8+
30.9
Comp-UV 580_20-A :: CD4
Comp-UV 610_20-A :: CD8
M
MAIT cells
1.32
Va7.2+
5.58
CD161+
12.3
Non-MAIT
78.6
Comp-V 710_50-A :: Va7-2
Comp-YG 710_50-A :: CD161
L
CD3+TCRgd-
96.7
CD3+TCRgd+
2.73
Comp-R 780_60-A :: CD3
Comp-V 450_50-A :: gdTCR
K
CD3-
16.0
CD3+
79.9
SSC-A
Comp-R 780_60-A :: CD3
O
Tregs
3.29
Non-TRegs
89.8
Comp-R 730_45-A :: FoxP3
Comp-B 710_50-A :: CD25
P
TRegs
0
Non-TRegs
55.3
Comp-R 730_45-A :: FoxP3
Comp-B 710_50-A :: CD25
Q
HLA-DR+
97.7
Comp-V 810_40-A :: HLA-DR
Comp-V 525_50-A :: CD19
R
B cells
12.5
non-B cells
87.5
Comp-V 525_50-A :: CD19
Comp-R 780_60-A :: CD3
U
Exhausted
0
Naive
10.8
Terminal
1.06
Effector Memory
27.4
Central Memory
57.7
Comp-V 677_20-A :: CD45RA
Comp-YG 610_20-A :: CD27
T
Exhausted
0.66
Naiive
40.4
Terminal
1.53
Effector Memory
9.61
Central Memory
43.0
Comp-V 677_20-A :: CD45RA
Comp-YG 610_20-A :: CD27
S
NK cells
77.8
Comp-YG 780_60-A :: CD16
Comp-UV 670_20-A :: CD56

Figure 5.3. **Scatter plot depicting gating of Flow-Count Fluorospheres in FlowJo.**

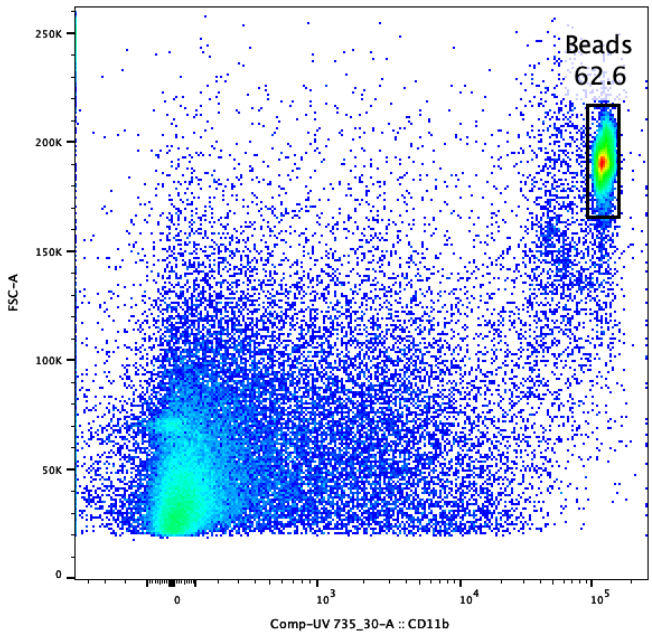

5.4.3 Luminex® assay

Functional analyses were performed on the supernatant (50μl) of the samples. We used Luminex® technology to multiplex inflammatory analytes including interleukin (IL)-1β, IL-6, IL-8, IL-10, interleukin 1 Receptor antagonist (IL-1Ra), interleukin-12p40 (IL-12p40), tumour necrosis factor-α (TNF-α), interferon-γ (IFN-γ), IFN-α, vascular endothelial growth factor (VEGF), monocyte chemoattractant protein 1 (MCP-1), macrophage inflammatory protein 1 & 2 (MIP-1 & MIP-2) and interferon-inducible protein 10 (IP-10).

The principle of this assay involves the addition of samples to a microparticle cocktail – with the fluorophore-embedded microparticles being pre-coated with analyte-specific antibodies. The antibodies subsequently bind to their respective antigens of the analytes of interest. With the further addition of analyte-specific biotinylated antibodies, an 'antigen-antibody sandwich' is created. Lastly, streptavidin-phycoerythrin conjugate (Streptavidin-PE) is added which binds to the biotinylated antibodies. The fluorescent microparticles are then read and detected on a flow-based Luminex® instrument containing two lasers, Red and Green. The first laser (Red) excites the fluorophore within each microparticle, and identifies the analyte being detected through identifying the microparticle region. The second laser (Green) quantifies the amount of analyte bound to the microparticle by exciting PE and determining the size of the subsequent signal detected.

To perform this analysis, an R&D systems™ (Bio-Techne® brand) human premixed multi-analyte kit was used (lot number L153814). On the day of analysis, supernatant samples were thawed and prepared prior to commencement of the assay run. A supernatant volume of 30μL of CSF with a 1 in 2 dilution was used as per manufacturer instructions. All necessary reagents were also prepared prior to commencement of the assay run. These included the Wash Buffer, Standards, diluted Microparticle Cocktail, diluted Biotin-Antibody Cocktail, and Streptavidin-PE. This sample and reagent preparation is fully outlined in the supplementary methods section.

The plates used were 96-well plates. Standards were run in duplicate. After 50μl of sample was added to each remaining well, 50μL of the diluted Microparticle Cocktail was then added

to each well, followed by a 2-hour incubation period at room temperature on a shaker at 800 rpm. An automatic wash step was then performed, involving 3 cycles of removing the liquid from each well, addition of 100μL of wash buffer and then removal of the liquid again. Subsequently, 50μL of the diluted Biotin-Antibody Cocktail was added to each well. The plate was then covered in foil and underwent a 1-hour incubation period at room temperature on a shaker at 800 rpm. The wash step was then repeated. Following this, 50μL of the diluted Streptavidin-PE was added to each well, followed by a 30-minute incubation period at room temperature on a shaker at 800 rpm. The wash step was then repeated for the final time. Finally, 100μL of wash buffer was then added to each well, with a 2-minute incubation of the plate at room temperature on a shaker at 800 rpm. The plate was then read using a Luminex® Bio-Plex 200 analyser. Concentrations below the lower limit of detection (LLOD) were assigned a value of 0.01.

5.5 Statistical analysis

Statistical analyses were performed using IBM® SPSS Statistics (version 28.0.1.1). Given that the aim of this project was to collect pilot data, we did not perform a formal power calculation. Tests of normality were performed on all datasets to determine the nature of the data's distribution. Statistical significance was set at $p < 0.05$.

To describe the profile of immune cells and inflammatory mediators

Descriptive statistics included measures of central tendency (median, interquartile range and minimum to maximum range), and frequencies. To ascertain which is the *most abundant cell type* the Independent-Samples Median test was employed to both cell proportion and concentration datasets to compare the major cell populations – namely lymphocytes, monocytes, neutrophils, microglia, and astrocytes. This was performed on admission samples. Given that most patients in this cohort had TBM, the Mann-Whitney test was used to compare CSF cell proportions, absolute counts, and inflammatory mediator concentrations to establish whether their profiles were being driven by one prominent CNS infection phenotype. This analysis was performed on admission samples.

To *describe the temporal profile* of cells and cytokines the first 8 days – taken as the first week – following a patient's admission to RCWMCH were split up into four 48-hour epochs (day 1-2, 3-4, 5-6 and 7-8). Descriptive statistics were calculated for these time epochs as most samples fell within this time frame, and for the few samples taken thereafter. To explore whether the changes observed over time were significantly different the Wilcoxon Signed Ranks Test was used to compare CSF cell proportions, absolute cell concentrations, and inflammatory mediators between the first and fourth 48-hour epochs – i.e. days 1-2 and days 7-8, respectively.

To explore the association between CSF cells and inflammatory mediators

A Spearman's correlation test was performed between 1) CSF cell proportions and CSF inflammatory markers, and between 2) absolute CSF cell concentrations and CSF inflammatory markers. Correlations were performed in admission and week 1 samples.

5.6 Ethics statement

This study received scientific approval from the Department of Surgery Research Committee (DRC REF 2023/015), ethics approval from the UCT Faculty of Health Sciences Human Research Ethics Committee (HREC REF 114/2023). Hospital approval was also received. As previously mentioned, informed consent was obtained from parents/legal guardians for all patients recruited for this study. For children over the age of 8 years who had a Glasgow Coma Scale (GCS) score of 15 (i.e. fully conscious), assent was requested

Chapter 6 – Results

6.1 Patient cohort

There were 30 patients, median age 2.6 (IQR: 1.3 – 3.9) years enrolled in this study. Two patients were treated for clinically suspected ventriculitis (6.7%), two patients treated for clinically suspected bacterial meningitis (6.7%), five patients treated for clinically suspected shunt infection (16.6%) and twenty one patients treated for TBM (70% of the total, of whom 81% had definite TBM).

A total of 61 ventricular CSF samples were collected and analysed; 30 (49%) were admission samples. Serial samples were obtained for 22 patients (71%). There were 31 serial samples – of which 68% were from week 1. The median time since admission for receiving a serial sample was 2.5 days. As part of clinical routine patient CSF samples are sent to the National Health Laboratory Service for cell counts, which include concentrations of granulocytes and lymphocytes only. Patients were prescribed appropriate antimicrobial treatment from admission at the discretion of the neurosurgical team. Demographic and clinical characteristics of the patient cohort are outlined in table 6.1. The median duration of hospital stay was 49 days, and the mortality rate was 23% (n=7/30). The majority of these patients had TBM and were in-hospital deaths (57%), with a median of 19 days post admission.

Table 6.1: Patient cohort demographic & clinical characteristics

Variable	Value
Patients	30
Age (years)	2.6 (1.3-3.9)[a]
Sex (female)	15 (50)
Immunisations UTD	17 (61)[b]
Clinical characteristics (on admission)	
○ HIV status (negative) ○ GCS ○ Focal neurology	30 (100) 12 (8-13)[a,c] 17 (57)[d]
○ *Diagnosis*	
▪ TBM ▪ Other bacterial CNS infections	21 (70) 9 (30)
○ *Admission CSF characteristics*	
▪ Lymphocytes (cells/μL) ▪ PMNs (cells/μL) ▪ Glucose (mmol/L) ▪ Protein (g/L)	25 (13-46) 5 (0-11) 3 (1.8-3.6)[e] 0.68 (0.36-2.8)[f]
Mortality (deaths)	7 (23)

Values represented as number (percent) or as median (IQR – interquartile range).
GCS: Glasgow Coma Scale; *PMNs*: polymorphonucleocytes; *UTD*: up to date
[a]Minimum – maximum ranges: age (0.06-11.75), GCS (3-15)
[b]Data missing in 2 patients
[c]GCS not noted in 2 patients
[d]Focal neurology included pupil reactivity, paresis, cranial nerve palsies and aphasia
[e]Normal range is 60-80% of plasma glucose in samples taken 15 minutes apart
[f]Normal range is 0.15-0.40 g/L

6.2 Flow Cytometry

6.2.1 Cell proportions

Admission

Measures of central tendency for proportions of main cell populations of interest – namely lymphocytes ($CD45^+$), monocytes ($CD45^+$), granulocytes ($CD45^+$), $CD45^-$ $TMEM119^+$ microglia and astrocytes ($CD45^-TMEM119^-$) – in admission samples are reported in Table 6.2. Overall, 76.2% of cells were viable and $CD45^-$ cells accounted for the largest proportion of cells (81.2%). Of these, microglia ($CD45^-$ $TMEM119^+$) were the most predominant (median 48.4%). Astrocytes ($CD45\text{-}ACSA^+$) accounted for a small proportion of the $CD45^-$ $TMEM119^-$ cells (5.7%). $CD45^-$ microglia were significantly higher than monocytes ($p < 0.001$), lymphocytes ($p = 0.01$) and granulocytes ($p < 0.001$). Amongst the $CD45^+$ cells lymphocytes accounted for a significantly higher proportion than monocytes ($p = 0.002$) and granulocytes ($p < 0.001$). Graphical representation of these cell populations and their relevant sub-groups is depicted in figure 6.1. Descriptive statistics are shown in tables 6.2-6.4. Figures including outliers can be found in Appendix B.

Table 6.2: Descriptive statistics for cell proportions upon admission: **Major cell populations**

Cell type	**$CD45^+$ Cells (12.19%)**				**$CD45^-$ Cells (81.2%)**		
	Granulocytes ($CD45^+$) **Neutrophils** ($CD11b^+CD16^+$)		**Lymphocytes** ($CD45^+$)	**Monocytes** ($CD45^+CD14^+$)	**Microglia** ($CD45^-$ $TMEM119^+$)	**Astrocytes** ($CD45^-ACSA^+$) **Reactive astrocytes** ($ACSA^+GFAP^+$)	
Admission	*n = 30*	*n = 30*	*n = 30*	*n = 30*	*n = 30*	*n = 30*	*n = 30*
Median	1.19	33.85	7.33	1.63	48.40	5.70	0.37
Min	0	4	0	0	2	0	0
Max	58	99	47	22	99	29	5
p25	0.41	20.40	1.52	0.56	7.74	2.15	0.10
p75	3.16	76.75	15.75	5.27	62.93	9.56	0.91

Values represent proportion (%), n represents number of samples.
CD: cluster of differentiation marker; *max:* maximum; *min:* minimum; *p:* percentile

Table 6.3: Descriptive statistics for cell proportions upon admission: **Lymphocytic sub-groups**

Parent cell group	**Lymphocytes** ($CD45^+$)			
Sub-group	**$CD3^+$ cells**		**$CD3^-$ cells**	
Admission	*n = 30*		*n = 30*	
Median	81.05		15.35	
Min	0		0	
Max	95		29	
IQR	73.93-87.83		8.6-21.78	
Sub-group	**$\gamma\delta^+$ cells** ($CD3^+$ $\gamma\delta$ TCR^+)	**$\gamma\delta^-$ cells** ($CD3^+$ $\gamma\delta$ TCR^-)	**B cells** ($CD3^-CD19^+$)	**Non-B cells** ($CD3^-CD19^-$)
Admission	*n = 30*	*n = 30*	*n = 30*	*n = 30*
Median	2.58	95	33	65.65
Min	0	0	0	0
Max	8	100	75	100
IQR	1.3-4.38	91.75-97.25	16.27-53.75	65.33-83.60

Sub-group	**MAIT cells** ($CD3^+V\alpha7.2^+$ $CD161^+$)	**Non-MAIT cells** ($CD3^+V\alpha7.2^-$ $CD161^-$)	**Vα7.2+ cells** ($CD3^+V\alpha7.2^+$)	**CD161+ cells** ($CD3^+CD161^+$)	**Activated B cells** ($CD19^+HLA\text{-}DR^+$)	**NK cells** ($CD16^+CD56^+$)
Admission	*n = 30*	*n = 30*	*n = 30*	*n = 30*	*n = 30*	*n = 30*
Median	0.74	68.50	11	3.50	98.95	73.30
Min	0	0	0	0	0	0
Max	14	99	79	29	100	100
IQR	0.09-2.18	47.25-79.50	4.50-21.25	1-13.25	95.15-100	65.33-83.60

Parent cell group	Non-MAIT cells			
Sub-group	**CD4⁺ cells** ($CD3^+CD4^+$)		**CD8⁺ cells** ($CD3^+CD8^+$)	
Admission	*n = 30*		*n = 30*	
Median	51.90		32.55	
Min	0		0	
Max	84		67	
IQR	44.18-57.18		24.35-37.20	
Sub-group	**Treg cells** ($CD4^+CD25^+FoxP3^+$)	**Non-Treg cells** ($CD4^+CD25^+FoxP3^-$)	**Treg cells** ($CD8^+CD25^+FoxP3^+$)	**Non-Treg cells** ($CD8^+CD25^+FoxP3^-$)
Admission	*n = 30*	*n = 30*	*n = 30*	*n = 30*
Median	5.72	90.50	0	86
Min	0	0	0	0
Max	27	100	9	100
IQR	2.37-11.10	82.75-94.25	0-0.21	60.75-97

Sub-group	Central memory T cells ($CD45RA^-CD27^+$)	Effector memory T cells ($CD45RA^-CD27^-$)	Naïve T cells ($CD45RA^+CD27^+$)	Exhausted T cells ($CD45RA^{++}CD27^-$)	Terminal T cells ($CD45RA^+CD27^-$)	Central memory T cells ($CD45RA^-CD27^+$)	Effector memory T cells ($CD45RA^-CD27^-$)	Naïve T cells ($CD45RA^+CD27^+$)	Exhausted T cells ($CD45RA^{++}CD27^-$)	Terminal T cells ($CD45RA^+CD27^-$)
Admission	*n = 30*	*n = 30*	*n = 30*	*n = 30*	*n = 30*	*n = 30*	*n = 30*	*n = 30*	*n = 30*	*n = 30*
Median	49	14.5	19.5	0	1.5	19.5	1	55.5	3	2.5
Min	0	0	0	0	0	0	0	0	0	0
Max	100	75	70	17	50	74	25	100	32	75
IQR	23.75-57.25	6-26.25	8-36.75	0-0.25	1-5.25	12-26.5	0-8.25	34.5-66.5	0-9.75	0-8.25

Values represent proportion (%), n represents number of samples.
CD: cluster of differentiation marker; *IQR:* inter-quartile range; *max:* maximum; *min:* minimum; *Treg*: regulatory T cells

Table 6.4: Descriptive statistics for cell proportions upon admission: **Monocytic sub-groups**

Parent cell group	**Monocytes** ($CD45^+$)		
Sub-group	**$CD14^+$ cells**		**$CD14^-$ cells**
Admission	*n = 30*		*n = 30*
Median	22.85		65.90
Min	1		20
Max	76		93
IQR	12.14-40.80		46.68-79.30
Sub-group	**Non-classical monocytes** ($CD14^+CD16^+$)	**Classical monocytes** ($CD14^+CD16^-$)	**$CD45^+$ microglia** ($TMEM119^+$)
Admission	*n = 30*	*n = 30*	*n = 30*
Median	68.05	22.05	41.80
Min	11	2	1
Max	99	84	90
IQR	37.58-85.13	12.23-61.95	16.42-73.90

Values represent proportion (%), n represents number of samples.
CD: cluster of differentiation marker; *IQR:* inter-quartile range; *max:* maximum; *min:* minimum

Figure 6.1 (below). **Box plot of admission cell proportions for major peripheral and brain-derived immune cell populations**. Cell proportions of **A:** all major $CD45^+$ (granulocytes, lymphocytes, and monocytes) & $CD45^-$ cell populations, **B:** peripheral leukocyte populations only, **C:** lymphocytic ($CD3^+$ & $CD3^-$) and monocytic ($CD14^+$ & $CD14^-$) sub-groups, **D:** brain-derived $CD45^-$ microglia ($CD45^-TMEM119^+$) and non-microglia cell populations only, **E:** astrocytes ($CD45^-ACSA^+$) and **F:** reactive astrocytes ($ACSA^+GFAP^+$).

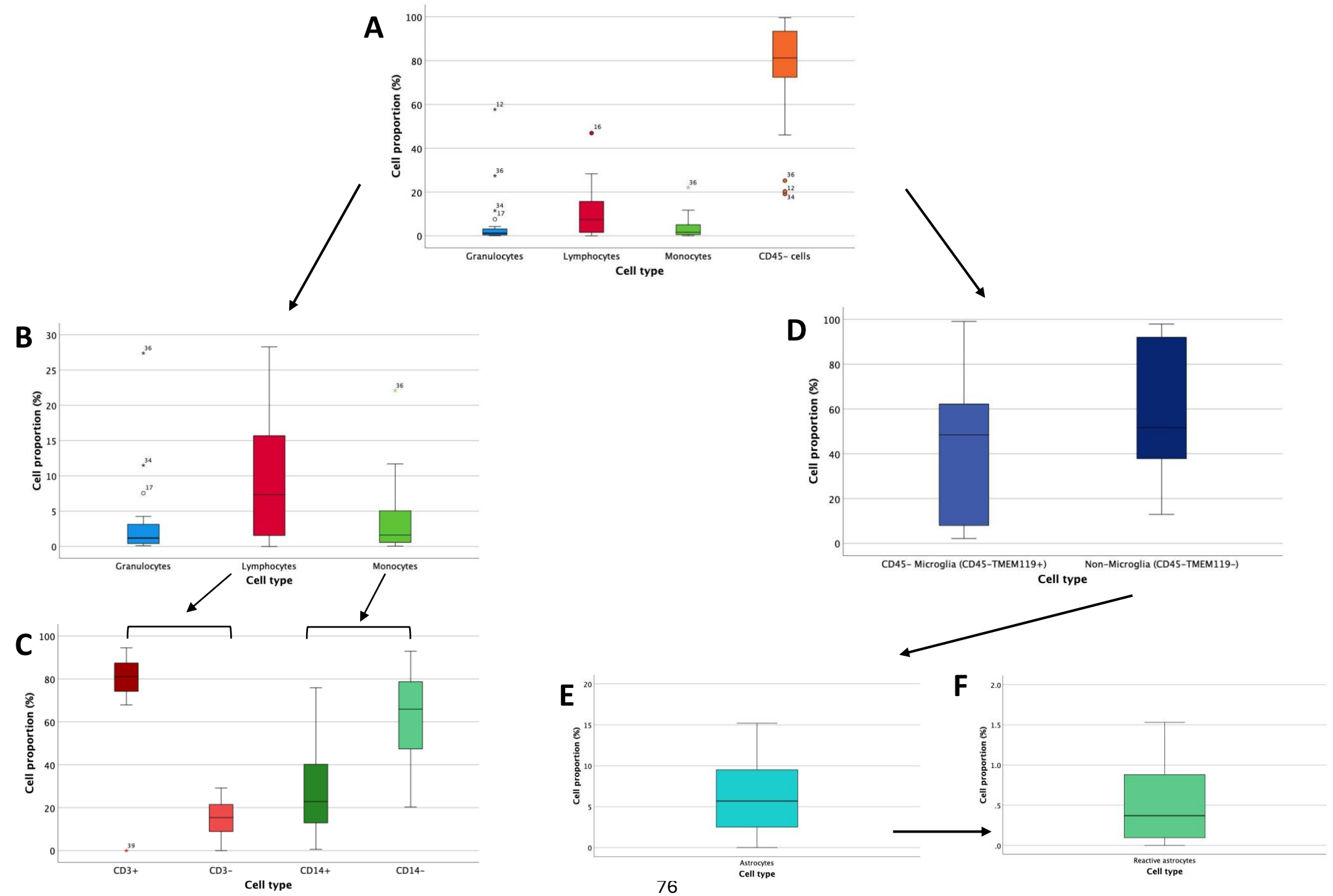
A
Cell proportion (%)
Granulocytes
Lymphocytes
Monocytes
CD45- cells
Cell type
B
Cell proportion (%)
Granulocytes
Lymphocytes
Monocytes
Cell type
C
Cell proportion (%)
CD3+
CD3-
CD14+
CD14-
Cell type
D
Cell proportion (%)
CD45- Microglia (CD45-TMEM119+)
Non-Microglia (CD45-TMEM119-)
Cell type
E
Cell proportion (%)
Astrocytes
Cell type
F
Cell proportion (%)
Reactive astrocytes
Cell type

Temporal profile

Table 6.5 includes descriptive statistics over day 1-8 time epochs for the proportions of the main cell populations. Table 6.6 and table 6.7 include lymphocytic and monocytic sub-groups respectively. There was a marked decrease in the number of patient samples from day 3 onwards. Temporal profile analysis is based on samples available for the cohort overall at each time point, not necessarily for individual patients at each time point. Comparisons between days 1-2 and days 7-8 showed a significant decrease in the proportions of monocytes (1.63-0.22%; $p = 0.028$), $CD14^+$ cells (22.85-12.75%; $p = 0.046$), astrocytes (5.70-0.22%; $p = 0.028$), and reactive astrocytes (0.37-0.06%; $p = 0.028$), but a significant increase in $CD45^-$ cells ($p = 0.046$). However, the change in CD45- microglia was not significant. Figure 6.2 demonstrates these changes over time – figures with outliers can be found in Appendix B.

Table 6.5: Descriptive statistics for cell proportions per 48-hour epoch: **Major cell populations**

Cell type	CD45$^+$ Cells				CD45$^-$ Cells		
	Granulocytes (CD45$^+$) **Neutrophils** (CD11b$^+$CD16$^+$)		**Lymphocytes** (CD45$^+$)	**Monocytes** (CD45$^+$CD14$^+$)	**Microglia** (CD45$^-$ TMEM119$^+$)	**Astrocytes** (CD45$^-$ACSA$^+$) **Reactive astrocytes** (ACSA$^+$GFAP$^+$)	
Days 1-2	*n = 30*	*n = 30*	*n = 30*	*n = 30*	*n = 30*	*n = 30*	*n = 30*
Median	1.19	33.85	7.33	1.63	48.40	5.70	0.37
Min	0	4	0	0	2	0	0
Max	58	99	47	22	99	29	5
IQR	0.41-3.16	20.40-76.75	1.52-15.75	0.56-5.27	7.74-62.93	2.15-9.56	0.10-0.91
Days 3-4	*n = 9*	*n = 9*	*n = 9*	*n = 9*	*n = 9*	*n = 9*	*n = 9*
Median	1.18	27.20	14.70	1.25	18.30*	0.33	0.15
Min	0	9	1	0	2	0	0
Max	5	79	39	8	84	11	3
IQR	0.58-2.78	20.25-70.90	5.06-25.20	0.63-4.65	14.40-64.65	0.11-4.30	0.01-1.30
Days 5-6	*n = 6*	*n = 6*	*n = 6*	*n = 6*	*n = 6*	*n = 6*	*n = 6*
Median	0.36	18.30	11.64	0.74	62.60	0.43	0.08
Min	0	3	4	0	22	0	0
Max	4	49	47	6	80	7	0
IQR	0.15-1.64	10.67-27.70	5.13-27.15	0.30-2.30	37.10-77.88	0.27-3.07	0.01-0.22
Days 7-8	*n = 6*	*n = 6*	*n = 6*	*n = 6*	*n = 6*	*n = 6*	*n = 6*
Median	0.39	20.55	1.32	0.22	58.45	0.22	0.06
Min	0	1	0	0	7	0	0
Max	1	31	31	1	87	2	1
IQR	0.18-0.81	12.10-26.25	0.51-9.55	0.08-0.86	35.24-81.55	0.01-0.89	0.01-0.34

Values represent proportion (%), n represents number of samples. *CD:* cluster of differentiation marker; *max:* maximum; *min:* minimum; *p:* percentile.
*The decrease in CD45-microglia seen on days 3-4 is attributable to 9 patients, for whom their admission median proportion was 11.5%.

Table 6.6a: Descriptive statistics for cell proportions of lymphocytic sub-groups: **days 1-2**

Parent cell group	**Lymphocytes** ($CD45^+$)			
Sub-group	**$CD3^+$ cells**		**$CD3^-$ cells**	
Days 1-2	*n = 30*		*n = 30*	
Median (range)*	81.05 (0-95)		15.35 (0-29)	
IQR	73.93-87.83		8.6-21.78	
Sub-group	**$\gamma\delta^+$ cells** ($CD3^+$ $\gamma\delta$ TCR^+)	**$\gamma\delta^-$ cells** ($CD3^+$ $\gamma\delta$ TCR^-)	**B cells** ($CD3^-CD19^+$)	**Non-B cells** ($CD3^-CD19^-$)
Median (range)	2.58 (0-8)	95 (0-100)	33 (0-75)	65.65 (0-100)
IQR	1.3-4.38	91.75-97.25	16.27-53.75	65.33-83.60

Sub-group	**MAIT cells** ($CD3^+V\alpha7.2^+$ $CD161^+$)	**$CD161^+$ cells** ($CD3^+CD161^+$)	**$V\alpha7.2^+$ cells** ($CD3^+V\alpha7.2^+$)	**Non-MAIT cells** ($CD3^+V\alpha7.2^-$ $CD161^-$)	**Activated B cells** ($CD19^+HLA\text{-}DR^+$)	**NK cells** ($CD16^+CD56^+$)
Median (range) IQR	0.74 (0-14) 0.09-2.18	3.50 (0-29) 1-13.25	11 (0-79) 4.50-21.25	68.50 (0-99) 47.25-79.50	98.95 (0-100) 95.15-100	73.30 (0-100) 65.33-83.60

Sub-group	**$CD4^+$ cells** ($CD3^+CD4^+$)		**$CD8^+$ cells** ($CD3^+CD8^+$)	
Days 1-2	*n = 30*		*n = 30*	
Median (range)	51.90 (0-84)		32.55 (0-67)	
IQR	44.18-57.18		24.35-37.20	
Sub-group	**Treg cells** ($CD4^+CD25^+FoxP3^+$)	**Non-Treg cells** ($CD4^+CD25^+FoxP3^-$)	**Treg cells** ($CD8^+CD25^+FoxP3^+$)	**Non-Treg cells** ($CD8^+CD25^+FoxP3^-$)
Median (range)	5.72 (0-27)	90.50 (0-100)	0 (0-9)	86 (0-100)
IQR	2.37-11.10	82.75-94.25	0-0.21	60.75-97

	CD4+ Non-Tregs					CD8+ Non-Tregs				
Sub-group	**Central memory T cells** ($CD45RA^-$ $CD27^+$)	**Effector memory T cells** ($CD45RA^-$ $CD27^-$)	**Naïve T cells** ($CD45RA^+$ $CD27^+$)	**Exhausted T cells** ($CD45RA^{++}$ $CD27^-$)	**Terminal T cells** ($CD45RA^+$ $CD27^-$)	**Central memory T cells** ($CD45RA^-$ $CD27^+$)	**Effector memory T cells** ($CD45RA^-$ $CD27^-$)	**Naïve T cells** ($CD45RA^+$ $CD27^+$)	**Exhausted T cells** ($CD45RA^{++}$ $CD27^-$)	**Terminal T cells** ($CD45RA^+$ $CD27^-$)
Days 1-2	*n = 30*	*n = 30*	*n = 30*	*n = 30*	*n = 30*	*n = 30*	*n = 30*	*n = 30*	*n = 30*	*n = 30*
Median (range) IQR	49 (0-100) 23.75-57.25	14.5 (0-75) 6-26.25	19.5 (0-70) 8-36.75	0 (0-17) 0-0.25	1.5 (0-50) 1-5.25	19.5 (0-74) 12-26.5	1 (0-25) 0-8.25	55.5 (0-100) 34.5-66.5	3 (0-32) 0-9.75	2.5 (0-75) 0-8.25

Values represent proportion (%), n represents number of samples.
CD: cluster of differentiation marker; *IQR:* inter-quartile range; *MAIT:* mucosal-associated T cell; *NK:* natural killer; *Treg:* regulatory T cell
*min-max range

Table 6.6b: Descriptive statistics for cell proportions of lymphocytic sub-groups: **days 3-4**

Parent cell group	**Lymphocytes** ($CD45^+$)			
Sub-group	**$CD3^+$ cells**		**$CD3^-$ cells**	
Days 3-4	*n = 9*		*n = 9*	
Median (range)* IQR	85 (69-97) 75.90-88.45		13.5 (3-27) 9.10-21.70	
Sub-group	**$\gamma\delta^+$ cells** ($CD3^+$ $\gamma\delta$ TCR^+)	**$\gamma\delta^-$ cells** ($CD3^+$ $\gamma\delta$ TCR^-)	**B cells** ($CD3^-CD19^+$)	**Non-B cells** ($CD3^-CD19^-$)
Median (range) IQR	2.57 (0-6) 0.88-3.84	97 (85-100) 94-98.50	54 (11-74) 16.05-65.70	46 (25-88) 34.25-81.05

Sub-group	**MAIT cells** ($CD3^+V\alpha7.2^+$ $CD161^+$)	**$CD161^+$ cells** ($CD3^+CD161^+$)	**$V\alpha7.2^+$ cells** ($CD3^+V\alpha7.2^+$)	**Non-MAIT cells** ($CD3^+V\alpha7.2^-$ $CD161^-$)	**Activated B cells** ($CD19^+HLA\text{-}DR^+$)	**NK cells** ($CD16^+CD56^+$)
Median (range) IQR	0.69 (0-44) 0.11-9.72	2 (0-16) 0-9.50	8 (3-32) 4.50-26.50	75 (13-90) 62-88	98.70 (93-100) 97.45-100	60.10 (41-81) 52.95-78.25

Sub-group	**$CD4^+$ cells** ($CD3^+CD4^+$)		**$CD8^+$ cells** ($CD3^+CD8^+$)	
Days 3-4	*n = 9*		*n = 9*	
Median (range) IQR	45.70 (2-54) 43.85-51.50		34.40 (3-51) 24.25-38.15	
Sub-group	**Treg cells** ($CD4^+CD25^+FoxP3^+$)	**Non-Treg cells** ($CD4^+CD25^+FoxP3^-$)	**Treg cells** ($CD8^+CD25^+FoxP3^+$)	**Non-Treg cells** ($CD8^+CD25^+FoxP3^-$)
Median (range) IQR	6.11 (1-43) 3.13-12.90	84 (44-97) 60-95	0.07 (0-1) 0-0.62	88 (2-99) 46-96

	CD4+ Non-Tregs					CD8+ Non-Tregs				
Sub-group	**Central memory T cells** ($CD45RA^-$ $CD27^+$)	**Effector memory T cells** ($CD45RA^-$ $CD27^-$)	**Naïve T cells** ($CD45RA^+$ $CD27^+$)	**Exhausted T cells** ($CD45RA^{++}$ $CD27^-$)	**Terminal T cells** ($CD45RA^+$ $CD27^-$)	**Central memory T cells** ($CD45RA^-$ $CD27^+$)	**Effector memory T cells** ($CD45RA^-$ $CD27^-$)	**Naïve T cells** ($CD45RA^+$ $CD27^+$)	**Exhausted T cells** ($CD45RA^{++}$ $CD27^-$)	**Terminal T cells** ($CD45RA^+$ $CD27^-$)
Days 3-4	*n = 9*	*n = 9*	*n = 9*	*n = 9*	*n = 9*	*n = 9*	*n = 9*	*n = 9*	*n = 9*	*n = 9*
Median (range) IQR	38 (8-68) 24-49	32 (3-58) 15.50-42.50	19 (8-46) 12-28.50	0 (0-1) 0-0	5 (2-19) 3.50-12	16 (0-33) 13.50-26	5 (1-64) 2-16	57 (0-75) 39-68	5 (0-14) 0.50-7	10 (0-27) 2.50-15.50

Values represent proportion (%), n represents number of samples.
CD: cluster of differentiation marker; *IQR:* inter-quartile range; *MAIT:* mucosal-associated T cell; *NK:* natural killer; *Treg:* regulatory T cell
*min-max range

Table 6.6c: Descriptive statistics for cell proportions of lymphocytic sub-groups: **days 5-6**

Parent cell group	**Lymphocytes** ($CD45^+$)			
Sub-group	**$CD3^+$ cells**		**$CD3^-$ cells**	
Days 5-6	*n = 6*		*n = 6*	
Median (range)*	87.90 (80-94)		11.20 (6-16)	
IQR	80.88-93.32		6.35-13.20	
Sub-group	**$\gamma\delta^+$ cells** ($CD3^+$ $\gamma\delta$ TCR^+)	**$\gamma\delta^-$ cells** ($CD3^+$ $\gamma\delta$ TCR^-)	**B cells** ($CD3^-CD19^+$)	**Non-B cells** ($CD3^-CD19^-$)
Median (range)	1.05 (0-3)	98 (94-99)	50.30 (27-87)	49.50 (13-73)
IQR	0.58-2.25	94.75-99	38.35-80.20	19.33-61.63

Sub-group	**MAIT cells** ($CD3^+V\alpha7.2^+$ $CD161^+$)	**$CD161^+$ cells** ($CD3^+CD161^+$)	**$V\alpha7.2^+$ cells** ($CD3^+V\alpha7.2^+$)	**Non-MAIT cells** ($CD3^+V\alpha7.2^-$ $CD161^-$)	**Activated B cells** ($CD19^+HLA\text{-}DR^+$)	**NK cells** ($CD16^+CD56^+$)
Median (range)	0.78 (0-4)	4.50 (4-12)	20.50 (4-27)	67.50 (56-88)	99.50 (91-100)	77.70 (61-88)
IQR	0.47-2.13	4-7.50	4-24	60.50-88	94.58-100	69.80-83.90

Sub-group	**$CD4^+$ cells** ($CD3^+CD4^+$)		**$CD8^+$ cells** ($CD3^+CD8^+$)	
Days 5-6	*n = 6*		*n = 6*	
Median (range)	57.85 (25-91)		25.25 (8-45)	
IQR	33.50-82.25		15.37-42.20	
Sub-group	**Treg cells** ($CD4^+CD25^+FoxP3^+$)	**Non-Treg cells** ($CD4^+CD25^+FoxP3^-$)	**Treg cells** ($CD8^+CD25^+FoxP3^+$)	**Non-Treg cells** ($CD8^+CD25^+FoxP3^-$)
Median (range)	8.09 (2-26)	81.50 (68-88)	0.40 (0-1)	89.50 (1-97)
IQR	4.78-20.02	77-88	0.05-0.96	59.50-97

	CD4+ Non-Tregs					CD8+ Non-Tregs				
Sub-group	**Central memory T cells** ($CD45RA^-$ $CD27^+$)	**Effector memory T cells** ($CD45RA^-$ $CD27^-$)	**Naïve T cells** ($CD45RA^+$ $CD27^+$)	**Exhausted T cells** ($CD45RA^{++}$ $CD27^-$)	**Terminal T cells** ($CD45RA^+$ $CD27^-$)	**Central memory T cells** ($CD45RA^-$ $CD27^+$)	**Effector memory T cells** ($CD45RA^-$ $CD27^-$)	**Naïve T cells** ($CD45RA^+$ $CD27^+$)	**Exhausted T cells** ($CD45RA^{++}$ $CD27^-$)	**Terminal T cells** ($CD45RA^+$ $CD27^-$)
Days 5-6	*n = 6*	*n = 6*	*n = 6*	*n = 6*	*n = 6*	*n = 6*	*n = 6*	*n = 6*	*n = 6*	*n = 6*
Median (range) IQR	45 (32-62) 37.25-55.25	32 (18-45) 24.75-42.75	14 (1-24) 7.75-18.75	0 (0-0) 0-0	2 (1-5) 1-2.75	27 (17-79) 19.25-57.25	6.50 (0-36) 0.75-28.50	41.50 (17-66) 18.50-63	0.50 (0-11) 0-3.50	4 (1-11) 1-6.50

Values represent proportion (%), n represents number of samples.
CD: cluster of differentiation marker; *IQR:* inter-quartile range; *MAIT:* mucosal-associated T cell; *NK:* natural killer; *Treg:* regulatory T cell
*min-max range

Table 6.6d: Descriptive statistics for cell proportions of lymphocytic sub-groups: **days 7-8**

Parent cell group	**Lymphocytes** ($CD45^+$)			
Sub-group	**$CD3^+$ cells**		**$CD3^-$ cells**	
Days 7-8	*n = 6*		*n = 6*	
Median (range)*	85.50 (0-97)		11.59 (2-97)	
IQR	0-96.18		3.41-87.80	
Sub-group	**$\gamma\delta^+$ cells** ($CD3^+$ $\gamma\delta$ TCR^+)	**$\gamma\delta^-$ cells** ($CD3^+$ $\gamma\delta$ TCR^-)	**B cells** ($CD3^-CD19^+$)	**Non-B cells** ($CD3^-CD19^-$)
Median (range)	0.64 (0-2)	96.50 (0-99)	48.90 (0-83)	50.65 (17-92)
IQR	0-1.59	0-98.25	6.16-67.33	32.67-79.97

Sub-group	**MAIT cells** ($CD3^+V\alpha7.2^+$ $CD161^+$)	**$CD161^+$ cells** ($CD3^+CD161^+$)	**$V\alpha7.2^+$ cells** ($CD3^+V\alpha7.2^+$)	**Non-MAIT cells** ($CD3^+V\alpha7.2^-$ $CD161^-$)	**Activated B cells** ($CD19^+HLA\text{-}DR^+$)	**NK cells** ($CD16^+CD56^+$)
Median (range)	0.27 (0-34)	2 (0-17)	13 (0-43)	38 (0-81)	99.30 (56-100)	44.65 (0-66)
IQR	0-11.51	0-7.25	0-22	0-75.75	82.68-100	11.93-55.15

Sub-group	**$CD4^+$ cells** ($CD3^+CD4^+$)		**$CD8^+$ cells** ($CD3^+CD8^+$)	
Days 7-8	*n = 6*		*n = 6*	
Median (range)	42.10 (0-85)		6.29 (0-49)	
IQR	0-72.08		0-42.83	
Sub-group	**Treg cells** ($CD4^+CD25^+FoxP3^+$)	**Non-Treg cells** ($CD4^+CD25^+FoxP3^-$)	**Treg cells** ($CD8^+CD25^+FoxP3^+$)	**Non-Treg cells** ($CD8^+CD25^+FoxP3^-$)
Median (range)	2.89 (0-11)	71.50 (0-92)	0 (0-0)	46.50 (0-90)
IQR	0-6.69	0-91.25	0-0	0-77.25

	CD4+ Non-Tregs					CD8+ Non-Tregs				
Sub-group	**Central memory T cells** ($CD45RA^-$ $CD27^+$)	**Effector memory T cells** ($CD45RA^-$ $CD27^-$)	**Naïve T cells** ($CD45RA^+$ $CD27^+$)	**Exhausted T cells** ($CD45RA^{++}$ $CD27^-$)	**Terminal T cells** ($CD45RA^+$ $CD27^-$)	**Central memory T cells** ($CD45RA^-$ $CD27^+$)	**Effector memory T cells** ($CD45RA^-$ $CD27^-$)	**Naïve T cells** ($CD45RA^+$ $CD27^+$)	**Exhausted T cells** ($CD45RA^{++}$ $CD27^-$)	**Terminal T cells** ($CD45RA^+$ $CD27^-$)
Days 7-8	*n = 6*	*n = 6*	*n = 6*	*n = 6*	*n = 6*	*n = 6*	*n = 6*	*n = 6*	*n = 6*	*n = 6*
Median (range) IQR	28 (0-37) 0-32.50	15 (0-65) 0-47.75	6.50 (0-55) 0-37.75	0 (0-1) 0-0.25	0 (0-6) 0-3.75	17 (0-71) 0-38	6 (0-36) 0-19.50	15 (0-82) 0-61	0 (0-3) 0-0.75	0.50 (0-7) 0-4

Values represent proportion (%), n represents number of samples.
CD: cluster of differentiation marker; *IQR:* inter-quartile range; *MAIT:* mucosal-associated T cell; *NK:* natural killer; *Treg:* regulatory T cell
*min-max range

Table 6.7a: Descriptive statistics for cell proportions of monocytic sub-groups: **days 1-2 & 3-4**

Parent cell group	**Monocytes** ($CD45^+$)		
Sub-group	**$CD14^+$ cells**		**$CD14^-$ cells**
Days 1-2	*n = 30*		*n = 30*
Median (range)* IQR	22.85 (1-76) 12.14-40.80		65.90 (20-93) 46.68-79.30
Sub-group	**Non-classical monocytes** ($CD14^+CD16^+$)	**Classical monocytes** ($CD14^+CD16^-$)	**$CD45^+$ microglia** ($TMEM119^+$)
Days 1-2	*n = 30*	*n = 30*	*n = 30*
Median (range) IQR	68.05 (11-99) 37.58-85.13	22.05 (2-84) 12.23-61.95	41.80 (1-90) 16.42-73.90

Parent cell group	**Monocytes** ($CD45^+$)		
Sub-group	**$CD14^+$ cells**		**$CD14^-$ cells**
Days 3-4	*n = 9*		*n = 9*
Median (range) IQR	18.60 (2-53) 5.60-44.65		65.80 (35-97) 52.20-84.05
Sub-group	**Non-classical monocytes** ($CD14^+CD16^+$)	**Classical monocytes** ($CD14^+CD16^-$)	**$CD45^+$ microglia** ($TMEM119^+$)
Days 3-4	*n = 9*	*n = 9*	*n = 9*
Median (range) IQR	55.10 (26-94) 35.30-91.65	42.90 (4-71) 6.65-62.60	51.40 (11-91) 39-69.70

Values represent proportion (%), n represents number of samples.
CD: cluster of differentiation marker; *IQR:* inter-quartile range
*min-max range

Table 6.7b: Descriptive statistics for cell proportions of monocytic sub-groups: **days 5-6 & 7-8**

Parent cell group	**Monocytes** ($CD45^+$)		
Sub-group	**$CD14^+$ cells**		**$CD14^-$ cells**
Days 5-6	*n = 6*		*n = 6*
Median (range)*	14.80 (0-71)		80 (26-94)
IQR	4.06-33.20		58.68-86.68
Sub-group	**Non-classical monocytes** ($CD14^+CD16^+$)	**Classical monocytes** ($CD14^+CD16^-$)	**$CD45^+$ microglia** ($TMEM119^+$)
Days 5-6	*n = 6*	*n = 6*	*n = 6*
Median (range)	47.35 (15-86)	44.85 (12-78)	60.55 (22-70)
IQR	24.25-76.05	20-71.95	39.38-65.50

Parent cell group	**Monocytes** ($CD45^+$)		
Sub-group	**$CD14^+$ cells**		**$CD14^-$ cells**
Days 7-8	*n = 6*		*n = 6*
Median (range)	12.75 (3-20)		81.85 (55-97)
IQR	3.30-18.20		67.85-94.13
Sub-group	**Non-classical monocytes** ($CD14^+CD16^+$)	**Classical monocytes** ($CD14^+CD16^-$)	**$CD45^+$ microglia** ($TMEM119^+$)
Days 7-8	*n = 6*	*n = 6*	*n = 6*
Median (range)	63.95 (0-84)	31.55 (10-100)	43.40 (16-61)
IQR	15-82.98	12-85	29.75-60.80

Values represent proportion (%), n represents number of samples.
CD: cluster of differentiation marker; *IQR:* inter-quartile range
*min-max range

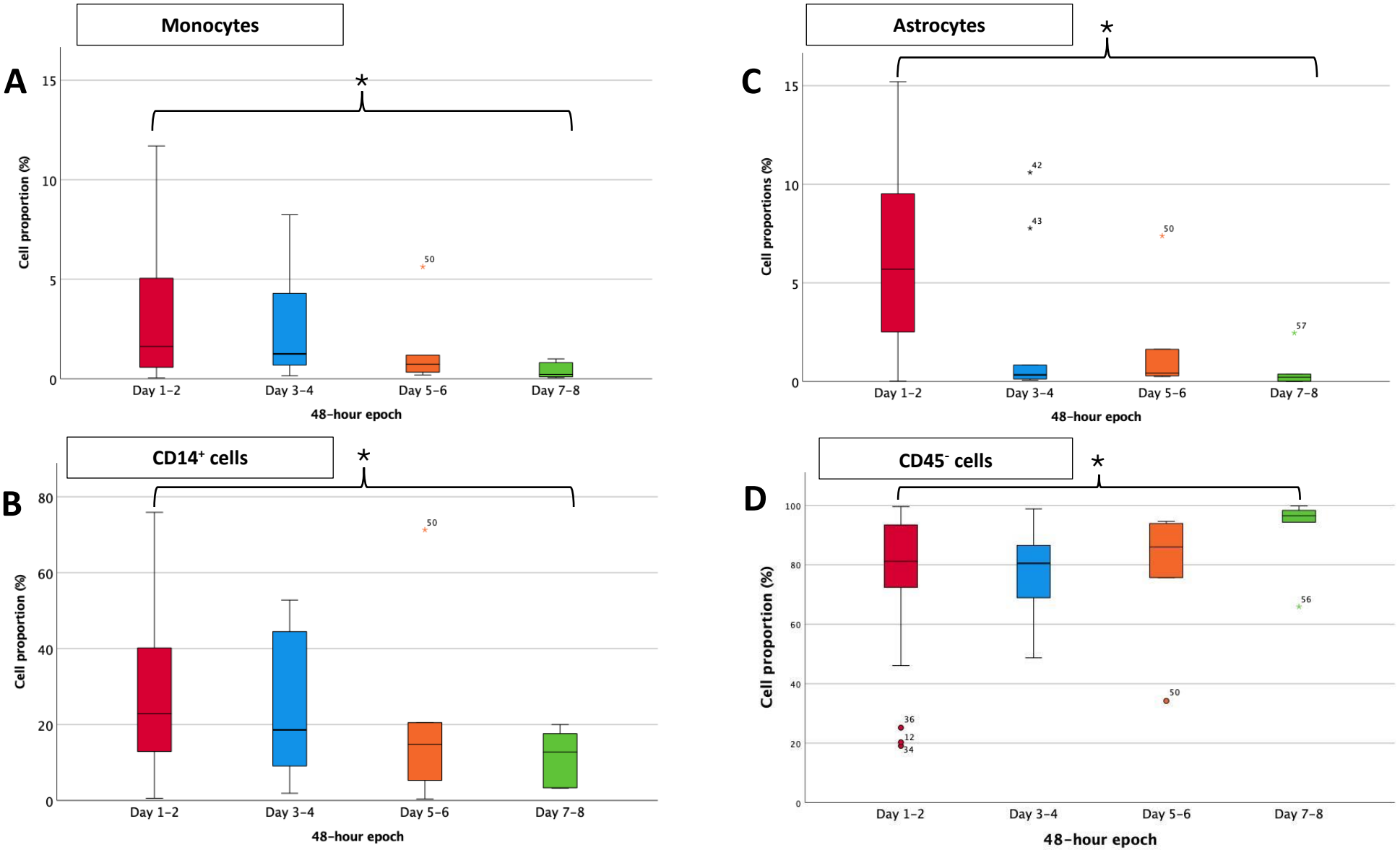

Figure 6.2. **Significant changes in cell proportion over the first week of hospital admission.** Changes in cell proportions over four 48-hour epochs for **A:** monocytes ($CD45^+$)**, B:** $CD14^+$, **C:** astrocytes ($CD45^-ACSA^+$)and **D:** $CD45^-$ cells.

6.2.2 Absolute cell concentrations

Admission

Absolute counts/concentrations were available in 23 of the 30 patients. Descriptive statistics for main cell populations – lymphocytes, monocytes, granulocytes, $CD45^-$ microglia and astrocytes and their sub-groups – are shown in table 6.8a, 6.9 and 6.10, with $CD45^-$ microglia having the highest concentration (median of 129.85 cells/μL). These microglia were significantly more abundant than granulocytes ($p < 0.001$), monocytes ($p < 0.001$) and astrocytes ($p < 0.001$). Lymphocyte concentrations were significantly higher than granulocytes ($p < 0.001$), monocytes ($p < 0.001$) and astrocytes ($p < 0.001$). as depicted in Figure 6.3 – figure with outliers included in Appendix B. Cell concentrations from our National Health Laboratory Services (NHLS) were not significantly different from the cell concentrations derived from the flow cytometry. NHLS concentrations are shown in Table 6.8b.

Table 6.8a: Descriptive statistics for absolute cell concentrations upon admission: **Major cell populations (flow cytometry data)**

Cell type	$CD45^+$ Cells (cells/μL)				$CD45^-$ Cells		
	Granulocytes ($CD45^+$) **Neutrophils** ($CD11b^+CD16^+$)		**Lymphocytes** ($CD45^+$)	**Monocytes** ($CD45^+CD14^+$)	**Microglia** ($CD45^-$ $TMEM119^+$)	**Astrocytes** ($CD45^-ACSA^+$) **Reactive astrocytes** ($ACSA^+GFAP^+$)	
Admission	*n = 23*	*n = 23*	*n = 23*	*n = 23*	*n = 23*	*n = 23*	*n = 23*
Median	3.97	1.45	34.04	5.71	129.85	9.43	0.56
Min	0	0	0	1	2	0	0
Max	115	62	1305	932	17024	123	19
p25	2.15	0.19	13.10	2.92	45.34	4.26	0.09
p75	16.97	15.33	75.75	21.85	1025.84	34.14	1.31

Values represent absolute cell concentration (cells/μL), n represents number of samples.
CD: cluster of differentiation marker; *max:* maximum; *min:* minimum; *p:* percentile

Table 6.8b: Descriptive statistics for absolute cell concentrations upon admission: **Major cell populations (NHLS counts)**

Cell type	**Granulocytes** ($CD45^+$)	**Lymphocytes** ($CD45^+$)
Admission	*n = 23*	*n = 23*
Median	3	28
Min	0	2
Max	250	239
IQR	0-11	13-75

Values represent absolute cell concentration (cells/μL), n represents number of samples.
CD: cluster of differentiation marker; *IQR:* inter-quartile range; *max:* maximum; *min:* minimum

Table 6.6: Descriptive statistics for absolute cell concentrations upon admission: **Lymphocytic sub-groups**

Parent cell group	**Lymphocytes** ($CD45^+$)			
Sub-group	**$CD3^+$ cells**		**$CD3^-$ cells**	
Admission	*n = 23*		*n = 23*	
Median	28.24		4.43	
Min	0		0	
Max	1189		71	
IQR	11.23-65.62		1.87-10.85	
Sub-group	**$\gamma\delta^+$ cells** ($CD3^+$ $\gamma\delta$ TCR^+)	**$\gamma\delta^-$ cells** ($CD3^+$ $\gamma\delta$ TCR^-)	**B cells** ($CD3^-CD19^+$)	**Non-B cells** ($CD3^-CD19^-$)
Median	0.50	27.32	1.20	2.41
Min	0	0	0	0
Max	44	1101	23	94
IQR	0.14-1.45	11.23-64.21	0.66-2.62	0.80-7.25

Sub-group	**MAIT cells** ($CD3^+V\alpha7.2^+$ $CD161^+$)	**Non-MAIT cells** ($CD3^+V\alpha7.2^-$ $CD161^-$)	**$V\alpha7.2^+$ cells** ($CD3^+V\alpha7.2^+$)	**$CD161^+$ cells** ($CD3^+CD161^+$)	**Activated B cells** ($CD19^+HLA\text{-}DR^+$)	**NK cells** ($CD16^+CD56^+$)
Median	0.32	21.46	2.04	1.63	1.18	1.74
Min	0	0	0	0	0	0
Max	44	604	246	81	23	43
IQR	0.08-0.82	3.90-44.37	1.05-4.92	0.47-7.43	0.65-2.60	0.49-3.88

	Non-MAIT cells			
Sub-group	**CD4⁺ cells** ($CD3^+CD4^+$)		**CD8⁺ cells** ($CD3^+CD8^+$)	
Admission	*n = 23*		*n = 23*	
Median IQR	10.96 (0-367) 1.89-21.48		6.66 (0-107) 1.25-14.40	
Sub-group	**Treg cells** ($CD4^+CD25^+FoxP3^+$)	**Non-Treg cells** ($CD4^+CD25^+FoxP3^-$)	**Treg cells** ($CD8^+CD25^+FoxP3^+$)	**Non-Treg cells** ($CD8^+CD25^+FoxP3^-$)
Median IQR	0.51 (0-43) 0.19-1.04	9.88 (0-310) 1.66-19.92	0.01(0-0) 0-0.03	4.44 (0-64) 1.15-12.45

Sub-group	**Central memory T cells** ($CD45RA^-CD27^+$)	**Effector memory T cells** ($CD45RA^-CD27^-$)	**Naïve T cells** ($CD45RA^+CD27^+$)	**Exhausted T cells** ($CD45RA^{++}CD27^-$)	**Terminal T cells** ($CD45RA^+CD27^-$)	**Central memory T cells** ($CD45RA^-CD27^+$)	**Effector memory T cells** ($CD45RA^-CD27^-$)	**Naïve T cells** ($CD45RA^+CD27^+$)	**Exhausted T cells** ($CD45RA^{++}CD27^-$)	**Terminal T cells** ($CD45RA^+CD27^-$)
Admission	*n = 23*	*n = 23*	*n = 23*	*n = 23*	*n = 23*	*n = 23*	*n = 23*	*n = 23*	*n = 23*	*n = 23*
Median IQR	5.57 (0-68) 0.39-9.76	2.36 (0-10) 0.10-3.80	1.06 (0-218) 0.3-4.03	0 (0-0) 0-0.01	0.16 (0-8) 0.01-0.32	1.30 (0-9) 0.25-2.86	0.05 (0-1) 0-0.35	2.53 (0-60) 0.58-7.7	0.02 (0-2) 0-0.15	0.05 (0-2) 0-0.24

Values represent absolute cell concentrations (cells/μL); n represents number of samples.
CD: cluster of differentiation marker; *IQR:* inter-quartile range; *MAIT:* mucosal-associated T cell; *NK:* natural killer; *Treg:* regulatory T cell
*min-max range

Table 6.7: Descriptive statistics for absolute cell concentrations upon admission: **Monocytic sub-groups**

Parent cell group	**Monocytes** ($CD45^+$)		
Sub-group	**$CD14^+$ cells**		**$CD14^-$ cells**
Admission	*n = 23*		*n = 23*
Median	1.60		3.48
Min	0		0
Max	74		847
IQR	0.74-4.88		1.34-16.84
Sub-group	**Non-classical monocytes** ($CD14^+CD16^+$)	**Classical monocytes** ($CD14^+CD16^-$)	**$CD45^+$ microglia** ($TMEM119^+$)
Admission	*n = 23*	*n = 23*	*n = 23*
Median	0.94	0.37	1.62
Min	0	0	0
Max	36	31	127
IQR	0.20-3.33	0.17-1.04	0.74-5.57

Values represent absolute cell concentrations (cells/μL); n represents number of samples.
CD: cluster of differentiation marker; *IQR:* inter-quartile range; *max:* maximum; *min:* minimum

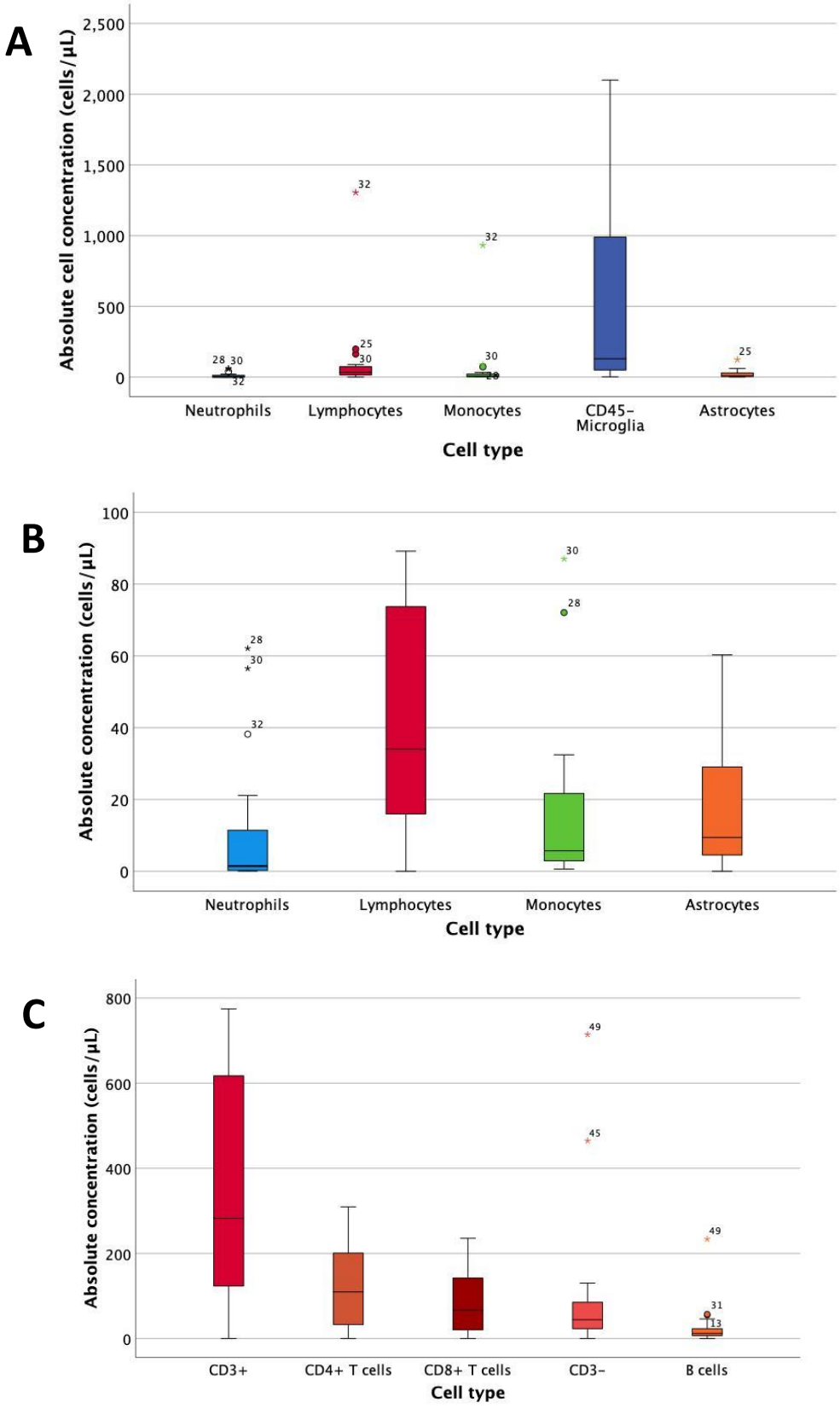

Figure 6.3. **Box plots for admission absolute cell concentrations for major peripheral and brain-derived immune cell populations.** Absolute cell concentrations for **A:** all major cell populations, **B:** populations excluding $CD45^-$ microglia and **C:** relevant lymphocytic ($CD45^+$) sub-groups.

Temporal profile

Measures of central tendency for concentrations of the major cell populations were compared between days 1-2 and days 7-8. The increase in lymphocyte concentration at days 5-6 was driven by patients 18 and 24, and at days 7-8 by patient 38. Microglial increase at days 5-6 was driven by patients 11, 18 and 24, and at days 7-8 by patients 18, 37 and 38. Non-MAIT cells ($p = 0.043$ – although this was not significant for the CD4 and CD8 sub-groups), $\gamma\delta$ T cells ($p = 0.043$) and non-classical monocytes ($p = 0.046$) demonstrated significant decreases in concentration, as seen in figure 6.4. Figures with outliers are included in Appendix B. Descriptive statistics for the major cell populations and their sub-groups over the first 8 days of hospital stay are included in tables 6.11, 6.12 and 6.13, respectively. To ascertain whether the high proportion of microglia may have been due to tissue fragments released during the insertion of the EVD, we compared the median microglial counts between days 1-2 and 3-4. There was no significant difference ($p = 0.666$).

Table 6.8: Descriptive statistics for absolute cell concentrations per 48-hour epoch: **Major cell populations**

Cell type	CD45⁺ Cells				CD45⁻ Cells		
	Granulocytes (CD45⁺) **Neutrophils** (CD11b⁺CD16⁺)		**Lymphocytes** (CD45⁺)	**Monocytes** (CD45⁺CD14⁺)	**Microglia** (CD45⁻ TMEM119⁺)	**Astrocytes** (CD45⁻ACSA⁺) **Reactive astrocytes** (ACSA⁺GFAP⁺)	
Days 1-2	*n = 23*	*n = 23*	*n = 23*	*n = 23*	*n = 23*	*n = 23*	*n = 23*
Median	3.97	1.45	34.04	5.71	129.85	9.43	0.56
Min	0	0	0	1	2	0	0
Max	115	62	1305	932	17024	123	19
IQR	2.15-16.97	0.19-15.33	13.10-75.75	2.92-21.85	45.34-1025.84	4.26-34.14	0.09-1.31
Days 3-4	*n = 7*	*n = 7*	*n = 7*	*n = 7*	*n = 7*	*n = 7*	*n = 7*
Median	2.53	1.29	32.53	6.80	94.80	0.46	0.05
Min	1	0	7	0	5	0	0
Max	49	13	1371	186	3131	42	14
IQR	0.91-18.25	0.14-3.41	7.56-344.93	0.88-115.27	7.33-2151.36	0.06-5.10	0-0.93
Days 5-6	*n = 6*	*n = 6*	*n = 6*	*n = 6*	*n = 6*	*n = 6*	*n = 6*
Median	3.42	0.67	67.89	5.06	783.65	2.13	0.12
Min	0	0	26	0	10	0	0
Max	20	4	601	46	1967	9	1
IQR	1.36-10.87	0.18-2.86	31.67-479.13	1.94-28.08	96.30-1268.23	0.47-4.74	0.02-0.41
Days 7-8	*n = 6*	*n = 6*	*n = 6*	*n = 6*	*n = 6*	*n = 6*	*n = 6*
Median	3.59	0.54	73.29	4.29	1235.62	0.90	0.13
Min	1	0	0	0	33	0	0
Max	81	20	1748	24	3096	80	5
IQR	1.75-25.12	0.10-5.99	1.08-594.66	1.14-12.87	137.26-2729.41	0.01-21.12	0.01-4.02

Values represent absolute cell concentration (cells/μL), n represents number of samples.
CD: cluster of differentiation marker; *max:* maximum; *min:* minimum; *p:* percentile

Table 6.12a: Descriptive statistics for absolute cell concentrations of lymphocytic subgroups: **Days 1-2**

Parent cell group	**Lymphocytes** ($CD45^+$)			
Sub-group	**$CD3^+$ cells**		**$CD3^-$ cells**	
Days 1-2	*n = 23*		*n = 23*	
Median (range)*	28.24 (0-1189)		4.43 (0-71)	
IQR	11.23-65.62		1.87-10.85	
Sub-group	**$\gamma\delta^+$ cells** ($CD3^+$ $\gamma\delta$ TCR^+)	**$\gamma\delta^-$ cells** ($CD3^+$ $\gamma\delta$ TCR^-)	**B cells** ($CD3^-CD19^+$)	**Non-B cells** ($CD3^-CD19^-$)
Median (range)	0.50 (0-44)	27.32 (0-1101)	1.20 (0-23)	2.41 (0-94)
IQR	0.14-1.45	11.23-64.21	0.66-2.62	0.80-7.25

Sub-group	**MAIT cells** ($CD3^+V\alpha7.2^+$ $CD161^+$)	**$CD161^+$ cells** ($CD3^+CD161^+$)	**$V\alpha7.2^+$ cells** ($CD3^+V\alpha7.2^+$)	**Non-MAIT cells** ($CD3^+V\alpha7.2^-$ $CD161^-$)	**Activated B cells** ($CD19^+HLA\text{-}DR^+$)	**NK cells** ($CD16^+CD56^+$)
Median (range)	0.32 (0-44)	1.63 (0-81)	2.04 (0-246)	21.46 (0-604)	1.18 (0-23)	1.74 (0-43)
IQR	0.08-0.82	0.47-7.43	1.05-4.92	3.90-44.37	0.65-2.60	0.49-3.88

Sub-group	**$CD4^+$ cells** ($CD3^+CD4^+$)		**$CD8^+$ cells** ($CD3^+CD8^+$)	
Days 1-2	*n = 23*		*n = 23*	
Median (range)	10.96 (0-367)		6.66 (0-107)	
IQR	1.89-21.48		1.25-14.40	
Sub-group	**Treg cells** ($CD4^+CD25^+FoxP3^+$)	**Non-Treg cells** ($CD4^+CD25^+FoxP3^-$)	**Treg cells** ($CD8^+CD25^+FoxP3^+$)	**Non-Treg cells** ($CD8^+CD25^+FoxP3^-$)
Median (range)	0.51 (0-43)	9.88 (0-310)	0.01(0-0)	4.44 (0-64)
IQR	0.19-1.04	1.66-19.92	0-0.03	1.15-12.45

	CD4⁺ Non-Tregs						CD8⁺ Non-Tregs				
Sub-group	**Central memory T cells** (CD45RA⁻ CD27⁺)	**Effector memory T cells** (CD45RA⁻ CD27⁻)	**Naïve T cells** (CD45RA⁺ CD27⁺)	**Exhausted T cells** (CD45RA⁺⁺ CD27⁻)	**Terminal T cells** (CD45RA⁺ CD27⁻)		**Central memory T cells** (CD45RA⁻ CD27⁺)	**Effector memory T cells** (CD45RA⁻ CD27⁻)	**Naïve T cells** (CD45RA⁺ CD27⁺)	**Exhausted T cells** (CD45RA⁺⁺ CD27⁻)	**Terminal T cells** (CD45RA⁺ CD27⁻)
Days 1-2	*n = 30*	*n = 30*	*n = 30*	*n = 30*	*n = 30*		*n = 30*	*n = 30*	*n = 30*	*n = 30*	*n = 30*
Median (range) IQR	5.57 (0-68) 0.39-9.76	2.36 (0-10) 0.10-3.80	1.06 (0-218) 0.3-4.03	0 (0-0) 0-0.01	0.16 (0-8) 0.01-0.32		1.30 (0-9) 0.25-2.86	0.05 (0-1) 0-0.35	2.53 (0-60) 0.58-7.7	0.02 (0-2) 0-0.15	0.05 (0-2) 0-0.24

Values represent absolute concentrations (cells/μL); n represents number of samples.
CD: cluster of differentiation marker; *IQR:* inter-quartile range; *MAIT:* mucosal-associated T cell; *NK:* natural killer; *Treg:* regulatory T cell
*min-max range

Table 6.12b: Descriptive statistics for absolute cell concentrations of lymphocytic subgroups: **Days 3-4**

Parent cell group	**Lymphocytes** ($CD45^+$)			
Sub-group	**$CD3^+$ cells**		**$CD3^-$ cells**	
Days 3-4	*n = 7*		*n = 7*	
Median (range)*	27.67 (6-1176)		4.38 (1-123)	
IQR	6.26-310.68		1.18-31.89	
Sub-group	**$\gamma\delta^+$ cells** ($CD3^+$ $\gamma\delta$ TCR^+)	**$\gamma\delta^-$ cells** ($CD3^+$ $\gamma\delta$ TCR^-)	**B cells** ($CD3^-CD19^+$)	**Non-B cells** ($CD3^-CD19^-$)
Median (range)	1.05 (0-2)	25.72 (6-1172)	2.14 (0-84)	2.23 (0-38)
IQR	0.20-2.40	5.91-300.84	0.52-19.96	0.95-11.86

Sub-group	**MAIT cells** ($CD3^+V\alpha7.2^+$ $CD161^+$)	**$CD161^+$ cells** ($CD3^+CD161^+$)	**$V\alpha7.2^+$ cells** ($CD3^+V\alpha7.2^+$)	**Non-MAIT cells** ($CD3^+V\alpha7.2^-$ $CD161^-$)	**Activated B cells** ($CD19^+HLA\text{-}DR^+$)	**NK cells** ($CD16^+CD56^+$)
Median (range)	0.18 (0-512)	0.58 (0-31)	0.94 (0-377)	23.02 (4-174)	2.14 (0-82)	1.79 (0-20)
IQR	0.03-41.81	0.49-29.40	0.25-32.06	4.75-147.13	0.51-19.60	0.65-6.97

Sub-group	**$CD4^+$ cells** ($CD3^+CD4^+$)		**$CD8^+$ cells** ($CD3^+CD8^+$)	
Days 3-4	*n = 7*		*n = 7*	
Median (range)	10.31 (2-88)		5.91 (1-60)	
IQR	2.04-71.26		1.93-36.62	
Sub-group	**Treg cells** ($CD4^+CD25^+FoxP3^+$)	**Non-Treg cells** ($CD4^+CD25^+FoxP3^-$)	**Treg cells** ($CD8^+CD25^+FoxP3^+$)	**Non-Treg cells** ($CD8^+CD25^+FoxP3^-$)
Median (range)	0.50 (0-6)	8.94 (1-81)	0 (0-0)	5 (0-46)
IQR	0.13-3.90	1.90-43.77	0-0.02	0.29-34.58

	CD4⁺ Non-Tregs						CD8⁺ Non-Tregs				
Sub-group	**Central memory T cells** (CD45RA⁻ CD27⁺)	**Effector memory T cells** (CD45RA⁻ CD27⁻)	**Naïve T cells** (CD45RA⁺ CD27⁺)	**Exhausted T cells** (CD45RA⁺⁺ CD27⁻)	**Terminal T cells** (CD45RA⁺ CD27⁻)		**Central memory T cells** (CD45RA⁻ CD27⁺)	**Effector memory T cells** (CD45RA⁻ CD27⁻)	**Naïve T cells** (CD45RA⁺ CD27⁺)	**Exhausted T cells** (CD45RA⁺⁺ CD27⁻)	**Terminal T cells** (CD45RA⁺ CD27⁻)
Days 3-4	*n = 7*	*n = 7*	*n = 7*	*n = 7*	*n = 7*		*n = 7*	*n = 7*	*n = 7*	*n = 7*	*n = 7*
Median IQR	5 (0-29) 0.92-15.37	1.13 (0-40) 0.42-14.01	2.97 (0-10) 0.36-6.69	0 (0-0) 0-0.01	0.18 (0-3) 0.06-2.99		1.60 (0-13) 0.05-5	0.09 (0-7) 0.01-2.25	0.85 (0-28) 0.04-13.04	0.06 (0-2) 0-0.08	0.03 (0-5) 0.01-3

Values represent absolute cell concentrations (cells/μL); n represents number of samples.
CD: cluster of differentiation marker; *IQR:* inter-quartile range; *MAIT:* mucosal-associated T cell; *NK:* natural killer; *Treg:* regulatory T cell
*min-max range

Table 6.12c: Descriptive statistics for absolute cell concentrations of lymphocytic subgroups: **Days 5-6**

Parent cell group	**Lymphocytes** ($CD45^+$)			
Sub-group	**$CD3^+$ cells**		**$CD3^-$ cells**	
Days 5-6	*n = 6*		*n = 6*	
Median (range)*	59.87 (24-479)		5.93 (2-96)	
IQR	28.10-409.63		3.47-57.75	
Sub-group	**$\gamma\delta^+$ cells** ($CD3^+$ $\gamma\delta$ TCR^+)	**$\gamma\delta^-$ cells** ($CD3^+$ $\gamma\delta$ TCR^-)	**B cells** ($CD3^-CD19^+$)	**Non-B cells** ($CD3^-CD19^-$)
Median (range)	0.77 (1-2)	58.57 (23-475)	3.54 (2-96)	2.93 (1-33)
IQR	0.56-2.22	26.61-406.04	3.47-57.75	0.96-17.55

Sub-group	**MAIT cells** ($CD3^+V\alpha7.2^+$ $CD161^+$)	**$CD161^+$ cells** ($CD3^+CD161^+$)	**$V\alpha7.2^+$ cells** ($CD3^+V\alpha7.2^+$)	**Non-MAIT cells** ($CD3^+V\alpha7.2^-$ $CD161^-$)	**Activated B cells** ($CD19^+HLA\text{-}DR^+$)	**NK cells** ($CD16^+CD56^+$)
Median (range) IQR	0.46 (0-19) 0.23-6.04	3.63 (1-25) 1.85-17.76	11.51 (2-97) 3.98-37.09	44.65 (15-339 15.58-306.99	3.40 (1-83) 1.68-29.84	2.52 (1-24) 0.77-11.70

Sub-group	**$CD4^+$ cells** ($CD3^+CD4^+$)		**$CD8^+$ cells** ($CD3^+CD8^+$)	
Days 5-6	*n = 6*		*n = 6*	
Median (range)	32.92 (7-124)		8.41 (1-151)	
IQR	12.55-85.46		5.05-105.92	
Sub-group	**Treg cells** ($CD4^+CD25^+FoxP3^+$)	**Non-Treg cells** ($CD4^+CD25^+FoxP3^-$)	**Treg cells** ($CD8^+CD25^+FoxP3^+$)	**Non-Treg cells** ($CD8^+CD25^+FoxP3^-$)
Median (range)	3.9 (0-9)	24.53 (6-102)	0.06 (0-0)	6.44 (1-133)
IQR	1.03-8.08	10.98-69.07	0.03-0.16	1.22-39.21

	CD4⁺ Non-Tregs						CD8⁺ Non-Tregs				
Sub-group	**Central memory T cells** (CD45RA⁻ CD27⁺)	**Effector memory T cells** (CD45RA⁻ CD27⁻)	**Naïve T cells** (CD45RA⁺ CD27⁺)	**Exhausted T cells** (CD45RA⁺⁺ CD27⁻)	**Terminal T cells** (CD45RA⁺ CD27⁻)		**Central memory T cells** (CD45RA⁻ CD27⁺)	**Effector memory T cells** (CD45RA⁻ CD27⁻)	**Naïve T cells** (CD45RA⁺ CD27⁺)	**Exhausted T cells** (CD45RA⁺⁺ CD27⁻)	**Terminal T cells** (CD45RA⁺ CD27⁻)
Days 5-6	*n = 6*	*n = 6*	*n = 6*	*n = 6*	*n = 6*		*n = 6*	*n = 6*	*n = 6*	*n = 6*	*n = 6*
Median (range) IQR	10.54 (2-64) 5.52-35.57	9.26 (2-26) 3.06-20.60	3.75 (1-17) 1.35-7.83	0.01 (0-0) 0-0.01	0.37 (0-1) 0.24-0.65		1.42 (0-39) 0.76-12.66	1.16 (0-8) 0.01-3.58	1.33 (0-83) 0.57-24.56	0.07 (0-0) 0-0.18	0.26 (0-1) 0.10-0.60

Values represent absolute cell concentrations (cells/μL); n represents number of samples.
CD: cluster of differentiation marker; *IQR:* inter-quartile range; *MAIT:* mucosal-associated T cell; *NK:* natural killer; *Treg:* regulatory T cell
*min-max range

Table 6.12d: Descriptive statistics for absolute cell concentrations of lymphocytic subgroups: **Days 7-8**

Parent cell group	**Lymphocytes** ($CD45^+$)			
Sub-group	**$CD3^+$ cells**		**$CD3^-$ cells**	
Days 7-8	*n = 6*		*n = 6*	
Median (range)*	28.19 (0-202)		6.32 (0-23)	
IQR	0-139.81		0.92-18.23	
Sub-group	**$\gamma\delta^+$ cells** ($CD3^+$ $\gamma\delta$ TCR^+)	**$\gamma\delta^-$ cells** ($CD3^+$ $\gamma\delta$ TCR^-)	**B cells** ($CD3^-CD19^+$)	**Non-B cells** ($CD3^-CD19^-$)
Median (range)	0.30 (0-3)	59.65 (0-1491)	0.99 (0-13)	2.90 (0-13)
IQR	0-1.49	0-520.76	0.03-6.93	0.84-10.25

Sub-group	**MAIT cells** ($CD3^+V\alpha7.2^+$ $CD161^+$)	**$CD161^+$ cells** ($CD3^+CD161^+$)	**$V\alpha7.2^+$ cells** ($CD3^+V\alpha7.2^+$)	**Non-MAIT cells** ($CD3^+V\alpha7.2^-$ $CD161^-$)	**Activated B cells** ($CD19^+HLA\text{-}DR^+$)	**NK cells** ($CD16^+CD56^+$)
Median (range)	0.14 (0-40)	1.08 (0-246)	14.88 (0-163)	8.57 (0-160)	0.98 (0-13)	0.98 (0-5)
IQR	0-11.63	0-63.92	0-78.43	0-64.80	0.03-6.91	0-2.59

Sub-group	**$CD4^+$ cells** ($CD3^+CD4^+$)		**$CD8^+$ cells** ($CD3^+CD8^+$)	
Days 7-8	*n = 6*		*n = 6*	
Median (range)	6.94 (0-84)		0.49 (0-65)	
IQR	0-37.74		0-19.03	
Sub-group	**Treg cells** ($CD4^+CD25^+FoxP3^+$)	**Non-Treg cells** ($CD4^+CD25^+FoxP3^-$)	**Treg cells** ($CD8^+CD25^+FoxP3^+$)	**Non-Treg cells** ($CD8^+CD25^+FoxP3^-$)
Median (range)	0.06 (0-4)	3.83 (0-74)	0 (0-0)	0.29 (0-71)
IQR	0-1.94	0-33.69	0-0	0-61.71

	CD4⁺ Non-Tregs						CD8⁺ Non-Tregs				
Sub-group	**Central memory T cells** (CD45RA⁻ CD27⁺)	**Effector memory T cells** (CD45RA⁻ CD27⁻)	**Naïve T cells** (CD45RA⁺ CD27⁺)	**Exhausted T cells** (CD45RA⁺⁺ CD27⁻)	**Terminal T cells** (CD45RA⁺ CD27⁻)		**Central memory T cells** (CD45RA⁻ CD27⁺)	**Effector memory T cells** (CD45RA⁻ CD27⁻)	**Naïve T cells** (CD45RA⁺ CD27⁺)	**Exhausted T cells** (CD45RA⁺⁺ CD27⁻)	**Terminal T cells** (CD45RA⁺ CD27⁻)
Days 7-8	*n = 6*	*n = 6*	*n = 6*	*n = 6*	*n = 6*		*n = 6*	*n = 6*	*n = 6*	*n = 6*	*n = 6*
Median (range) IQR	1.19 (0-171) 0-63.21	2.44 (0-31) 0-21.50	0.10 (0-315) 0-96.26	0 (0-6) 0-1.61	0.01 (0-36) 0-1.61		0.09 (0-12) 0-10.42	0 (0-7) 0-1.84	0.08 (0-58) 0-38	0 (0-2) 0-0.9	0.01 (0-4) 0-1.55

Values represent absolute cell concentrations (cells/μL); n represents number of samples.
CD: cluster of differentiation marker; *IQR:* inter-quartile range; *MAIT:* mucosal-associated T cell; *NK:* natural killer; *Treg:* regulatory T cell
*min-max range

Table 6.13a: Descriptive statistics for absolute cell concentrations of monocytic sub-groups: **Days 1-2 & 3-4**

Parent cell group	**Monocytes** ($CD45^+$)		
Sub-group	**$CD14^+$ cells**		**$CD14^-$ cells**
Days 1-2	*n = 30*		*n = 30*
Median (range)*	1.60 (0-74)		3.48 (0-847)
IQR	0.74-4.88		1.34-16.84
Sub-group	**Non-classical monocytes** ($CD14^+CD16^+$)	**Classical monocytes** ($CD14^+CD16^-$)	**$CD45^+$ microglia** ($TMEM119^+$)
Days 1-2	*n = 30*	*n = 30*	*n = 30*
Median (range)	0.94 (0-36)	0.37 (0-31)	1.62 (0-127)
IQR	0.20-3.33	0.17-1.04	0.74-5.57

Parent cell group	**Monocytes** ($CD45^+$)		
Sub-group	**$CD14^+$ cells**		**$CD14^-$ cells**
Days 3-4	*n = 7*		*n = 7*
Median (range)	0.84 (0-4)		5.48 (0-180)
IQR	0.39-2.46		0.68-59.01
Sub-group	**Non-classical monocytes** ($CD14^+CD16^+$)	**Classical monocytes** ($CD14^+CD16^-$)	**$CD45^+$ microglia** ($TMEM119^+$)
Days 3-4	*n = 7*	*n = 7*	*n = 7*
Median (range)	0.35 (0-2)	0.17 (0-2)	0.57 (0-165)
IQR	0.21-1.31	0.07-0.56	0.44-43.52

Values represent absolute cell concentrations (cells/μL); n represents number of samples.
CD: cluster of differentiation marker; *IQR:* inter-quartile range
*min-max range

Table 6.13b: Descriptive statistics for absolute cell concentrations of monocytic sub-groups: **Days 5-6 & 7-8**

Parent cell group	**Monocytes** ($CD45^+$)		
Sub-group	**$CD14^+$ cells**		**$CD14^-$ cells**
Days 5-6	*n = 6*		*n = 6*
Median (range)*	0.30 (0-5)		2.29 (1-32)
IQR	0.17-4.68		1.78-20.55
Sub-group	**Non-classical monocytes** ($CD14^+CD16^+$)	**Classical monocytes** ($CD14^+CD16^-$)	**$CD45^+$ microglia** ($TMEM119^+$)
Days 5-6	*n = 6*	*n = 6*	*n = 6*
Median (range)	0.14 (0-5)	0.19 (0-3)	1.40 (1-10)
IQR	0.07-2.06	0.04-1.26	0.99-7.80

Parent cell group	**Monocytes** ($CD45^+$)		
Sub-group	**$CD14^+$ cells**		**$CD14^-$ cells**
Days 7-8	*n = 6*		*n = 6*
Median (range)	0.44 (0-2)		3.12 (0-23)
IQR	0.03-1		0.20-11.12
Sub-group	**Non-classical monocytes** ($CD14^+CD16^+$)	**Classical monocytes** ($CD14^+CD16^-$)	**$CD45^+$ microglia** ($TMEM119^+$)
Days 7-8	*n = 6*	*n = 6*	*n = 6*
Median (range)	0.23 (0-1)	0.08 (0-0)	1.07 (0-4)
IQR	0.01-0.81	0.02-0.26	0.12-3.66

Values represent absolute cell concentrations (cells/μL); n represents number of samples.
CD: cluster of differentiation marker; *IQR:* inter-quartile range
*min-max range

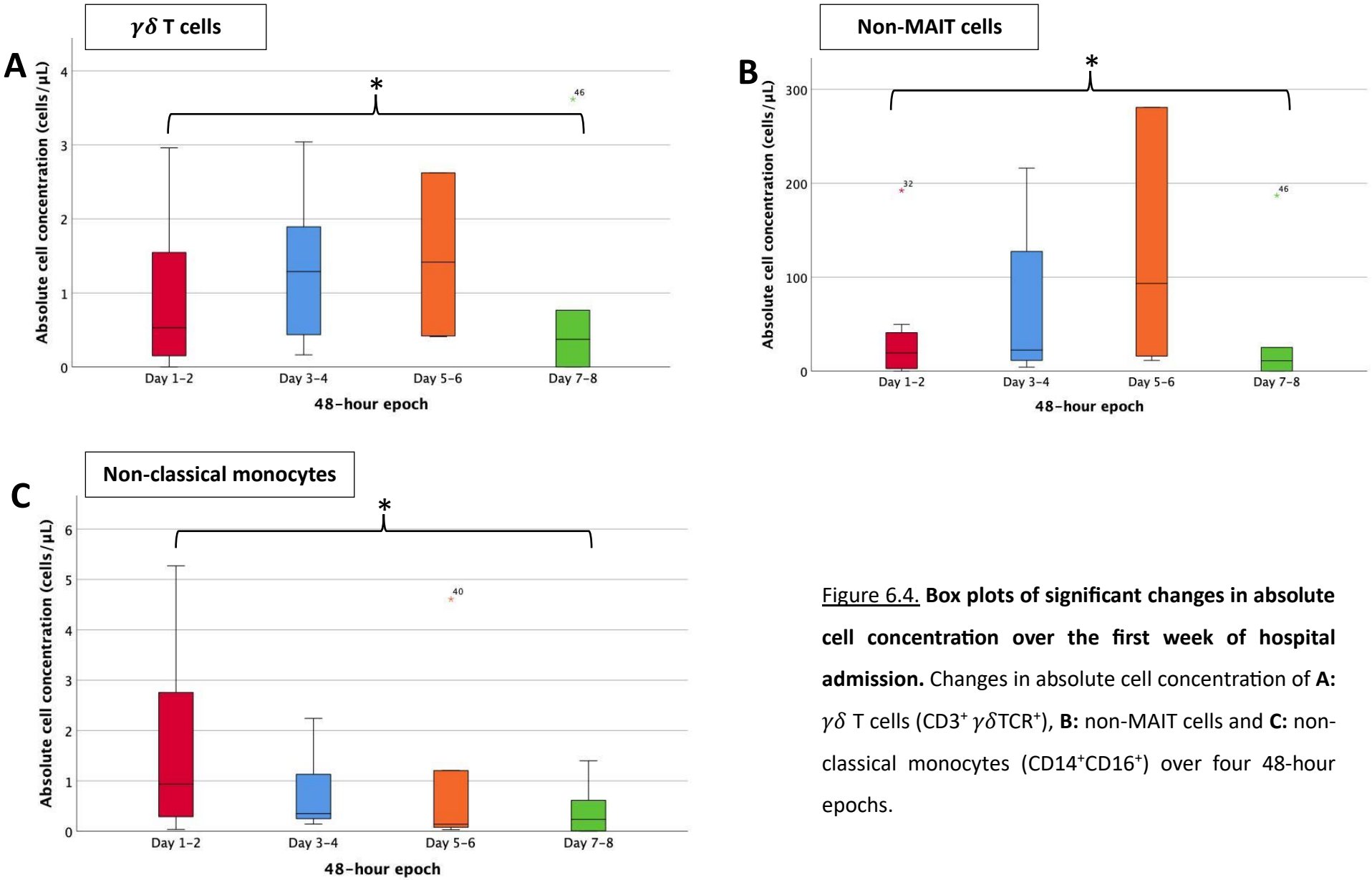

Figure 6.4. **Box plots of significant changes in absolute cell concentration over the first week of hospital admission.** Changes in absolute cell concentration of **A:** $\gamma\delta$ T cells ($CD3^+$ $\gamma\delta TCR^+$), **B:** non-MAIT cells and **C:** non-classical monocytes ($CD14^+CD16^+$) over four 48-hour epochs.

6.3 Luminex® Assay

Admission

The standard curves of the Luminex plates had median R^2 value of 0.878. Table 6.14 includes the lower limit of detection (LLOD) for all analytes for the two plates run, and the percentage of samples below this limit. Plate 2 included n=40 samples, whereas Plate 1 included n=24 samples (based on available wells as samples were run concurrently with other research samples), this may have contributed to the differential % of samples below the LLOD for MIP-1α and IL-1β.

Descriptive statistics for all twelve analytes in admission CSF are given in table 6.15. Overall the distribution of the cytokine concentrations was significantly different (*p = 0.000*), with IL-1Ra having the highest concentration (median conc. 4781.77pg/mL), followed by IP-10 (median 2279.50pg/mL) and MCP-1 (median 1604.76pg/mL) - Figure 6.5.

Table 6.9: Lower limit of detection (LLOD) for inflammatory analytes between the two Luminex® plates run

Analyte	Plate 1		Plate 2	
	LLOD	% samples <LLOD	LLOD	% samples <LLOD
MCP-1	463.68	0	210.03	0
IL-8	12.11	0	12.12	0
IP-10	9.38	0	13.3	0
MIP-1α	105.07	80	103.88	29.2
IL-1RA	208.29	0	231.75	0
IFN-γ	0.18	5	6.12	0
IL-6	2.45	0	3.8	0
IL-1β	0.24	60	0.79	29.2
TNF-α	1.18	0	2.6	4.2
IL-10	5.18	0	5.06	0
IFN-α	0.91	0	4.12	0
VEGF	5.74	0	6.45	0

Abbreviations: IFN: interferon; *IL*: interleukin; *IL-1Ra*: interleukin-1 receptor antagonist; *IP-10*: interferon-inducible protein 10; *LLOD:* lower limit of detection; *MCP-1*: monocyte chemoattractant protein-1; *MIP*: macrophage inflammatory protein; *TNF*: tumour necrosis factor; *VEGF*: vascular endothelial growth factor

Table 6.10: Descriptive statistics for admission inflammatory biomarkers

Marker	**MCP-1**	**IL-8**	**IP-10**	**IL-1Ra**	**IFN-γ**	**IL-6**	**TNF-α**	**IL-10**	**IFN-α**	**VEGF**	**IL-1β**	**MIP-1α**
Admission	*n = 30*	*n = 30*	*n = 30*	*n = 30*	*n = 30*	*n = 30*	*n = 30*	*n = 30*	*n = 30*	*n = 30*	*n = 30*	*n = 30*
Median	1604.76	277.16	2279.50	4781.77	167.33	284.04	28.73	21.11	3.17	118.45	0.52	0.01
Min	210.03	12.11	9.38	208.29	0.01	19.91	0.01	5.06	0.91	6.45	0.01	0.01
Max	6534.69	3328.24	3983.50	42313.60	1195.20	6835.00	235.19	513.81	24.78	472.65	286.80	746.71
p25	807.24	106.44	1213.57	1729.86	47.50	78.61	7.64	9.09	1.66	61.89	0.01	0.01
p75	2279.59	642.87	3056.54	23089.74	289.40	2217.21	53.83	334.71	11.03	168.19	32.46	246.72

Values reported as concentration (pg/mL).

Abbreviations: IFN: interferon; *IL*: interleukin; *IL-1Ra*: interleukin-1 receptor antagonist; *IP-10*: interferon-inducible protein 10; *max*: maximum; *MCP-1*: monocyte chemoattractant protein-1; *min*: minimum; *MIP-1α*: macrophage inflammatory protein; *p*: percentile; *TNF*: tumour necrosis factor; *VEGF*: vascular endothelial growth factor

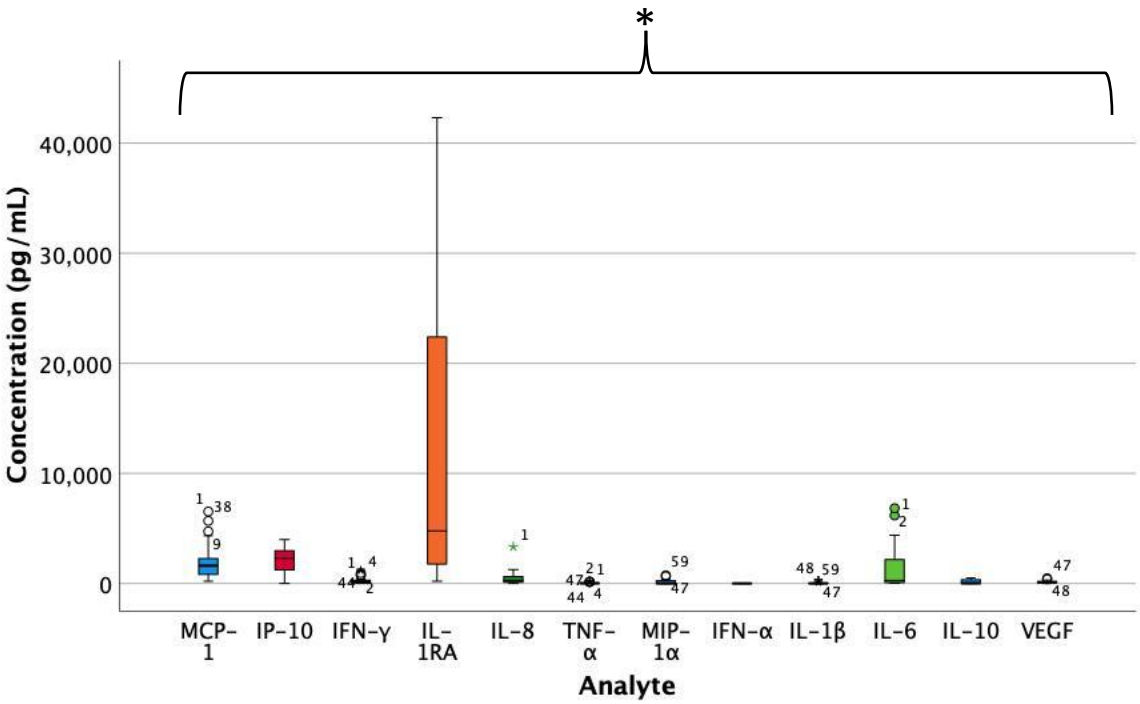

Figure 6.5. **Box plots of overall admission concentrations for all 12 inflammatory analytes.**

Temporal profile

Between days 1-2 and days 7-8, there were statistically significant decreases in IFN-γ (p = *0.046*), IP-10 (p = *0.046*), IFN-α (p = *0.043*) and IL-10 (p = *0.028*). Overall, analytes decreased in concentration between days 1-2 and days 7-8. Descriptive statistics for this first week are included in table 6.16, and a graphical demonstration of the significant changes over the time period is shown in figure 6.6.

Table 6.11: Descriptive statistics for inflammatory biomarkers: 48-hour epochs

Marker	MCP-1	IL-8	IP-10	IL-1Ra	IFN-γ	IL-6	TNF-α	IL-10	IFN-α	VEGF
Days 1-2	*n = 30*	*n = 30*	*n = 30*	*n = 30*	*n = 30*	*n = 30*	*n = 30*	*n = 30*	*n = 30*	*n = 30*
Median	1604.76	277.16	2279.50	4781.77	167.33	284.04	28.73	21.11	3.17	118.45
Min	210.03	12.11	9.38	208.29	0.01	19.91	0.01	5.06	0.91	6.45
Max	6534.69	3328.24	3983.50	42313.60	1195.20	6835.00	235.19	513.81	24.78	472.65
p25	807.24	106.44	1213.57	1729.86	47.50	78.61	7.64	9.09	1.66	61.89
p75	2279.59	642.87	3056.54	23089.74	289.40	2217.21	53.83	334.71	11.03	168.19
Days 3-4	*n = 9*	*n = 9*	*n = 9*	*n = 9*	*n = 9*	*n = 9*	*n = 9*	*n = 9*	*n = 9*	*n = 9*
Median	1622.44	342.92	2128.51	3632.93	126.82	285.68	15.70	11.48	3.17	84.90
Min	458.85	80.06	593.11	1377.87	36.06	76.43	3.86	8.45	0.91	68.98
Max	3895.78	1056.14	4260.74	15588.92	403.70	892.44	87.83	385.61	9.67	153.91
p25	546.68	170.02	1512.55	1957.10	66.35	101.54	11.34	9.22	2.04	69.43
p75	2843.34	775.54	2843.01	11503.82	190.49	574.22	65.22	259.92	8.35	144.47
Days 5-6	*n = 6*	*n = 6*	*n = 6*	*n = 6*	*n = 6*	*n = 6*	*n = 6*	*n = 6*	*n = 6*	*n = 6*
Median	1604.40	189.30	1176.30	1334.07	46.96	86.83	12.28	12.86	2.04	56.27
Min	418.16	57.92	511.06	337.92	12.36	4.25	2.48	5.18	0.91	26.71
Max	2475.63	566.75	2353.85	7850.54	112.93	354.87	46.24	252.81	6.53	193.68
p25	1145.34	92,92	601.62	767.28	24.83	44.00	3.65	6.84	1.47	31.91
p75	2131.12	439.79	2247.54	4052.44	81.58	194.86	33.29	221.93	6.07	116.22
Days 7-8	*n = 6*	*n = 6*	*n = 6*	*n = 6*	*n = 6*	*n = 6*	*n = 6*	*n = 6*	*n = 6*	*n = 6*
Median	1258.50	130.96	896.69	1371.92	28.98	63.81	10.28	6.31	1.66	110.62
Min	996.26	21.22	51.98	288.73	0.18	2.45	1.61	5.18	0.91	5.74
Max	1520.30	1259.92	2122.97	7198.81	205.33	1021.13	18.16	263.79	7.15	155.36
p25	1045.15	61.23	140.60	579.99	5.72	4.66	2.26	6.03	0.91	41.94
p75	1406.65	482.94	2050.01	7190.63	85.71	512.05	15.21	129.81	3.03	126.90

Values reported as concentration (pg/mL). *IFN*: interferon; *IL*: interleukin; *IL-1Ra*: interleukin-1 receptor antagonist; *IP-10*: interferon-inducible protein 10; *max*: maximum; *MCP-1*: monocyte chemoattractant protein-1; *min*: minimum; *p*: percentile; *TNF*: tumour necrosis factor; *VEGF*: vascular endothelial growth factor. Values below the LLOD for the respective analytes were given a value of 0.01; MIP-1α & IL-1β excluded because values mostly <LLOD.

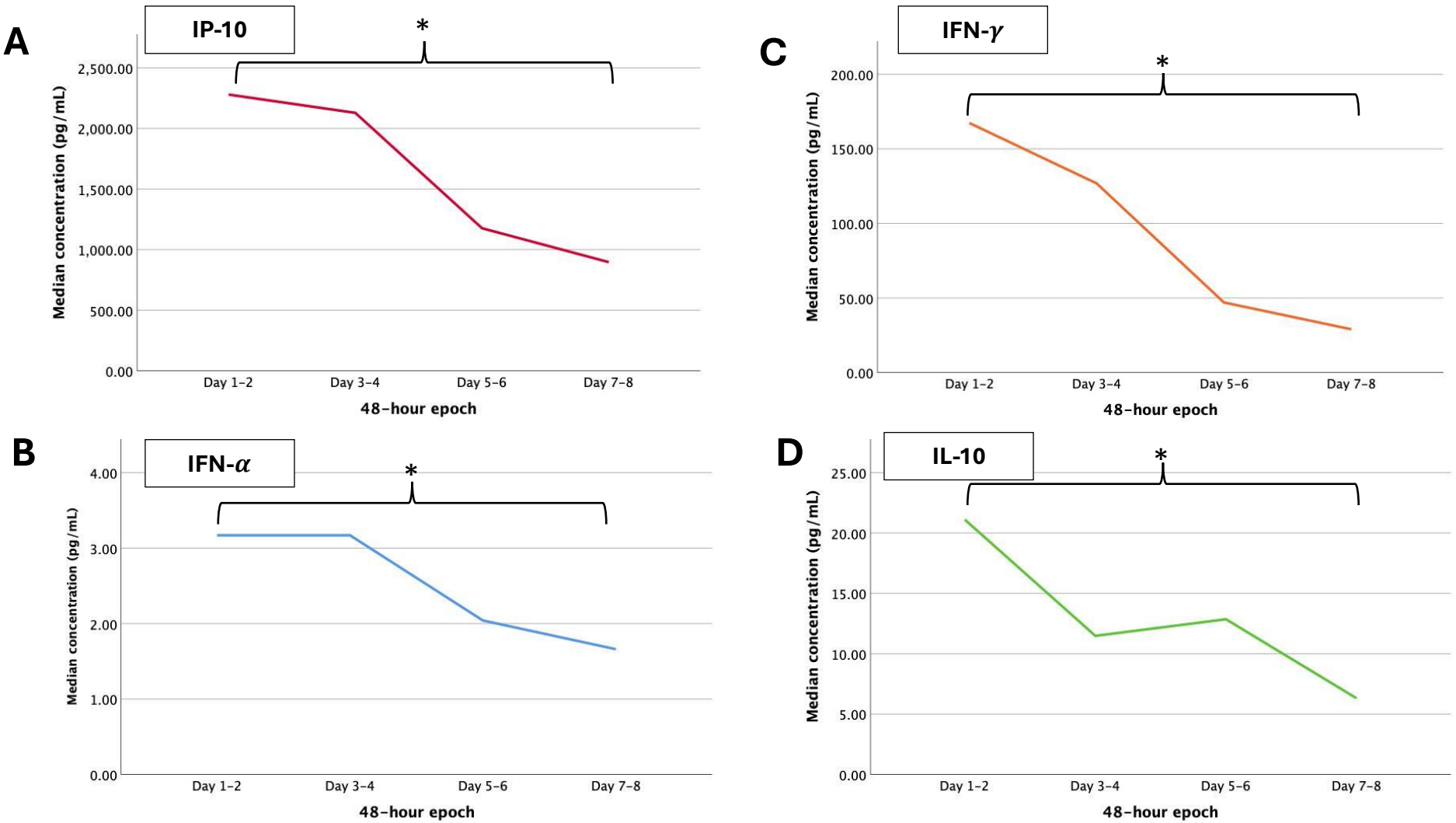

Figure 6.6. **Significant changes in analyte concentration over the first week of hospital admission**. Line graphs showing change in median concentration of **A:** IP-10, **B:** IFN-α, **C:** IFN-γ and **D:** IL-10 over four 48-hour epochs.

6.4 Correlations

6.4.1 Cell proportions

Correlations between immune cell proportions and inflammatory cytokines on admission and days 7-8 are shown in table 6.17.

Table 6.12: Correlation coefficients for significant correlations between immune cell proportions and inflammatory cytokines: Admission (**A**) & Days 7-8 (**B**)

A

Analyte	**MCP-1**	**IL-8**	**IP-10**	**IL-1Ra**	**IFN-γ**	**IL-6**	**TNF-α**	**IL-10**	**IFN-α**	**VEGF**
Admission	*n = 30*	*n = 30*	*n = 30*	*n = 30*	*n = 30*	*n = 30*	*n = 30*	*n = 30*	*n = 30*	*n = 30*
Cell type										
Lymphocytes			0.364							
Granulocytes			0.559	0.454		0.507	0.444	0.535	0.484	0.479
Neutrophils						0.372		0.404	0.413	0.362
Monocytes			0.379					0.384		0.413
$CD14^+$										-0.396
NC monocytes						0.440			0.371	0.429
C monocytes						-0.472			-0.396	-0.462
NK cells					0.490	0.476	0.470		0.396	
Non-B cells			0.620		0.4					
Gd T cells							0.393			
$CD4^+$ T cells										-0.443
CD4 Tregs					0.463					
$CD8^+$ T cells						0.368	0.441		0.397	0.372
Reactive astrocytes	0.363				0.369					

Moderate positive correlation Moderate negative correlation Strong positive correlation

C: classical; *CD:* cluster of differentiation marker*; IFN*: interferon; *IL*: interleukin; *IL-1Rα*: interleukin-1 receptor antagonist; *IP-10*: interferon-inducible protein 10; *MCP-1*: monocyte chemoattractant protein-1; *NC:* non-classical; *NK:* natural killer; *TNF*: tumour necrosis factor; *VEGF*: vascular endothelial growth factor.

Values represent correlation coefficients; n represents number of samples.
Weak correlation = 0.1 – 3.9; moderate correlation = 0.4 – 0.59; strong correlation = 0.6 – 1[202].

B

Analyte	MCP-1	IL-8	IP-10	IL-1Ra	IFN-γ	IL-6	TNF- α	IL-10	IFN-α	VEGF
Days 7-8	*n = 6*	*n = 6*	*n = 6*	*n = 6*	*n = 6*	*n = 6*	*n = 6*	*n = 6*	*n = 6*	*n = 6*
Cell type										
Granulocytes					0.943					
Neutrophils	0.829		0.943							
Monocytes		0.829		0.829		0.829				0.886
NK cells				0.829		0.829	0.829	0.880		0.886
Gd T cells										
$CD4^+$ T cells									0.939	
MAIT cells									0.939	
Astrocytes									0.926	
Reactive astrocytes	0.886	0.943								
$CD45^+$ microglia										-0.829
$CD45^-$ microglia					-1					

Strong positive correlation Strong negative correlation

CD: cluster of differentiation marker*; IFN*: interferon; *IL*: interleukin; *IL-1Ra*: interleukin-1 receptor antagonist; *IP-10*: interferon-inducible protein 10; *MAIT:* mucosal-associated invariant T cells; *MCP-1*: monocyte chemoattractant protein-1; *NK:* natural killer; *TNF*: tumour necrosis factor; *VEGF*: vascular endothelial growth factor.

Values represent correlation coefficients; n represents number of samples.
Weak correlation = 0.1 – 3.9; moderate correlation = 0.4 – 0.59; strong correlation = 0.6 – 1.

6.4.2 Absolute cell concentrations

As with cell proportions, correlations between cell concentrations and inflammatory analytes were assessed in admission samples and samples during days 7-8. The number of significant correlations demonstrated by most cells once again decreased over time, with an increase in the strength of significant correlations. Table 6.18 depict these changes.

Table 6.13 Correlation coefficients between absolute immune cell concentrations and inflammatory cytokines: Admission (**A**) & Days 7-8 (**B**)

A

Analyte	**MCP-1**	**IL-8**	**IP-10**	**IL-1Ra**	**IFN-γ**	**IL-6**	**TNF-α**	**IL-10**	**IFN-α**	**VEGF**
Admission	*n = 23*	*n = 23*	*n = 23*	*n = 23*	*n = 23*	*n = 23*	*n = 23*	*n = 23*	*n = 23*	*n = 23*
Cell type										
Lymphocytes		0.49		0.419		0.528	0.467	0.418		
$CD3^+$		0.479		0.422		0.528	0.458			
$CD3^-$										
Granulocytes				0.529		0.561		0.648	0.688	0.486
Neutrophils	-0.502	0.436		0.527				0.646	0.646	0.538
Monocytes	-0.485			0.527				0.653	0.483	0.475
$CD14^+$	-0.559							0.498	0.5	
CD14-	-0.453		0.444	0.558			0.47	0.676	0.426	0.477
NC monocytes	-0.466			0.433		0.648		0.483	0.526	
C monocytes								0.414		
NK cells		0.431	0.441		0.482	0.459	0.475			
Non-B cells								0.433		
Gd T cells			0.438	0.501		0.640	0.481			0.427
$CD8^+$ T cells		0.537		0.501			0.512	0.492		0.499
$CD4^+$ T cells		0.452								
CD4 Tregs					0.515		0.458			
MAIT cells						0.601				0.471
Non-MAIT cells		0.499				0.518	0.452			
$CD45^+$ microglia	-0.416	0.464		0.489		0.514	0.436	0.662	0.45	0.482

Moderate positive correlation Moderate negative correlation Strong positive correlation

C: classical; *CD:* cluster of differentiation marker*; IFN*: interferon; *IL*: interleukin; *IL-1Ra*: interleukin-1 receptor antagonist; *IP-10*: interferon-inducible protein 10; *MCP-1*: monocyte chemoattractant protein-1; *MAIT:* mucosal-associated invariant T cells; *NC:* non-classical; *NK:* natural killer*; TNF*: tumour necrosis factor; *VEGF*: vascular endothelial growth factor. Values represent correlation coefficients; n represents number of samples. Weak correlation = 0.1 – 3.9; moderate correlation = 0.4 – 0.59; strong correlation = 0.6 – 1.

B

Analyte	MCP-1	IL-8	IP-10	IL-1Ra	IFN-γ	IL-6	TNF-α	IL-10	IFN-α	VEGF
Days 7-8	*n = 6*	*n = 6*	*n = 6*	*n = 6*	*n = 6*	*n = 6*	*n = 6*	*n = 6*	*n = 6*	*n = 6*
Cell type										
Lymphocytes										
CD3+		0.812							0.814	
Granulocytes								0.82		
Neutrophils		0.886	0.886	0.829		0.829	0.829	0.82		
$CD14^+$								0.82		
CD14-								0.88		0.943
NC monocytes								0.82		
C monocytes		0.829								
NK cells								0.893		
B cells			0.829							
Activated B cells			0.829							
Gd T cells				0.812		0.812	0.812			
$CD4^+$ T cells				0.812		0.812	0.812			
CD4 Tregs				0.812		0.812	0.812			
MAIT cells									0.939	
Non-MAIT cells				0.812		0.812	0.812			
Reactive Astrocytes		0.943						0.82		
Astrocytes									0.926	
$CD45^+$ microglia								0.88		0.943

Moderate positive correlation Moderate negative correlation Strong positive correlation

C: classical; *CD:* cluster of differentiation marker*; IFN*: interferon; *IL*: interleukin; *IL-1Ra*: interleukin-1 receptor antagonist; *IP-10*: interferon-inducible protein 10; *MCP-1*: monocyte chemoattractant protein-1; *MAIT:* mucosal-associated invariant T cells; *NC:* non-classical; *NK:* natural killer*; TNF*: tumour necrosis factor; *VEGF*: vascular endothelial growth factor. Values represent correlation coefficients; n represents number of samples. Weak correlation = 0.1 – 3.9; moderate correlation = 0.4 – 0.59; strong correlation = 0.6 – 1.

6.5 TBM vs. Other Infections

6.5.1 Cell proportions & concentrations

In comparison to patients with non-TB brain infections, on admission TBM patients had significantly higher proportions of $CD4^+$ regulatory T cells ($p = 0.001$), $CD8^+$ regulatory T cells ($p = 0.013$), astrocytes ($p = 0.002$) and reactive astrocytes ($p = 0.004$), shown in figure 6.7. Patients with non-TB brain infections had significantly higher concentrations of granulocytes ($p = 0.011$), neutrophils ($p = 0.008$) and $CD14^+$ cells ($p = 0.038$) – figure 6.8. Graphs including outliers can be found in Appendix B. There were no significant difference in cell proportions or counts over time.

6.5.2 Luminex® analysis

Admission

TBM patients had higher concentrations of MCP-1 ($p = 0.007$) and IFN-γ ($p = 0.003$) on admission, are graphically represented in figure 6.8D. This was consistent at days 7-8 ($p = 0.009$ and $p = 0.002$ respectively). However, concentrations of MIP-1α ($p = 0.029$) and VEGF ($p = 0.043$) were significantly higher in other infections samples.

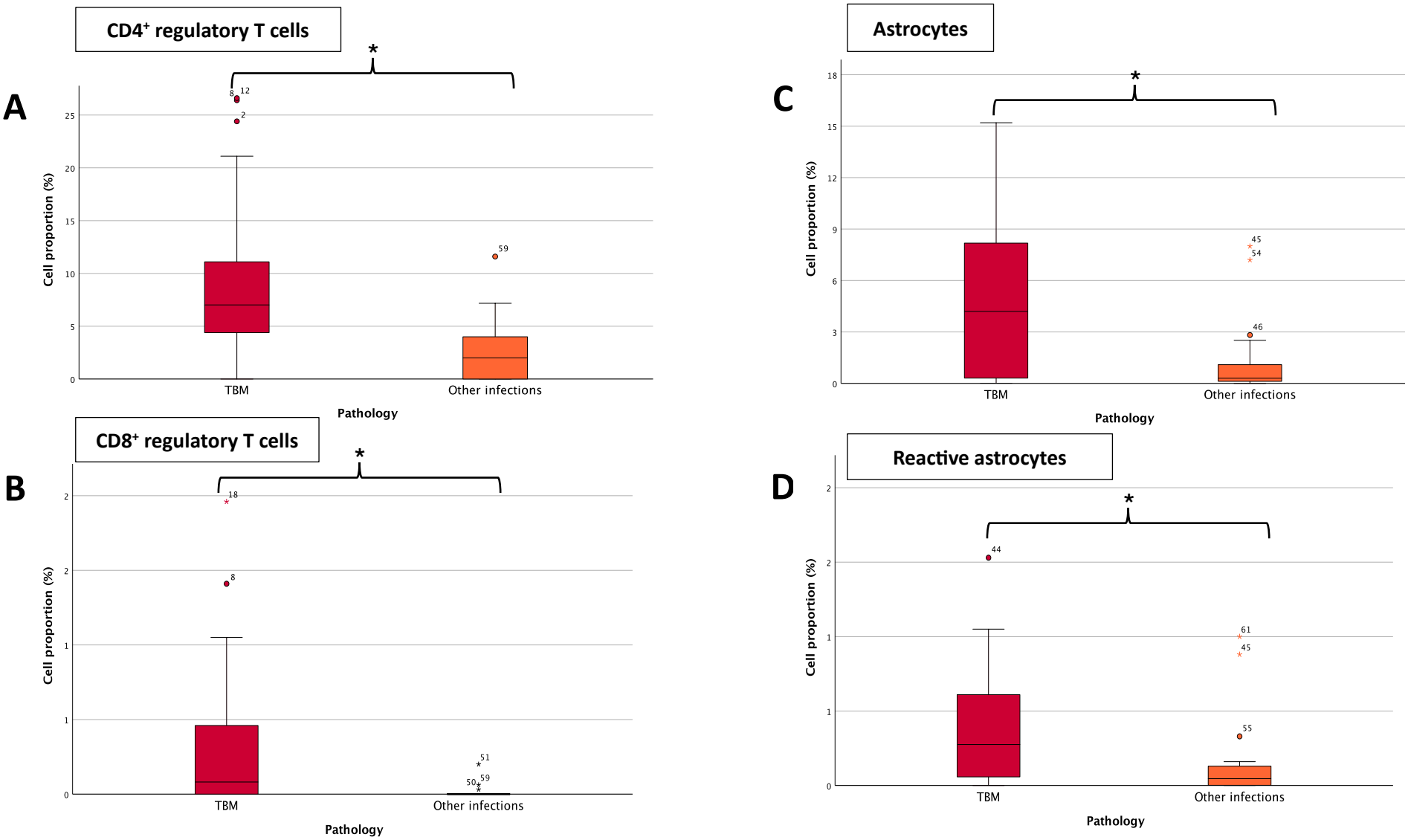

Figure 6.7. **Box plots of significant differences in admission cell proportions between TBM and other brain infections. A:** Cell proportions of $CD4^+$ regulatory T cells ($CD3^+CD4^+$). **B:** Cell proportions of $CD8^+$ regulatory T cells ($CD3^+CD8^+$). **C:** Cell proportions of astrocytes ($CD45^-ACSA^+$). **D:** Cell proportions of reactive astrocytes ($ACSA^+GFAP^+$).

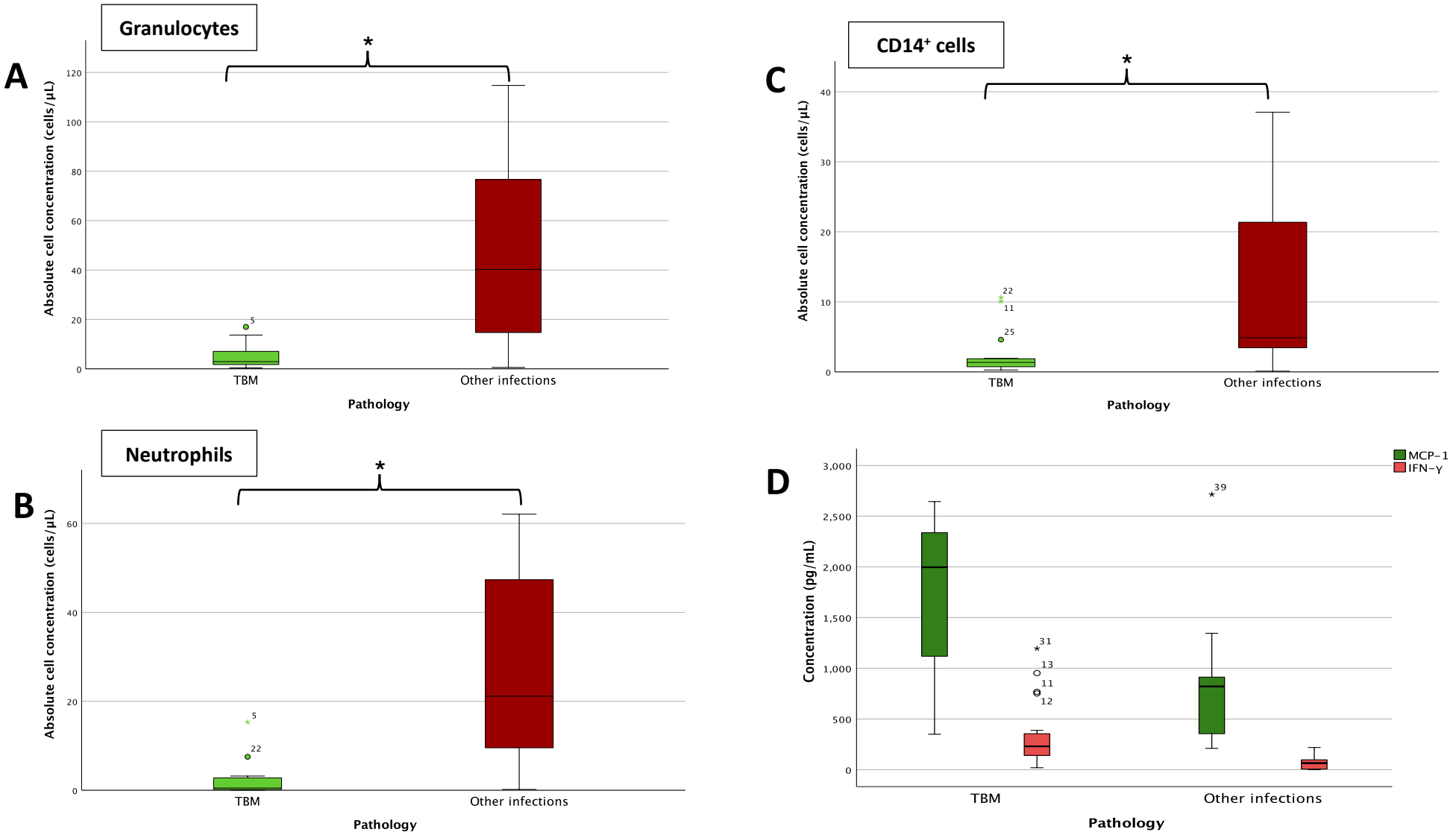

Figure 6.8. **Box plots of significant differences in absolute cell & analyte concentration between TBM and other brain infections, upon admission. A:** Absolute concentration of granulocytes ($CD45^+$). **B:** Absolute concentration of neutrophils ($CD11b^+CD16^+$). **C:** Absolute concentration of $CD14^+$ cells. **D:** Analyte concentrations of MCP-1 and IFN-γ.

Chapter 7 – Discussion

7.1. Brain-resident immune cells

This is the first study, to our knowledge, to examine brain resident cells, particularly microglia using the highly-specific marker TMEM119, together with an extensive panel of peripheral immune cells using flow cytometry in antemortem ventricular CSF in paediatric patients with CNS infections. $CD45^{-}$ microglia accounted for the highest cell proportion and concentration in ventricular CSF of the major cell populations – lymphocytes, granulocytes, monocytes and astrocytes. This was a noteworthy result given that leukocytes routinely serve as markers of inflammation in CNS infections and are the only cell types reported by clinical laboratories, although microglia are known as the primary CNS-resident innate immune cells[203,204]. These results imply that brain-resident immune cells likely play the largest role in the immune response to CNS infection, but that their contribution to the pathophysiology of CNS infections may be under-appreciated relative to the peripheral immune response. Clinical decision-making and interventional research studies concerning disease progression and resolution do not currently consider these cell types and rely on what we have arguably shown to be the minority of immune cells involved (as demonstrated by their decreased presence in the CSF) in CNS infection.

The presence of microglia in the CSF is not commonly considered, and therefore observing them as the majority cell population present raises important questions about their activity, movement and function. The persistence of the high microglial concentrations even after the admission sample argues against the possibility that the insertion of the ventricular catheter was the source of the microglial population. As alluded to in Chapter 2, the CNS is commonly deemed more immunologically quiescent than peripheral organs, due to strict control of peripheral immune cell influx by a tight BBB, low numbers of surveilling peripheral immune cells and the absence of a typical lymphatic system[119]. The data from this study, along with recent studies that the brain possesses a glymphatic system[205], add to the growing understanding that this organ may not be as immunologically quiescent as was originally thought.

Microglia may take on neuroprotective (restorative) or neuropathophysiological roles during infection[206,207]. As with peripheral innate immune cells, resting microglia are activated through recognition of pathogenic or pro-inflammatory stimuli such as lipopolysaccharide, myeline debris or certain cytokines[203,208,209]. Similar to peripheral macrophages, microglia are capable of proliferation, phagocytosis, antigen presentation, chemotaxis and cytokine release[208]. Reactive microglia are believed to contribute to the pathophysiology of neuroinflammation and thus brain infections[204], as their phagocytic activity is significantly increased in this activated state[209]. Their release of pro-inflammatory mediators such as TNF-α and IL-6 induces astrogliosis, increases the permeability of brain endothelium and contributes to breakdown of the BBB[204,210]. Recruitment by activated microglia of peripheral leukocytes and activation of adaptive immune cells through antigen presentation further solidifies their role as primary innate immune cells of the brain[208]. But this may also contribute to pathophysiology in the brain, as increased BBB permeability, leakage and leukocyte recruitment may contribute to downstream injury mechanisms like raised intracranial pressure and cytotoxic oedema, which could lead to brain damage and neuronal cell death[204].

In the same vein, activated microglia may also take on a more anti-inflammatory and neuroprotective (M2) phenotype[204]. In this case, microglia demonstrate an immunoregulatory role through phagocytosis of cellular debris, release of anti-inflammatory mediators and release of neuroprotective factors[204,208,209]. Taken together, it is evident that microglia are an important innate cell group in the initiation and possibly resolution of brain inflammation and infection. This is likely to manifest in their high initial and sustained concentrations in the admission and serial samples respectively of this patient cohort.

It is also important to consider that this was a population of young patients still undergoing brain development. Microglia demonstrate a crucial role in neurodevelopment through synaptic pruning and maturation of neural circuitry[70,206]. Entering the brain during early developmental stages, microglia serve as constant surveyors of the brain parenchyma and are rapid first responders in the case of injury and important contributors to maintaining homeostasis across the lifespan[206]. [206,207] It is therefore paramount to holistically consider their role in both the healthy and diseased CNS, particularly in the context of the developing brain.

We found an unexpected microglial cell population that express CD45 ($CD45^{+}TMEM119^{+}$), resembling both brain specific microglia as well as peripheral monocytes. Recent research has examined the origins of microglia from macrophage (myeloid) precursors, particularly from bone-marrow-derived monocytes, and their migration into the CNS[207]. *In vitro* murine experiments have demonstrated that in the case of bacterial CNS infection, such as meningitis caused by *Streptococcus pneumoniae*, monocytes in the bloodstream can engraft into the brain, differentiate into microglia and contribute to the neuroinflammatory response (including post-infectious tissue damage and pathology)[211]. These newly formed microglia were particularly dominant after the acute phase of the infection had passed, and appeared to be incorporated into the circulating microglial popultion[211]. Evolution of these cells into neurons or astrocytes does not occur, as shown in these murine experiments by staining with a microglia-specific fluorescent marker (Iba-1) and a macrophage-specific fluorescent marker (F4/80)[211]. Research using animal models depleted in microglia also demonstrate that microglia can be replenished through the infiltration of peripherally derived bone-marrow cells which become "microglial-like" in their morphology and dynamics[206]. Interestingly they appear to maintain a distinct genetic profile, and ongoing research in our group aims to conduct single cell RNA-sequencing on this cell population to further characterise them. While a very intriguing population, the absolute concentration of these cells was small, and thus caution in overinterpreting the data is warranted.

We demonstrated that the predominance of microglial cells does not appear to be reflective of surveillance alone, as both microglial and peripheral immune cell proportions decreased over time. This suggests that the high proportions of microglia seen in samples (particularly at early time points) reflect an active immune response. Given the relatively small numbers of samples after admission, conclusions about the temporal profile of these cells is tenuous, as the collection and timing of serial samples may have been biased by clinical imperatives. However, the progression or resolution of an immune response is clinically determined by the change in immune cell counts in serial samples, and therefore examining resident and peripheral immune cells in these samples was relevant. It is noteworthy that overall there was an increase in microglial proportions and absolute concentrations over time. Although this was not significant, this was different from the temporal patterns of other important immune cells, such as lymphocytes, which decreased in proportion over time, and while their absolute

concentration increased (again not significant), their rate of increase was not as great that of microglia.

Astrocytes, the other CNS-resident immune cell population, constituted a very small proportion and concentration of cells in comparison. This is likely because they are not the primary CNS-resident immune cell and their role is more structural and supportive. However, it is noteworthy that absolute astrocytic concentrations accounted for larger concentrations than monocytes and granulocytes. Astrocytes are known to be recruited to assist in the immune response, and evidence of their activation has been reported in previous studies examining the biomarker GFAP in TBM and other forms of meningitis[139].

7.2 Peripheral immune cells

On admission lymphocytes were significantly greater in proportion and concentration than monocytes and granulocytes. Considering that two thirds of the patient cohort were TBM patients, this was not unexpected given the association between TBM and lymphocytosis[21]. $CD3^+$ cells demonstrated a higher – albeit non-significant – cell proportion and concentration than $CD3^-$ cells. $CD3^+$ cells give rise to non-MAIT cells and ultimately helper ($CD4^+$) T cells and cytotoxic ($CD8^+$) T cells (Figure 5.2N). The recruitment of T cells and B cells into the CNS and therefore the elevation of lymphocytes on admission could be accounted for by the chemotactic capabilities of both microglia and astrocytes[212,213]. Upon activation through antigen presentation, $CD4^+$ T cells proliferate and differentiate into regulatory T cells (T_{reg}) or T-helper (T_H) cells specific to the offending pathogen[214]. The subsequent inflammatory mediators released from these cells, such as cytokines, are also specific to the offending pathogen[214].

On the other hand, $CD8^+$ T cells are cytotoxic, meaning that after activation they will kill the infected cell[214,215]. Cytotoxic T cells also release cytokines along with cytotoxic granules, both of which are known to induce apoptosis of the infected cell[212]. Taking into account that T cells are a hallmark population of any adaptive immune response and necessary for optimal clearance of a pathogen[215] and the lymphocytic predominance in TBM patients[21], it is not surprising that $CD3^+$ and non-MAIT cells are important peripheral cell populations in the context of CNS infection and neuroinflammation.

We included markers of T_{reg} cells to ascertain whether a predominance of regulatory vs non-regulatory cells is a potential mediator of paediatric vulnerability to CNS infection, given the suggested contribution of these regulatory cells towards "immaturity" of a child's immune system[216]. These cells constitute between 3-10% of all $CD4^+$ T lymphocytes in humans [160–162], and are primarily derived from cells in the thymus [162,217]. *In vitro* murine experiments and *in vivo* observations have elucidated the suppressive and anergic nature of T_{Reg} cells – enabling them to mediate and maintain immune tolerance, demonstrate immunomodulatory properties, and protect the body against autoimmunity [162,218]. As outlined by O'Garra *et al.*, these cells are capable of preventing naïve T cell expansion and proliferation through secretion of cytokines such as IL-10 and transforming growth factor (TGF)-β[160,217]. Other proposed mechanisms involve the direct killing of antigen-presenting cells (APCs) and pathogenic cells at the site of inflammation through cell-to-cell contact [160,161,218], along with prevention of migration of other peripheral immune cells [161]. The $CD4^+$ T_{Reg} cells identified in this study are classified as $CD4^+FoxP3^+CD25^+$ T_{Reg} cells (figure 5.2O) – also known as naturally occurring T_{Reg} cells [160,161]. Ultimately, these cells have been characterised to regulate autoimmunity and inflammation [160]. We also identified $CD8^+$ T_{Reg} cells, which employ the same suppressive cytokines to control the host's excessive immune responses as $CD4^+$ T_{Reg} cells [216,219]. Their functions also include suppressing activated T cells at the site of inflammation, keeping autoimmune diseases at bay and regulating immune tolerance in a healthy individual [219,220]. The low proportion and numbers of these regulatory cells does not appear to suggest a role in immune vulnerability to CNS infection or a strong contribution to immunomodulation, but this is a small study across a broad age range (given rapid immune change and development in the early years of life) and further work is required to make conclusive statements.

$\gamma\delta$ T cells are typically a minor subset of $CD3^+$ cells[221], which is mirrored in this study population's concentrations and proportions. Capable of a rapid response to a wide range of stimuli[221,222], there is generally an increase in their number a few days after the onset of infection[222]. Therefore, the significant decrease in $\gamma\delta$ T cells we observed over time could suggest resolution of the inflammatory response. Exhausted and terminal T cells were included in this study to observe whether the immune response had been ongoing for some time and possibly reaching its end. The low numbers for these cell types, however, suggest that this was

not the case. However, as stated, this was a small study, and these cell numbers were small, therefore our conclusions are limited.

Considering $CD4^+$ T cells vs $CD8^+$ T cells, there was a greater proportion and concentration of non-MAIT cells that were $CD4^+$. A possible explanation for this is the specific role of $CD8^+$ T cells in clearing CNS infections caused by intracellular pathogens such as viruses[212,223], whereas there were no viral infections in this study. Intriguingly, infiltrating T cells have been shown to activate microglial cells and are capable of modulating a more secretory or phagocytic microglial phenotype[213]. Activated $CD4^+$ T cells in particular are believed to enhance microglial antigen presentation in the context of infection and are important in orchestrating a protective immune response [213,224]. The interrelated roles of T-cell chemotaxis to the CNS by microglia and subsequent modulation of microglial activation by activated T cells demonstrates the complex interplay between the various components of the immune response in CNS infections. Whether the roles of $CD4^+$ and $CD8^+$ cells described above may have contributed to the finding that $CD4^+$ cells were almost 50% central memory T cells whereas $CD8^+$ cells were more than 50% naïve T cells, is unclear.

Of the monocyte-derived cells, classical monocytes accounted for a minority of $CD14^+$ cells, of which the larger proportion and concentration were non-classical monocytes. This is surprising, given that non-classical monocytes are considered to be patrolling, resident cells whereas their commonly reported more numerous classical counterparts are known to be more involved in the inflammatory response and promote tissue repair[225–227]. Non-classical monocytes, however, are responsible for stimulating and inducing proliferation in $CD4^+$ T cells[225]. It is possible that these cells may have contributed to the greater number of $CD4^+$ T cells vs $CD8^+$ T cells mentioned earlier, but this is purely conjecture.

In acute neuroinflammatory states, there is rapid chemotaxis of monocytes migrating from the bloodstream into the brain, followed by differentiation into innate immune responders – such as macrophages or dendritic cells[225,227], with the aim to prevent extensive spread of the pathogen and subsequent pathology[225]. The same can be said for granulocytes and their sub-group of neutrophils. The relatively low numbers of these cell populations seen on admission and their decline over the first week of treatment likely indicate a subsiding innate phase of

the immune response, giving way to a more prominent adaptive immune response. The increase in lymphocyte numbers correlates with this, and as alluded to previously is likely a reflection of lymphocytosis in the predominant TBM patient cohort. Neutrophils are known to be important cells in adult TBM, where patients are often co-infected with HIV[228], however, this is not the case in children. The overall decreasing trend in cell concentrations could be suggestive of resolving inflammation. Case illustrations of patients 34 and 38 mirror this, where their clinical improvement showed decreasing cell and cytokine concentrations.

7.3 Inflammatory analyte changes

On admission, the highest analyte concentration detected was that of IL-1Ra, followed by IP-10 and MCP-1. These cytokines are not as well described in the TBM literature as TNF-α and IFN-γ. It is possible that the difference may be explained by the ventricular nature of the CSF in this study compared to the lumbar spine source of CSF in most other studies. It is noteworthy that high MCP-1 concentrations persisted over time, whereas that of Il-1Ra and IP-10 significantly decreased. The persistence of MCP-1 was similar to the persistence of microglial concentrations, although there was no clear correlation demonstrated between the two. MCP-1 is one of the most abundant cytokines detected by our group in the brain, including in brain interstitial fluid[229]. Synthesized by microglia and astrocytes, it promotes chemotaxis of innate and adaptive cells into the CNS[174,175] while also potentially compromising the BBB and generating reactive oxygen species[176]. In a small study from our group, this analyte was associated with mortality and stroke in TBM patients[229]. Negative associations were found between MCP-1 and concentrations of numerous peripheral immune cells, suggesting that they were not the likely source of this cytokine. IP-10 similarly participates in chemotaxis with high CSF concentrations in neuroinflammatory conditions[179,180]. Both peripheral and brain-derived cells release IP-10, and it is known to be elevated in neuro-inflammatory conditions[179]. The high concentrations on admission suggest a pro-inflammatory milieu.

It is interesting that a high concentration of the anti-inflammatory, immunomodulatory cytokine IL-1Ra was also observed on admission, suggesting a simultaneous immunomodulatory mileu[147,148]. IL-1Ra is a well-known antagonist of the IL-1 receptor – a pro-inflammatory cytokine. The ratio of IL-1β and IL-1Ra is considered an important indicator of

disease severity[230], however, IL-1β is notoriously difficult to detect in CSF with Luminex analysis[231]. Therefore, we were not able to assess this ratio and postulate its significance in disease severity. The inverse increase in IL-1RA and decrease in IP-10 over time suggests that immunoregulatory mechanisms were likely at play. In conjunction with IL-1β, low concentrations of MIP-1α were found, which may indicate poor detection of this analyte by the kit or low presence of the analyte itself. Helmy *et al.* (2011) have also found IL-1β concentrations to be low[231]. This could correlate with and account for the low concentrations of neutrophils, given its role in recruitment of neutrophils to the CNS and its synthesis by neutrophils[178].

Once again, the low sample numbers warrant caution in the interpretation of serial cytokine data – as was the case with cell populations. Overall, most cytokine concentrations did not change significantly. The demonstrated decreasing trend in concentration was suggestive of resolving inflammation.

7.4 Correlations

Correlations between cells and cytokines were conducted to explore whether certain populations of cells may be accounting for certain cytokine concentrations. As shown by the correlation data, there were several (largely weak) correlations. This is likely indicative of the fact that multiple cells secrete multiple cytokines, as is reported across the literature. Additionally, this suggests that immune cells and downstream immune mediators co-exist in an elaborately orchestrated immune response. Arguably there may be differences in how cells and cytokines inter-relate in different conditions; therefore, analysing the TBM and Other Infection groups (with larger sample numbers) separately may yield different findings.

Given that the start of an infection is difficult to predict, the temporal phase of the immune response is difficult to determine. At day 7-8 the correlations were strong, which could reflect an overall decreasing trend across immune cells and mediators over time. However, as sample numbers were low (n = 6) we are cautious not to over-interpret the data. The differential direction between correlations of classical versus non-classical monocyte proportions and immune mediators was an interesting and unique correlation. This could be explained by the

fairly different roles exhibited by classical (inflammatory) and non-classical (resident, patrolling) monocytes as alluded to above[225–227].

7.5 TBM vs. other infections

Although comparisons were made between patients with TBM and patients with other infections (OI) of the brain, the results are exploratory. This is because the OI group was small and heterogenous, and it is thus difficult to comment on the degree to which different pathogens result in differential cell and cytokine profiles in CSF of patients with CNS infections. This study aimed to encompass more brain infections than TBM, however, the fact that most of the patient cohort had TBM reflects our local disease burden of TB – with TBM being the commonest cause of meningitis in our province and a common indication for neurosurgical prcoedures[232]. It is also noteworthy that most of the patients who died were TBM patients. We are unable to say what the impact of death was on cell and cytokine concentrations; the low mortality rate did not warrant comparison across mortality as this was a descriptive study that was not powered to examine outcome.

Bearing in mind the limitation of comparison between the groups, there were a few differences that suggest further study would be meaningful. As expected, the lymphocytic predominance in TBM patients (likely driven by the $CD4^+$ and $CD8^+$ predominance in this group), versus the granulocytic and monocytic ($CD14^+$) predominance in OI patients aligns with the cell populations clinically associated with these disease phenotypes, and TBM is known to be pauci-cellular amongst CNS infections [233]. Astrocytes were significantly higher in TBM patients compared to patients with other CNS infections. When triggered by injury to the CNS or neuroinflammation, astrocytes morph into a reactive astrocytic form with unique phenotypic and functional features – a process known as astrogliosis[234,235]. *Mycobacterium tuberculosis*, the causative pathogen in TBM, is known to induce astrogliosis[235], which may explain the associated higher proportion of astrocytes and their reactive sub-group in this phenotype of brain infection, but the number of OI patients was low and the specificity of astrocytes for TBM would require larger numbers of patients with non-TBM infections. Given the differences in the underlying pathophysiology, it would also be expected that we would see a difference in the cytokine profile. Of interest, TBM patients had higher concentrations of MCP-1 and IFN-γ

on admission, and patients with other infections demonstrated higher concentrations of MIP-1α and VEGF. Further examination of the cytokine response in a larger group of patients may elucidate differences in the inflammatory response between TBM and other bacterial infections.

7.6 Limitations

Since this was a descriptive observational study, the patient cohort was a small convenience sample of patients presenting to our hospital and who required a ventricular catheter throughout the inclusion period. The resulting patient cohort largely consisted of TBM patients, which likely influenced the immune cell proportions/concentrations, and patterns of inflammatory cytokines. However, the aim of this study was to generate pilot data on the cellular immunophenotype of ventricular CSF, which currently does not exist, and therefore contributes novel insights into neuroimmunology that can be further explored. The timing and number of CSF samples was not pre-determined but rather based purely on clinical need. This limited our interpretations of temporal data. Future studies could formally target follow-up clinical surveillance sampling from external ventricular drains. However, the limited data do show changes over time. Lastly, given that this was a pilot study, the inclusion criteria (and definitions of the different infections) were based on the clinical teams' diagnostic decisions regarding each patient. There may be variability across centres in the definition of conditions like shunt infections, for example; however, we aimed to generate pilot data on infection in the CNS (rather than specific infections) and clinically this patient cohort was considered to have a CNS infection. The primary aim of the study was to characterize cells and inflammatory mediators in ventricular CSF rather than to explain the fundamental differences between different pathologies.

7.7 Remarks and future perspectives

The cell profiles described in this thesis represent the developing brain and developing immune system, and it is crucial to note that this may not mirror/reflect results that would be seen in adult patients. Furthermore, adults with CNS infections – particularly TBM – are often HIV co-infected[236]. This will alter the dynamics of the immune response, and could result in a

markedly different immune cell and cytokine profile. Given the high burden of disease that children carry, it is important to explore the concept of immunological vulnerability in children to infections in general, and particularly in CNS infections given that approximately 74% of meningitis was reported in children younger than 14 years across 5 countries in the African meningitis belt[237]. TBM specifically is known to be more common among children (as well as in immunocompromised adults) and is the most common form of meningitis in children in our local setting[238].

This study focused primarily on ventricular CSF. As demonstrated from protein, transcriptome and drug data, characteristics of ventricular CSF are different to lumbar CSF[29,138,139]. There are a number of contributing factors for this difference: the more permeable nature of the blood-spinal cord barrier compared to the BBB may allow more blood-derived cells to enter lumbar CSF[239]; spinal inflammation in the spinal sub-arachnoid space can disturb the flow of CSF between the brain and the spine often contributing to a same effect[240]; and the pathophysiology of TBM in the spine is characteristically more inflammatory compared to in the brain, which better reflects tissue injury[241].

Suggestions for future studies include: further study of immunological vulnerabilities predisposing children to CNS infection – our group is currently conducting a study involving examination of CSF and blood from children with TBM and other forms of CNS infection in comparison to healthy and TB-unexposed children. Further work on a larger sample size with more CNS infection phenotypes to determine whether significant differences exist in the immunophenotype of ventricular CSF cells, and downstream research to elucidate novel diagnostic and therapeutic markers that may be disease-specific are warranted. Work on the association with outcome could also be important for prognostic biomarkers or to guide clinical management. Research to characterise the difference in the adult and paediatric immune response (peripheral and CNS) would be important for age-specific treatment and possible biomarkers. Finally, future studies (especially in humans) that will expand our understanding of the pivotal role that microglia play in infection, healing, and development are needed and could offer exciting insights to benefit research and clinical practice.

Chapter 8 – Concluding remarks

Brain-resident immune cells, particularly microglia, are the most abundant cell type in the ventricular CSF of patients with CNS infection and likely play a pivotal role in the immune response to CNS infections. The implications of this both clinically and in research may be under-appreciated but represents an important and interesting avenue of research to explore, especially in the context of children and the developing brain. Having an objective measure of the scale of the neuroinflammatory response, as opposed to systemic inflammation, may assist in not only understanding the specifics of the inflammatory response of the organ of interest, but also in testing host-directed therapies. Microglia in particular accounted for the dominant proportion of brain-derived immune cells, and their holistic roles in the healthy and diseased CNS hold much potential for future studies. Lymphocytes constituted the largest peripheral immune cell population in infectious CSF, but this may be attributable to the large cohort of TBM patients in this study. Inflammatory analytes on admission were largely pro-inflammatory, but very high concentrations of anti-inflammatory IL-1Ra suggest an immunomodulatory environment. Multiple immune cells likely secrete multiple cytokines, as demonstrated by the weak correlations detected between cells and cytokines.

There are significant differences in the immunophenotype of ventricular CSF in TBM versus other infections. Samples from TBM patients were predominantly lymphocytic, whereas other infections were more granulocytic – which aligns with their known clinical presentations. Similarly, the inflammatory analyte milieu was different between these two cohorts. The host's immune response to distinct CNS infections is worth further research. Overall, the changing patterns of immune cells and cytokines over time suggests a shift from a more prominent innate immune response to an adaptive immune response, although the timing of the immune response is difficult to assess given that the start of an infection is not known. Over time, the general decrease in cell proportions and concentrations coupled with the decrease in inflammatory analyte concentrations points towards resolution of inflammation.

This study generated novel data that provided granular detail on the peripheral and resident immune cell populations in children with CNS infections, and contributes important insights

on which to grow our understanding of the immune response at the site of disease, in the context of neurodevelopment. With further research to grow these data, novel pathways for disease monitoring as well as intervention may be identifiable.

Appendix A – Methods

A.1 Flow cytometry analysis

Antibody titrations – performed for each of the 21 antibodies within this study's panel

Seven Eppendorf tubes were labelled with the dilution factor:

1. 1:30
2. 1:60
3. 1:120
4. 1:240
5. 1:480
6. 1:960
7. 1:1920

For the peripheral immune cells, blood was used for the titrations. But for the brain-derived immune cells, CSF was used. Brain-derived cell titrations were performed similarly to titrations of peripheral immune cells, except that the FACSlyse step that is mentioned below was excluded. In the first Eppendorf tube, 90μL of flow staining buffer was added, with 50μL being added to the remaining six Eppendorf tubes. Subsequently, 10μL of the antibody was added to the first Eppendorf tube, and resuspended thoroughly within the flow staining buffer. Crucially, the tube of the specific antibody being titrated was vortexed for around 5 seconds prior to use. To begin the dilution series, 50μL of solution was transferred from Eppendorf tube one into Eppendorf tube two. Following transfer, resuspension within tube two ensured optimal mixing of the two solutions. This process was repeated for the remaining Eppendorf tubes, and the same pipette tip could be used. The 50μL of solution removed from the last (7th) Eppendorf tube was discarded. Whole blood (100μL) was then added to each of the seven Eppendorf tubes – the same pipette was used but care was taken not to touch the solution in the bottom of the tubes. The tubes were then vortexed for around 3 seconds each, covered in foil and incubated for 30 minutes in a 5℃ fridge.

Following this incubation, 1.5mL of FACSlysing solution was added to each tube. Mixing was achieved by inverting the tubes, after which they were covered in foil and incubated for 10

minutes in a 5℃ fridge. The tubes were subsequently centrifuged (510 x g for 5 minutes), followed by decanting of the supernatant. A volume of 250μL of flow staining buffer was added to the seven tubes and the tubes were vortexed. Lastly, the tubes were covered in foil and placed in a 5℃ fridge until analysis on the flow cytometer. The optimal titres for all the antibodies on the 21-colour panel are provided in the table below.

Table A.1: Optimal antibody titres

Antibody	Dilution factor	Volume (μL)
CD45	1:120	1.25
Viability (UViD)	*	1
CD4	1:120	1.25
CD8	1:240	0.625
CD56	1:240	0.625
CD11b	1:120	1.25
γδTCR	1:240	0.625
CD19	1:120	1.25
CD14	1:60	2.5
CD45RA	1:240	0.625
Vα7.2	1:120	1.25
HLA-DR	1:240	0.625
TMEM119	1:60	2.5
CD25	1:240	0.625
GFAP	1:120	1.25
CD27	1:960	0.156
CD161	1:60	2.5
CD16	1:960	0.156
ACSA	1:60	2.5
FoxP3	1:120	1.25
CD3	1:120	1.25

ACSA: astrocyte cell surface antigen; *CD:* cluster of differentiation; *CD45RA*: CD45 receptor antagonist; *FoxP3:* forkhead box P3 or scurfin; *GFAP*: glial fibrillary acidic protein; *HLA-DR*: human leukocyte antigen-DR isotype; *TCR*: T-cell receptor; *TMEM119*: transmembrane protein 119. An extra 10% of volume for each antibody was added when making the antibody cocktail, to account for any pipetting errors.

*Viability was not titrated, the manufacturer's recommendation of 1μL was used

Table A.2: Specific antibody characteristics

Antibody	Company	Clone
BD Horizon™, Mouse Anti-Human CD45	BD Biosciences	HI30
Invitrogen, Viability Dye (blue-fluorescent reactive dye)	Life Technologies Corporation	2483570
BD Horizon™, Mouse Anti-Human CD4	BD Biosciences	SK3
BD Horizon™, Mouse Anti-Human CD8	BD Biosciences	SK1
BD OptiBuild™, Mouse Anti-Human CD56 (NCAM-1)	BD Biosciences	B159
BD OptiBuild™, Mouse Anti-Human CD11b	BD Biosciences	D12
BD Horizon™, Mouse Anti-Human TCR γδ	BD Biosciences	B1
BD Horizon™, Mouse Anti-Human CD19	BD Biosciences	SJ25C1
BD Horizon™, Mouse Anti-Human CD14	BD Biosciences	M5E2
BD Horizon™, Mouse Anti-Human CD45RA	BD Biosciences	HI100
BD OptiBuild™, Mouse Anti-Human TCR Vα7.2	BD Biosciences	OF-5A12
BD Horizon™, Mouse Anti-Human HLA-DR	BD Biosciences	G46-6
Human TMEM119	R&D Systems®	1689026
BD Horizon™, Mouse Anti-Human CD25	BD Biosciences	M-A251
BD Pharmingen™, Mouse anti-GFAP	BD Biosciences	1B4
BD Horizon™, Mouse Anti-Human CD27	BD Biosciences	M-T271
BD Pharmingen™, Mouse Anti-Human CD161	BD Biosciences	DX12
BD Pharmingen™, Mouse Anti-Human CD16	BD Biosciences	3G8
MACS, Mouse Anti-Human/Mouse/Rat ACSA	Miltenyi Biotec	ACSA-1
BD Horizon™, Mouse Anti-Human FoxP3	BD Biosciences	259D/C7
BD Pharmingen™, Mouse Anti-Human CD3	BD Biosciences	SK7
Additional reagents	**Company**	**Catalogue number**
BD™ CompBead Anti-Mouse Ig, κ/Negative Control Compensation Particles Set	BD Biosciences	BD/552843
Rainbow Calibration Particles (8 peaks), 3.0-3.4 µm	BD Biosciences	559123

ACSA: astrocyte cell surface antigen; *CD:* cluster of differentiation; *CD45RA*: CD45 receptor antagonist; *FoxP3:* forkhead box P3 or scurfin; *GFAP*: glial fibrillary acidic protein; *HLA-DR*: human leukocyte antigen-DR isotype; *TCR*: T-cell receptor; *TMEM119*: transmembrane protein 119; *Treg*: T regulatory cells; *UViD*: ultraviolet-induced detection

A.2 Luminex® analysis

Samples were subjected to a 2-fold dilution, entailing 50μL of sample being mixed with 50μL of Calibrator Diluent RD6-52. 500mL of Wash Buffer was made by adding 20mL of Wash Buffer Concentrate to 480mL of distilled water. Six standards were created using a 3-fold dilution series. Standard 1 served as the high standard and consisted of 100μL of each of the three unique standard cocktails provided, added to 700μL of Calibrator Diluent RD6-52. For the remaining 5 standards, 200μLof Calibrator Diluent RD6-52 was added to 5 test tubes, which were labelled standard 2-6. The dilution series was then carried out. This involved transferring 100μL of the Standard 1 solution into the Standard 2 test tube, resuspending this well with the calibrator diluent, and then transferring 100μL of the Standard 2 solution into the Standard 3 test tube. This process was carried out until the Standard 6 test tube was reached.

For the diluted Microparticle Cocktail, the Microparticle Cocktail vial was centrifuged (1000 x g for 30 seconds). The vial was then gently vortexed to resuspend the microparticles, after which 500μL of this cocktail was diluted with 5mL of Diluent RD2-1. Importantly, the microparticles were protected from light at all times, and were prepared within 30 minutes of use. The Biotin-Antibody Cocktail vial was centrifuged (1000 x g for 30 seconds), followed by gentle vortexing of the vial. 500μL this cocktail was then diluted with 5mL of Diluent RD2-1. Lastly, the Streptavidin-PE vial was centrifuged (1000 x g for 30 seconds) and the vial gently vortexed. 220μL of the Streptavidin-PE concentrate was then diluted with 5,35mL of Wash Buffer. All three dilutions were determined based on the number of wells in the plate.

Appendix B – Results

Graphs including outliers

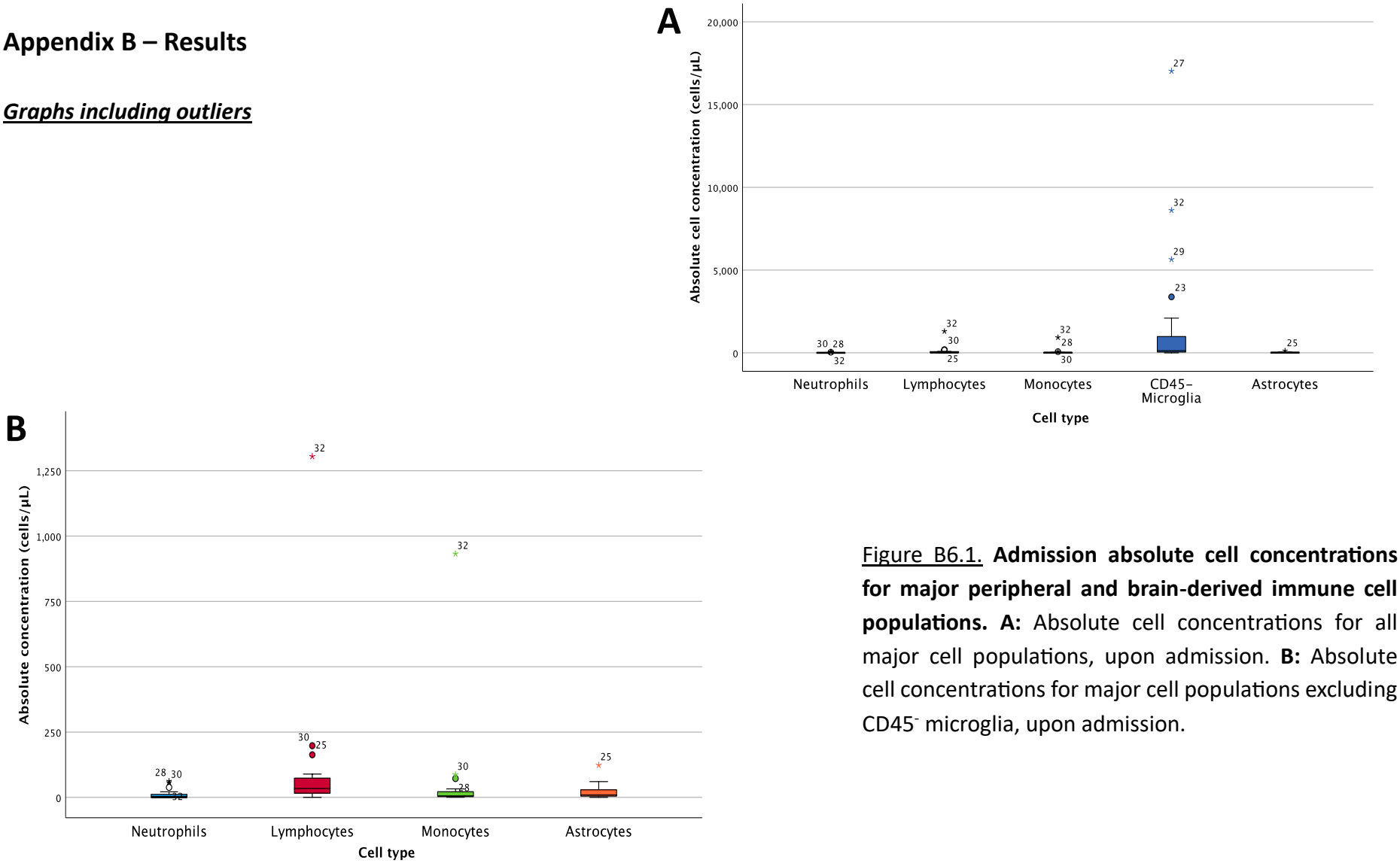

Figure B6.1. **Admission absolute cell concentrations for major peripheral and brain-derived immune cell populations. A:** Absolute cell concentrations for all major cell populations, upon admission. **B:** Absolute cell concentrations for major cell populations excluding $CD45^-$ microglia, upon admission.

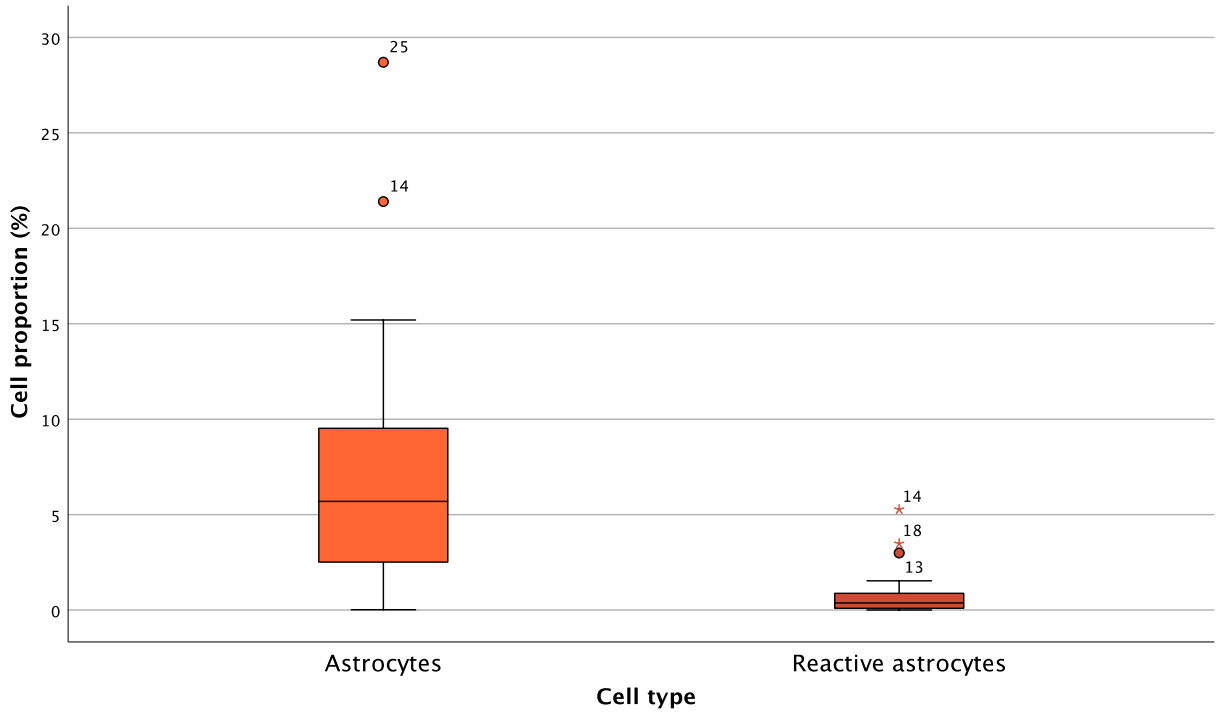

Figure B6.2. **Cell proportions for major peripheral and brain-derived immune cell populations**. Above: Cell proportions of the astrocytic ($CD45^{-}ACSA^{+}$) sub-group (reactive astrocytes ($ACSA^{+}GFAP^{+}$)) upon admission.

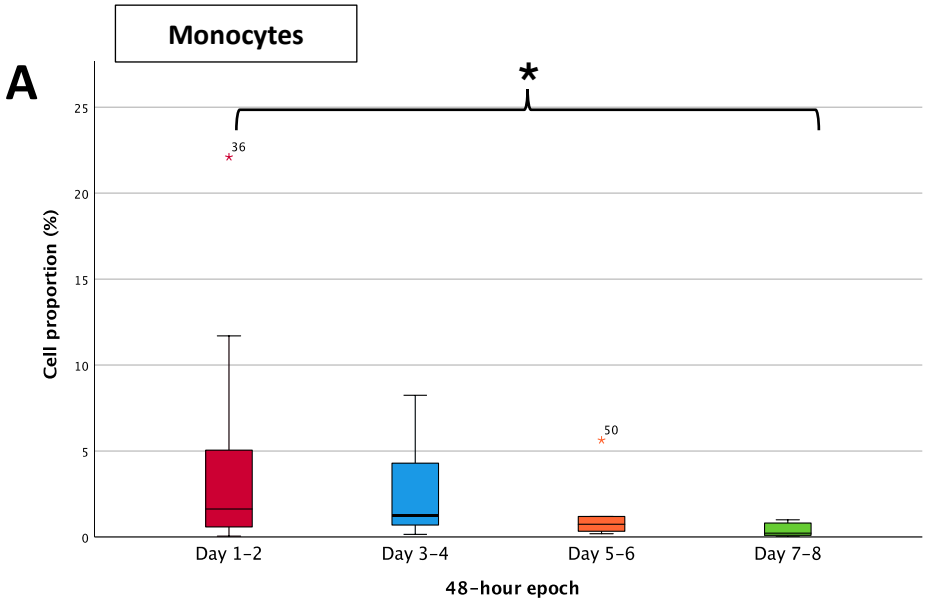

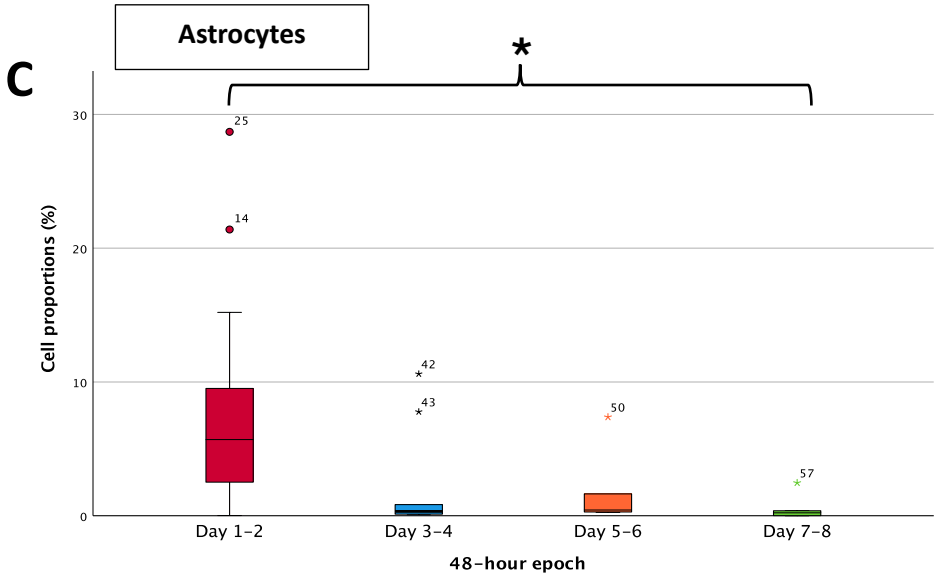

Figure B6.3. **Significant changes in cell proportion over the first week of hospital admission. A:** Changes in cell proportions for monocytes ($CD45^{+}$) over four 48-hour epochs. **C:** Changes in cell proportions for astrocytes ($CD45^{-}ACSA^{+}$) over four 48-hour epochs.

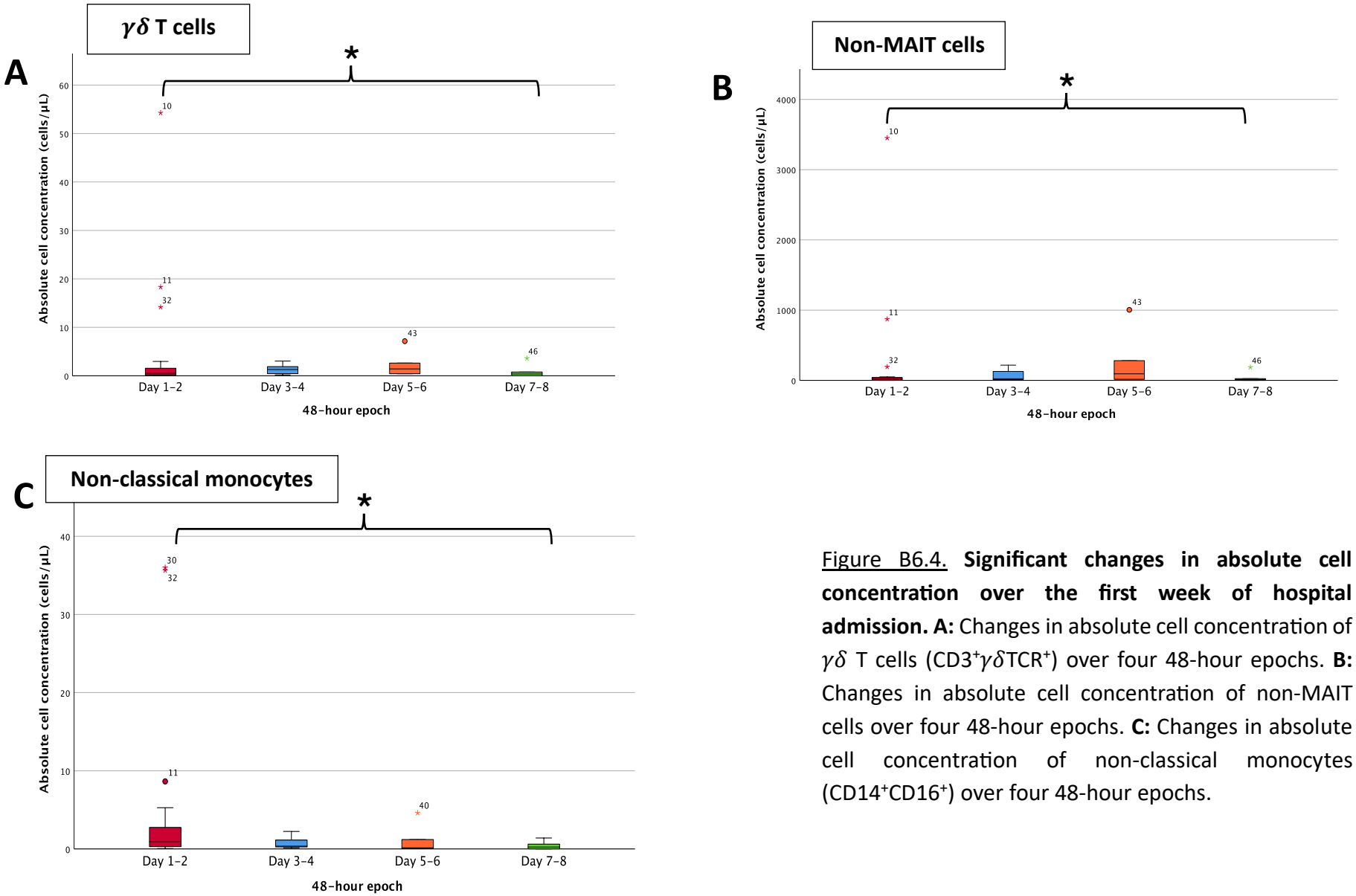

Figure B6.4. **Significant changes in absolute cell concentration over the first week of hospital admission. A:** Changes in absolute cell concentration of $\gamma\delta$ T cells ($CD3^+\gamma\delta TCR^+$) over four 48-hour epochs. **B:** Changes in absolute cell concentration of non-MAIT cells over four 48-hour epochs. **C:** Changes in absolute cell concentration of non-classical monocytes ($CD14^+CD16^+$) over four 48-hour epochs.

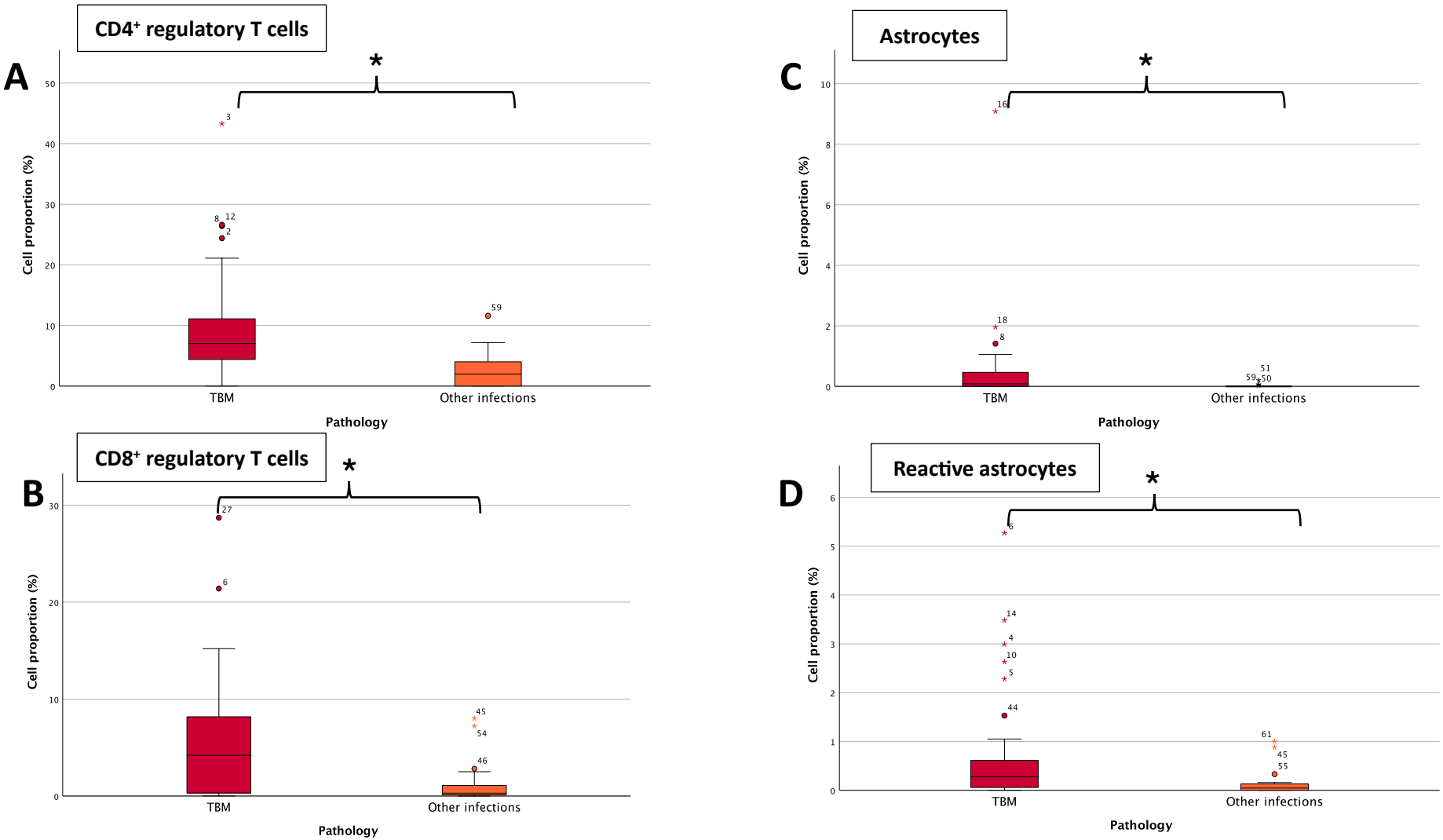

Figure B6.5. **Significant differences in admission cell proportions between TBM and other brain infections. A:** Admission cell proportions of $CD4^+$ regulatory T cells split by pathology. **B:** Admission cell proportions of $CD8^+$ regulatory T cells split by pathology. **C:** Admission cell proportions of astrocytes ($CD45^-ACSA^+$) split by pathology. **D:** Admission cell proportions of reactive astrocytes ($ACSA^+GFAP^+$)split by pathology.

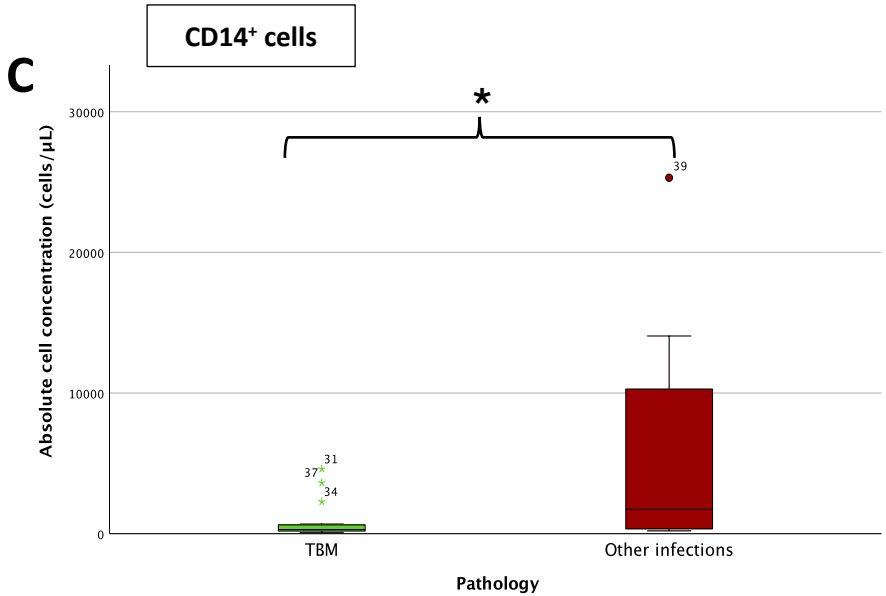

Figure B6.6. **Significant differences in absolute cell concentration between TBM and other brain infections, upon admission. C:** Absolute concentration of $CD14^+$ cells per pathology, upon admission. **D:** Absolute concentration of live cells per pathology, upon admission.

References

1. Robertson, F. C. *et al.* Epidemiology of central nervous system infectious diseases: a meta-analysis and systematic review with implications for neurosurgeons worldwide. *J Neurosurg* **130**, 1107–1126 (2019).
2. Sigfrid, L. *et al.* A systematic review of clinical guidelines on the management of acute, community-acquired CNS infections. *BMC Med* **17**, 170 (2019).
3. Turner, P. *et al.* The aetiologies of central nervous system infections in hospitalised Cambodian children. *BMC Infect Dis* **17**, 806 (2017).
4. Singh, G., Tucker, E. W. & Rohlwink, U. K. Infection in the Developing Brain: The Role of Unique Systemic Immune Vulnerabilities. *Front Neurol* **12**, (2022).
5. John, C. *et al.* Global research priorities for infections that affect the nervous system. *Nature* **527**, S178–S186 (2015).
6. Saba Villarroel, P. M. *et al.* A clinical, aetiological, and public health perspective on central nervous system infections in Bolivia, 2017–2018. *Sci Rep* **11**, 23235 (2021).
7. Sahu, R., Kumar, R. & Mahapatra, A. Central nervous system infection in the pediatric population. *J Pediatr Neurosci* **4**, 20–24 (2009).
8. Ziai, W. C. & Lewin, J. J. Update in the Diagnosis and Management of Central Nervous System Infections. *Neurol Clin* **26**, 427–468 (2008).
9. Alamarat, Z. & Hasbun, R. Management of Acute Bacterial Meningitis in Children. *Infect Drug Resist* **13**, 4077–4089 (2020).
10. Kim, K. S. Acute bacterial meningitis in infants and children. *Lancet Infect Dis* **10**, 32–42 (2010).
11. Zainel, A., Mitchell, H. & Sadarangani, M. Bacterial Meningitis in Children: Neurological Complications, Associated Risk Factors, and Prevention. *Microorganisms* **9**, (2021).
12. Agrawal, S. & Nadel, S. Acute bacterial meningitis in infants and children: epidemiology and management. *Pediatric Drugs* **13**, 385–400 (2011).
13. Fontes, F. L., de Araújo, L. F., Coutinho, L. G., Leib, S. L. & Agnez-Lima, L. F. Genetic polymorphisms associated with the inflammatory response in bacterial meningitis. *BMC Med Genet* **16**, 70 (2015).
14. Sáez-Llorens, X. & McCracken Jr, G. H. Bacterial meningitis in children. *The Lancet* **361**, 2139–2148 (2003).
15. Gerber, J. & Nau, R. Mechanisms of injury in bacterial meningitis. *Curr Opin Neurol* **23**, (2010).
16. Pinho-Ribeiro FA *et al.* Bacteria hijack a meningeal neuroimmune axis to facilitate brain invasion. *Nature* **615**, 472–481 (2023).
17. Bourgi, K., Fiske, C. & Sterling, T. R. Tuberculosis Meningitis. *Curr Infect Dis Rep* **19**, 39 (2017).
18. Thwaites, G. *et al.* Tuberculous meningitis. *Journal of Neurology, Neurosurgery & Psychiatry* **68**, 289 (2000).
19. Huynh, J. *et al.* Tuberculous Meningitis in Children: Reducing the Burden of Death and Disability. *Pathogens* **11**, (2022).

20. Figaji, A. & Fieggen, G. The neurosurgical and acute care management of tuberculous meningitis: evidence and current practice. *Tuberculosis (Edinb.)* **90**, 393–400 (2010).
21. Rohlwink, U. K. *et al.* Clinical characteristics and neurodevelopmental outcomes of children with tuberculous meningitis and hydrocephalus. *Dev Med Child Neurol* **58**, 461–468 (2016).
22. Andronikou, S., Smith, B., Hatherhill, M., Douis, H. & Wilmshurst, J. Definitive neuroradiological diagnostic features of tuberculous meningitis in children. *Pediatr Radiol* **34**, 876–885 (2004).
23. Donovan, J., Thwaites, G. E. & Huynh, J. Tuberculous meningitis: where to from here? *Curr Opin Infect Dis* **33**, 259–266 (2020).
24. Daniel, B., Grace, G. & Natrajan, M. TBM in children: Clinical management and outcome. *Indian Journal of Medical Research* **150**, 117–130 (2019).
25. Schoeman JF & Donald PR. Tuberculous meningitis. *Handb Clin Neurol.* **112**, 1135–1138 (2013).
26. Padayatchi, N., Bamber, S., Dawood, H. & Bobat, R. Multidrug-Resistant Tuberculous Meningitis in Children in Durban, South Africa. *Pediatr Infect Dis J* **25**, (2006).
27. Wilkinson, R. J. *et al.* Tuberculous meningitis. *Nat Rev Neurol* **13**, 581–598 (2017).
28. Miftode, E. G. *et al.* Tuberculous Meningitis in Children and Adults: A 10-Year Retrospective Comparative Analysis. *PLoS One* **10**, e0133477- (2015).
29. Rohlwink, U. K. *et al.* Tuberculous meningitis in children is characterized by compartmentalized immune responses and neural excitotoxicity. *Nat Commun* **10**, 3767 (2019).
30. Principi, N. & Esposito, S. Diagnosis and therapy of tuberculous meningitis in children. *Tuberculosis* **92**, 377–383 (2012).
31. Isaacs AM *et al.* Age-specific global epidemiology of hydrocephalus: Systematic review, metanalysis and global birth surveillance. *PLoS One* **13**, e0204926 (2018).
32. Kahle, K., Kulkarni, A., Limbrick, D. & Warf, B. Hydrocephalus in children. *Lancet* **387**, 788–799 (2016).
33. Robert SM *et al.* Inflammatory hydrocephalus. *Childs Nerv Syst.* **37**, 3341–3353 (2021).
34. Tai, M. L. S. *et al.* Cerebral infarction pattern in tuberculous meningitis. *Sci Rep* **6**, (2016).
35. Donovan, J. *et al.* Xpert MTB/RIF ultra for the diagnosis of tuberculous meningitis: a small step forward. *Clinical Infectious Diseases* **71**, 2002–2005 (2020).
36. Marais, S. *et al.* Tuberculous meningitis: a uniform case definition for use in clinical research. *Lancet Infect Dis* **10**, 803–812 (2010).
37. Thwaites, G. *et al.* British Infection Society guidelines for the diagnosis and treatment of tuberculosis of the central nervous system in adults and children. *Journal of Infection* **59**, 167–187 (2009).
38. Schoeman, J. F. & Donald, P. R. Tuberculous meningitis. in *Handbook of Clinical Neurology* vol. 112 1135–1138 (2013).
39. Santos, M. M. *et al.* Infant hydrocephalus in sub-Saharan Africa: The reality on the Tanzanian side of the lake. *J Neurosurg Pediatr* **20**, 423–431 (2017).
40. Bauman, N. & Poenaru, D. Hydrocephalus in Africa-surgical perspective. *The Annals of African Surgery* **2**, 30–37 (2008).

41. Warf, B. C. Pediatric hydrocephalus in east Africa: Prevalence, causes, treatments, and strategies for the future. *World Neurosurg* **73**, 296–300 (2010).
42. Heij, H. A. The fate of ventriculo-peritonea1 shunts and outcome of revision surgery. *East Cent Afr J Surg* **5**, (2000).
43. Hosainey, S. A. M., Hald, J. K. & Meling, T. R. Risk of early failure of VP shunts implanted for hydrocephalus after craniotomies for brain tumors in adults. *Neurosurg Rev* **45**, 479–490 (2022).
44. Jackson, I. J. & Snodgrass, S. R. Peritoneal shunts in the treatment of hydrocephalus and increased intracranial pressure. *J Neurosurg* **12**, 216–222 (1955).
45. Scarff, J. E. Treatment of hydrocephalus: an historical and critical review of methods and results PATHOLOGICAL CONSIDERATIONS OF THE BASIC PRINCIPLES OF THERAPY. *J. Neurol. Neurosurg. Psychiat* **26**, 1 (1963).
46. Enger, P., Svendsen, F. & Wester, K. CSF shunt infections in children: Experiences from a population-based study. *Acta Neurochir (Wien)* **145**, 243–248 (2003).
47. Hanak, B. W., Bonow, R. H., Harris, C. A. & Browd, S. R. Cerebrospinal Fluid Shunting Complications in Children. *Pediatr Neurosurg* **52**, 381–400 (2017).
48. Vinchon, M. & Dhellemmes, P. Cerebrospinal fluid shunt infection: Risk factors and long-term follow-up. *Child's Nervous System* **22**, 692–697 (2006).
49. Mcgirt, M. J. *et al.* Risk Factors for Pediatric Ventriculoperitoneal Shunt Infection and Predictors of Infectious Pathogens. *Clinical Infectious Diseases* **36**, 858–862 (2003).
50. Mwang, N., Lecturer, S. & Omulo, T. VENTRICULOPERITONEAL SHUNT SURGERY AND SHUNT INFECTIONS IN CHILDREN WITH NON-TUMOUR HYDROCEPHALUS AT THE KENYATTA NATIONAL HOSPITAL, NAIROBI. *East Afr Med J* **77**, (2000).
51. Riva-Cambrin, S. et al. Risk factors for shunt malfunction in pediatric hydrocephalus: a multicenter prospective cohort study. *J Neurosurg Pediatr* **17**, 382–390 (2016).
52. Duhaime, A. C. Evaluation and management of shunt infections in children with hydrocephalus. *Clin Pediatr (Phila)* **45**, 705–713 (2006).
53. Turgut, M. *et al.* Cerebrospinal fluid shunt infections in children. *Pediatr Neurosurg* **41**, 131–136 (2005).
54. Mallucci, C. L. *et al.* Antibiotic or silver versus standard ventriculoperitoneal shunts (BASICS): a multicentre, single-blinded, randomised trial and economic evaluation. *The Lancet* **394**, 1530–1539 (2019).
55. Renier, D., Lacombe, J., Pierre-Kahn, A., Sainte-Rose, C. & Hirsch, J.-F. Factors causing acute shunt infection Computer analysis of 1174 operations. *J. Neurosurg* **61**, 1072–1078 (1984).
56. Ochieng, N., Okechi, H., Ferson, S. & Albright, A. L. Bacteria causing ventriculoperitoneal shunt infections in a Kenyan population. *J Neurosurg Pediatr* **15**, 150–155 (2015).
57. Bayston, R. Hydrocephalus shunt infections. *Journal of Antimicrobial Chemotherapy* **34**, 75–84 (1994).
58. Sarguna, P. & Lakshmi, V. Ventriculoperitoneal shunt infections. *Indian J Med Microbiol* **24**, 52–56 (2006).
59. Braxton, E. E. *et al.* Role of biofilms in neurosurgical device-related infections. *Neurosurg Rev* **28**, 249–255 (2005).

60. Davis, L. E., Cook, G. & William Costerton, J. Biofilm on Ventriculoperitoneal Shunt Tubing as a Cause of Treatment Failure in Coccidioidal Meningitis. *Emerging Infectious Diseases* • **8**, (2002).
61. Gutierrez-Murgas, Y. & Snowden, J. N. Ventricular shunt infections: Immunopathogenesis and clinical management. *J Neuroimmunol* **276**, 1–8 (2014).
62. Schreffler, R., Schreffler, A. & Wittler, R. Treatment of cerebrospinal fluid shunt infections: a decision analysis. *Pediatr Infect Dis J* **21**, 632–636 (2002).
63. Ochoa, A., Argañaraz, R. & Mantese, B. Neuroendoscopic lavage for the treatment of pyogenic ventriculitis in children: personal series and review of the literature. *Child's Nervous System* **38**, 597–604 (2022).
64. Stubljar, D. *et al.* Diagnostic Accuracy of Presepsin (sCD14-ST) for Prediction of Bacterial Infection in Cerebrospinal Fluid Samples from Children with Suspected Bacterial Meningitis or Ventriculitis. *J Clin Microbiol* 1239–1244 (2015) doi:10.1128/JCM.03052.
65. Agrawal, A., Cincu, R. & Timothy, J. Current concepts and approach to ventriculitis. *Infectious Diseases in Clinical Practice* **16**, 100–104 (2008).
66. Pezzullo, J., Tung, G., Mudigonda, S. & Rogg, J. Diffusion-Weighted MR Imaging of Pyogenic Ventriculitis. *AJR* **180**, 71–75 (2003).
67. Beer, R., Lackner, P., Pfausler, B. & Schmutzhard, E. Nosocomial ventriculitis and meningitis in neurocritical care patients. *J Neurol* **255**, 1617–1624 (2008).
68. Tunkel, A. R. *et al.* 2017 Infectious Diseases Society of America's Clinical Practice Guidelines for Healthcare-Associated Ventriculitis and Meningitis*. *Clinical Infectious Diseases* **64**, E34–E65 (2017).
69. Kim, J., Erice, C., Rohlwink, U. K. & Tucker, E. W. Infections in the Developing Brain: The Role of the Neuro-Immune Axis. *Front Neurol* **13**, (2022).
70. Kim, J., Erice, C., Rohlwink, U. K. & Tucker, E. W. Infections in the Developing Brain: The Role of the Neuro-Immune Axis. *Front Neurol* **13**, (2022).
71. Huttunen, P. *et al.* Differential diagnosis of acute central nervous system infections in children using modern microbiological methods. *Acta Paediatr* **98**, 1300–1306 (2009).
72. Horsnell, W. IBS1007S Introduction to the Immune System Lecture 1A. Preprint at (2023).
73. Schenten, D. & Medzhitov, R. Chapter 3 - The Control of Adaptive Immune Responses by the Innate Immune System. in (ed. Alt, F. W.) vol. 109 87–124 (Academic Press, 2011).
74. Medzhitov, R. & Janeway Jr, C. A. Innate immune recognition and control of adaptive immune responses. *Semin Immunol* **10**, 351–353 (1998).
75. Tosi, M. F. Innate immune responses to infection. *Journal of Allergy and Clinical Immunology* **116**, 241–249 (2005).
76. Medzhitov, R. & Janeway, C. A. Innate immunity: impact on the adaptive immune response. *Curr Opin Immunol* **9**, 4–9 (1997).
77. Thaiss, C. A., Levy, M., Itav, S. & Elinav, E. Integration of Innate Immune Signaling. *Trends Immunol* **37**, 84–101 (2016).
78. Dempsey, P. W., Vaidya, S. A. & Cheng, G. The Art of War: Innate and adaptive immune responses. *Cellular and Molecular Life Sciences* **60**, 2604–2621 (2003).

79. Janeway CA Jr, Travers P, Walport M & et al. Principles of innate and adaptive immunity. in *Immunobiology: The Immune System in Health and Disease*. (Garland Science, New York, 2001).
80. Ransohoff, R. M. & Brown, M. A. Innate immunity in the central nervous system. *Journal of Clinical Investigation* **122**, 1164–1171 (2012).
81. Horsnell, W. IBS1007S Introduction to the Immune System Lecture 1B. Preprint at (2023).
82. Medzhitov, R. & Janeway, C. A. Innate immunity: the virtues of a nonclonal system of recognition. *Cell* **91**, 295–298 (1997).
83. Weissman, I. L. & Cooper, M. D. How the Immune System Develops. *Sci Am* **269**, 64–71 (1993).
84. Rook, G. A. W., Lowry, C. A. & Raison, C. L. Hygiene and other early childhood influences on the subsequent function of the immune system. *Brain Res* **1617**, 47–62 (2015).
85. Thomas, G. D. *et al.* Human Blood Monocyte Subsets: A New Gating Strategy Defned Using Cell Surface Markers Identifed by Mass Cytometry. *Arterioscler Thromb Vasc Biol* **37**, 1548–1558 (2017).
86. Stansfield, B. K. & Ingram, D. A. Clinical significance of monocyte heterogeneity. *Clin Transl Med* **4**, (2015).
87. Ziegler-Heitbrock, L. Blood monocytes and their subsets: Established features and open questions. *Front Immunol* **6**, (2015).
88. Wu, Z., Zhang, Z., Lei, Z. & Lei, P. CD14: Biology and role in the pathogenesis of disease. *Cytokine Growth Factor Rev* **48**, 24–31 (2019).
89. Lakschevitz, F. S. *et al.* Identification of neutrophil surface marker changes in health and inflammation using high-throughput screening flow cytometry. *Exp Cell Res* **342**, 200–209 (2016).
90. Weirich, E. *et al.* Neutrophil CD11b expression as a diagnostic marker for early-onset neonatal infection. *J Pediatr* **132**, 445–451 (1998).
91. Kuijpers, B. W. *et al.* Membrane Surface Antigen Expression on Neutrophils: A Reappraisal of the Use of Surface Markers for Neutrophil Activation. *Blood* **78**, 1105–1111 (1991).
92. Ziegler, S. *et al.* CD56 is a pathogen recognition receptor on human natural killer cells. *Sci Rep* **7**, (2017).
93. Montaldo, E. *et al.* Human NK cell receptors/markers: A tool to analyze NK cell development, subsets and function. *Cytometry Part A* **83**, 702–713 (2013).
94. Cooper, M., Fehniger, T. & Caligiuri, M. The biology of human natural killer-cell subsets. *Trends Immunol* **22**, 633–640 (2001).
95. Poli, A. *et al.* CD56bright natural killer (NK) cells: An important NK cell subset. *Immunology* **126**, 458–465 (2009).
96. Fergusson, J. R. *et al.* CD161 defines a transcriptional and functional phenotype across distinct human T cell lineages. *Cell Rep* **9**, 1075–1088 (2014).
97. Mahnke, Y. D., Brodie, T. M., Sallusto, F., Roederer, M. & Lugli, E. The who's who of T-cell differentiation: Human memory T-cell subsets. *Eur J Immunol* **43**, 2797–2809 (2013).
98. Geginat, J. *et al.* The CD4-centered universe of human T cell subsets. *Semin Immunol* **25**, 252–262 (2013).

99. Cano RLE & Lopera HDE. Introduction to T and B lymphocytes. in *Autoimmunity: From Bench to Bedside [Internet].* (eds. Anaya JM, Shoenfeld Y & Rojas-Villarraga A, et al.) (El Rosario University Press, Bogota, 2013).
100. Sweet, R. W., Truneh, A. & Hendrickson, W. A. CD4: Its structure, role in immune function and AIDS pathogenesis, and potential as a pharmacological target. *Curr Opin Biotechnol* **2**, 622–633 (1991).
101. Takata, H. & Takiguchi, M. Three Memory Subsets of Human CD8 T Cells Differently Expressing Three Cytolytic Effector Molecules 1. *The Journal of Immunology* **177**, 4330–4340 (2006).
102. O'Rourke, A. M. & Mescher, M. F. The roles of CD8 in cytotoxic T lymphocyte function. *Immunol Today* **14**, 177–183 (1993).
103. Kaufmann, S. Gamma-delta and other unconventional T-lymphocytes: What do they see and what do they do. *Proc. Natl. Acad. Sci. USA* **93**, 2272–2279 (1996).
104. Toro, J. R. *et al.* Gamma-delta T-cell phenotype is associated with significantly decreased survival in cutaneous T-cell lymphoma. *Blood* **101**, 3407–3412 (2003).
105. Pellicci, D. G., Koay, H. F. & Berzins, S. P. Thymic development of unconventional T cells: how NKT cells, MAIT cells and γδ T cells emerge. *Nat Rev Immunol* **20**, 756–770 (2020).
106. Chien, Y. & Bonneville, M. Gamma delta T cell receptors. *Cell. Mol. Life Sci.* **63**, 2089–2094 (2006).
107. Provine, N. M. & Klenerman, P. MAIT Cells in Health and Disease. *Annu. Rev. Immunol.* **38**, 203–228 (2020).
108. Treiner, E. *et al.* Mucosal-associated invariant T (MAIT) cells: An evolutionarily conserved T cell subset. *Microbes Infect* **7**, 552–559 (2005).
109. Salou, M., Franciszkiewicz, K. & Lantz, O. MAIT cells in infectious diseases. *Curr Opin Immunol* **48**, 7–14 (2017).
110. Chen, X. & Jensen, P. E. The role of B lymphocytes as antigen-presenting cells. *Arch Immunol Ther Exp (Warsz)* **56**, 77–83 (2008).
111. Lebien, T. & Tedder, T. B lymphocytes: how they develop and function. *Blood* **112**, 1570–1580 (2008).
112. Ziegler-Heitbrock, L. *et al.* Nomenclature of monocytes and dendritic cells in blood. *Blood* **116**, e74–e80 (2010).
113. Klein, R. S. & Hunter, C. A. Protective and Pathological Immunity during Central Nervous System Infections. *Immunity* **46**, 891–909 (2017).
114. Wraith, D. C. & Nicholson, L. B. The adaptive immune system in diseases of the central nervous system. *Journal of Clinical Investigation* **122**, 1172–1179 (2012).
115. Russo, M. V & McGavern, D. B. Immune surveillance of the CNS following infection and injury. *Trends Immunol* **36**, 637–650 (2015).
116. Lampron, A., ElAli, A. & Rivest, S. Innate immunity in the CNS: redefining the relationship between the CNS and Its environment. *Neuron* **78**, 214–232 (2013).
117. Williams, K., Alvarez, X. & Lackner, A. A. Central nervous system perivascular cells are immunoregulatory cells that connect the CNS with the peripheral immune system. *Glia* **36**, 156–164 (2001).
118. Xu, J. *et al.* CNS and CNS diseases in relation to their immune system. *Front Immunol* **13**, 1063928 (2022).
119. Ousman, S. S. & Kubes, P. Immune surveillance in the central nervous system. *Nat Neurosci* **15**, 1096–1101 (2012).

120. Becher, B., Prat, A. & Antel, J. P. Brain-immune connection: Immuno-regulatory properties of CNS-resident cells. *Glia* **29**, 293–304 (2000).
121. Waisman, A., Liblau, R. S. & Becher, B. Innate and adaptive immune responses in the CNS. *Lancet Neurol* **14**, 945–955 (2015).
122. Carpentier, P. A. *et al.* Differential activation of astrocytes by innate and adaptive immune stimuli. *Glia* **49**, 360–374 (2005).
123. Prinz, M. & Priller, J. The role of peripheral immune cells in the CNS in steady state and disease. *Nat Neurosci* **20**, 136–144 (2017).
124. Matyszak, M. K. Inflammation in the CNS: Balance between immunological privilege and immune responses. *Prog Neurobiol* **56**, 19–35 (1998).
125. Jurga, A. M., Paleczna, M., Kadluczka, J. & Kuter, K. Z. Beyond the GFAP-astrocyte protein markers in the brain. *Biomolecules* **11**, (2021).
126. Clark, I. C. *et al.* Identification of astrocyte regulators by nucleic acid cytometry. *Nature* **614**, 326–333 (2023).
127. Escartin, C. *et al.* Reactive astrocyte nomenclature, definitions, and future directions. *Nat Neurosci* **24**, 312–325 (2021).
128. Jungblut, M. *et al.* Isolation and characterization of living primary astroglial cells using the new GLAST-specific monoclonal antibody ACSA-1. *Glia* **60**, 894–907 (2012).
129. Korzhevskii, D. E. & Kirik, O. V. Brain Microglia and Microglial Markers. *Neurosci Behav Physiol* **46**, 284–290 (2016).
130. Jurga, A. M., Paleczna, M. & Kuter, K. Z. Overview of General and Discriminating Markers of Differential Microglia Phenotypes. *Front Cell Neurosci* **14**, (2020).
131. Giulian, D. *et al.* Cell Surface Morphology Identifies Microglia as a Distinct Class of Mononuclear Phagocyte. *The Journal of Neuroscience* **15**, 7712–7726 (1995).
132. Libbey, J. E. & Fujinami, R. S. Adaptive immune response to viral infections in the central nervous system. in *Handbook of Clinical Neurology* vol. 123 225–247 (2014).
133. Green, J. A., Chau, T. T. H., Farrar, J. J., Friedland, J. S. & Thwaites, G. E. CNS infection, CSF matrix metalloproteinase concentrations, and clinical/laboratory features. *Neurology* **76**, 577–579 (2011).
134. Rohlwink, U. Neuroinflammation. *University of Cape Town* Preprint at (2021).
135. Dong, X. X., Wang, Y. & Qin, Z. H. Molecular mechanisms of excitotoxicity and their relevance to pathogenesis of neurodegenerative diseases. *Acta Pharmacol Sin* **30**, 379–387 (2009).
136. Jaerve, A. & Müller, H. W. Chemokines in CNS injury and repair. *Cell Tissue Res* **349**, 229–248 (2012).
137. Malik, P. & Shroff, M. Infection and inflammation: radiological insights into patterns of pediatric immune-mediated CNS injury. *Neuroradiology* **65**, 425–439 (2023).
138. Rohlwink, U. K. *et al.* Biomarkers of Cerebral Injury and Inflammation in Pediatric Tuberculous Meningitis. *Clinical Infectious Diseases* **65**, 1298–1307 (2017).
139. Rohlwink, U. K. & Figaji, A. A. Biomarkers of Brain Injury in Cerebral Infections. *Clin Chem* **60**, 823–834 (2014).
140. Skar, G. L. *et al.* Identification of Potential Cerebrospinal Fluid Biomarkers to Discriminate between Infection and Sterile Inflammation in a Rat Model of Staphylococcus epidermidis Catheter Infection. *Infect Immun* **87**, (2019).

141. Gaetani, L. *et al.* CSF and Blood Biomarkers in Neuroinflammatory and Neurodegenerative Diseases: Implications for Treatment. *Trends Pharmacol Sci* **41**, 1023–1037 (2020).
142. Harris, C. A., Morales, D. M., Arshad, R., McAllister, J. P. & Limbrick, D. D. Cerebrospinal fluid biomarkers of neuroinflammation in children with hydrocephalus and shunt malfunction. *Fluids Barriers CNS* **18**, 1–14 (2021).
143. Sahoo, M., Ceballos-Olvera, I., Del Barrio, L. & Re, F. Role of the inflammasome, IL-1β, and IL-18 in bacterial infections. *ScientificWorldJournal* **11**, 2037–2050 (2011).
144. Fernando López-Cortés, L. *et al.* Cerebrospinal fluid tumor necrosis factor-α , interleukin-1 β , interleukin-6, and interleukin-8 as diagnostic markers of cerebrospinal fluid infection in neurosurgical patients. *Crit Care Med* **28**, 215–219 (2000).
145. Lopez-Castejon, G. & Brough, D. Understanding the mechanism of IL-1β secretion. *Cytokine Growth Factor Rev* **22**, 189–195 (2011).
146. Rubartelli, A., Cozzolino, F., Talio, M. & Sitia, R. A novel secretory pathway for interleukin-1 beta, a protein lacking a signal sequence. *EMBO J* **9**, 1503–1510 (1990).
147. Dayer, J.-M. & Burger, D. IL-1Ra. *Cytokine reference* 319–336 (2000) doi:10.1006/rwcy.2000.04002.
148. Dinarello, C. A. Immunological and inflammatory functions of the interleukin-1 family. *Annu Rev Immunol* **27**, 519–550 (2009).
149. Arend, W. P. The balance between IL-1 and IL-1Ra in disease. *Cytokine Growth Factor Rev* **13**, 323–340 (2002).
150. Rock, R. B. *et al.* Role of microglia in central nervous system infections. *Clin Microbiol Rev* **17**, 942–964 (2004).
151. Simmons, C. P. *et al.* Pretreatment Intracerebral and Peripheral Blood Immune Responses in Vietnamese Adults with Tuberculous Meningitis: Diagnostic Value and Relationship to Disease Severity and Outcome. *The Journal of Immunology* **176**, 2007–2014 (2006).
152. Rose-John, S., Winthrop, K. & Calabrese, L. The role of IL-6 in host defence against infections: immunobiology and clinical implications. *Nat Rev Rheumatol* **13**, 399–409 (2017).
153. Cuff, S. M., Merola, J. P., Twohig, J. P., Eberl, M. & Gray, W. P. Toll-like receptor linked cytokine profiles in cerebrospinal fluid discriminate neurological infection from sterile inflammation. *Brain Commun* **2**, (2020).
154. Wagoner, N. J. Van, Oh, J.-W., Repovic, P. & Benveniste, E. N. Interleukin-6 (IL-6) Production by Astrocytes: Autocrine Regulation by IL-6 and the Soluble IL-6 Receptor. *The Journal of Neuroscience* **19**, 5236–5244 (1918).
155. Kotloff, R. M., Little, J. & Elias, J. A. Human alveolar macrophage and blood monocyte interleukin-6 production. *Am J Respir Cell Mol Biol* **3**, 497–505 (1990).
156. Ehrlich, L. C. *et al.* Cytokine Regulation of Human Microglial Cell IL-8 Production. *The Journal of Immunology* **160**, 1944–1948 (1998).
157. Nitta, T., Allegretta, M., Okumura, K., Sato, K. & Steinman, L. Neoplastic and reactive human astrocytes express interleukin-8 gene. *Neurosurg Rev* **15**, 203–207 (1992).

158. Aloisi, F. *et al.* Production of hemolymphopoietic cytokines (IL-6, IL-8, colony-stimulating factors) by normal human astrocytes in response to IL-1 beta and tumor necrosis factor-alpha. *J Immunol* **149**, 2358–2366 (1992).
159. Burmeister, A. R. & Marriott, I. The interleukin-10 family of cytokines and their role in the CNS. *Front Cell Neurosci* **12**, (2018).
160. O'Garra, A. & Vieira, P. Regulatory T cells and mechanisms of immune system control. *Nat Med* **10**, 801–805 (2004).
161. Wilczynski, J. R., Radwan, M. & Kalinka, J. The characterization and role of regulatory T cells in immune reactions. *Frontiers in Bioscience* **13**, 2266–2274 (2008).
162. Bacchetta, R., Gregori, S. & Roncarolo, M. G. CD4+ regulatory T cells: Mechanisms of induction and effector function. *Autoimmun Rev* **4**, 491–496 (2005).
163. Feuerstein, G. Z., Liu, T. & Barone, F. C. Cytokines, inflammation, and brain injury: role of tumor necrosis factor-alpha. *Cerebrovasc Brain Metab Rev* **6**, 341–360 (1994).
164. McCoy, M. K. & Tansey, M. G. TNF signaling inhibition in the CNS: Implications for normal brain function and neurodegenerative disease. *J Neuroinflammation* **5**, (2008).
165. Parameswaran, N. & Patial, S. Tumor necrosis factor-α signaling in macrophages. *Crit Rev Eukaryot Gene Expr* **20**, (2010).
166. Fischer, H. *et al.* Production of TNF-alpha and TNF-beta by staphylococcal enterotoxin A activated human T cells. *The Journal of Immunology* **144**, 4663–4669 (1990).
167. Chungt, I. & Benveniste, E. Tumor Necrosis Factor-c production by astrocytes - Induction by Lipopolysaccharide, IFN-7, and IL-16. *The Journal of Immunology* **144**, 2999–3007 (1990).
168. Monteiro, S., Roque, S., Marques, F., Correia-Neves, M. & Cerqueira, J. J. Brain interference: Revisiting the role of IFNγ in the central nervous system. *Prog Neurobiol* **156**, 149–163 (2017).
169. Thäle, C. & Kiderlen, A. F. Sources of interferon-gamma (IFN-γ) in early immune response to Listeria monocytogenes. *Immunobiology* **210**, 673–683 (2005).
170. Kak, G., Raza, M. & Tiwari, B. K. Interferon-gamma (IFN-γ): Exploring its implications in infectious diseases. *Biomol Concepts* **9**, 64–79 (2018).
171. Owens, T., Khorooshi, R., Wlodarczyk, A. & Asgari, N. Interferons in the central nervous system: A few instruments play many tunes. *Glia* **62**, 339–355 (2014).
172. Brassard, D. L., Grace, M. J. & Bordens, R. W. Interferon-α as an immunotherapeutic protein. *J Leukoc Biol* **71**, 565–581 (2002).
173. Fritz-French, C. & Tyor, W. Interferon-α (IFNα) neurotoxicity. *Cytokine Growth Factor Rev* **23**, 7–14 (2012).
174. Singh, S., Anshita, D. & Ravichandiran, V. MCP-1: Function, regulation, and involvement in disease. *Int Immunopharmacol* **101**, (2021).
175. Yadav, A., Saini, V. & Arora, S. MCP-1: Chemoattractant with a role beyond immunity: A review. *Clinica Chimica Acta* **411**, 1570–1579 (2010).
176. Yao, Y. & Tsirka, S. E. Monocyte chemoattractant protein-1 and the blood-brain barrier. *Cellular and Molecular Life Sciences* **71**, 683–697 (2014).

177. Diab, A. *et al.* Neutralization of Macrophage Inflammatory Protein 2 (MIP-2) and MIP-1 Attenuates Neutrophil Recruitment in the Central Nervous System during Experimental Bacterial Meningitis. *Infect Immun* **67**, 2590–2601 (1999).
178. Bhavsar, I., Miller, C. S. & Al-Sabbagh, M. Macrophage Inflammatory Protein-1 Alpha (MIP-1 alpha)/CCL3: As a biomarker. in *General Methods in Biomarker Research and their Applications* vols 1–2 223–249 (Springer International Publishing, 2015).
179. Kieseier, B. C. *et al.* Chemokines and chemokine receptors in inflammatory demyelinating neuropathies: a central role for IP-10. *Brain* **125**, 823–834 (2002).
180. Bhowmick, S. *et al.* Induction of IP-10 (CXCL10) in astrocytes following Japanese encephalitis. *Neurosci Lett* **414**, 45–50 (2007).
181. Liu, M. *et al.* CXCL10/IP-10 in infectious diseases pathogenesis and potential therapeutic implications. *Cytokine Growth Factor Rev* **22**, 121–130 (2011).
182. Madhurantakam, S., Lee, Z. J., Naqvi, A. & Prasad, S. Importance of IP-10 as a biomarker of host immune response: Critical perspective as a target for biosensing. *Curr Res Biotechnol* **5**, (2023).
183. Bhowmick, S. *et al.* Induction of IP-10 (CXCL10) in astrocytes following Japanese encephalitis. *Neurosci Lett* **414**, 45–50 (2007).
184. Ruiz De Almodovar, C., Lambrechts, D., Mazzone, M. & Carmeliet, P. Role and Therapeutic Potential of VEGF in the Nervous System. *Physiol Rev* **89**, 607–649 (2009).
185. Lange, C., Storkebaum, E., De Almodóvar, C. R., Dewerchin, M. & Carmeliet, P. Vascular endothelial growth factor: A neurovascular target in neurological diseases. *Nat Rev Neurol* **12**, 439–454 (2016).
186. Argaw, A. T. *et al.* Astrocyte-derived VEGF-A drives blood-brain barrier disruption in CNS inflammatory disease. *Journal of Clinical Investigation* **122**, 2454–2468 (2012).
187. Kut, C., Mac Gabhann, F. & Popel, A. S. Where is VEGF in the body? A meta-analysis of VEGF distribution in cancer. *Br J Cancer* **97**, 978–985 (2007).
188. McKinnon, K. M. Flow cytometry: An overview. *Curr Protoc Immunol* **120**, 5.1.1-5.1.11 (2019).
189. Adan, A., Alizada, G., Kiraz, Y., Baran, Y. & Nalbant, A. Flow cytometry: basic principles and applications. *Crit Rev Biotechnol* **37**, 163–176 (2017).
190. Henel, G. & Schmitz, J. L. Basic theory and clinical applications of flow cytometry. *Lab Med* **38**, 428–436 (2007).
191. Nunez, R. Introduction to the field of cytometry and its importance in biomedicine. *Curr Issues Mol Biol* **3**, 37–38 (2001).
192. Bignardi, G. E. Flow cytometry for the microscopy of body fluids in patients with suspected infection. *J Clin Pathol* **68**, 870 (2015).
193. Mandy, F. F., Bergeron, M. & Minkus, T. Principles of Flow Cytometry. *Transfus. Sci* **16**, 303–314 (1995).
194. Van Acker, J. T. *et al.* Automated flow cytometric analysis of cerebrospinal fluid. *Clin Chem* **47**, 556–560 (2001).
195. Dossou, N. *et al.* Evaluation of Flow Cytometry for Cell Count and Detection of Bacteria in Biological Fluids. *Microbiol Spectr* **10**, (2022).

196. Finn, W. G., Peterson, L. C., James, C. & Goolsby, C. L. Enhanced Detection of Malignant Lymphoma in Cerebrospinal Fluid by Multiparameter Flow Cytometry. *Am J Clin Pathol* **110**, 341–346 (1998).
197. Roma, A. A., Garcia, A., Avagnina, A., Rescia, C. & Elsner, B. Lymphoid and myeloid neoplasms involving cerebrospinal fluid: Comparison of morphologic examination and immunophenotyping by flow cytometry. *Diagn Cytopathol* **27**, 271–275 (2002).
198. Alvarez, R. *et al.* Clinical relevance of flow cytometric immunophenotyping of the cerebrospinal fluid in patients with diffuse large B-cell lymphoma. *Annals of Oncology* **23**, 1274–1279 (2012).
199. Nückel, H., Novotny, J. R., Noppeney, R., Savidou, I. & Dührsen, U. Detection of malignant haematopoietic cells in the cerebrospinal fluid by conventional cytology and flow cytometry. *Clin Lab Haematol* **28**, 22–29 (2006).
200. Han, S. *et al.* Comprehensive immunophenotyping of cerebrospinal fluid cells in patients with neuroimmunological diseases. *The Journal of Immunology* **192**, 2551–2563 (2014).
201. Singh, G. *et al.* The influence of fixation and cryopreservation of cerebrospinal fluid on antigen expression and cell percentages by flow cytometric analysis. *Sci Rep* **14**, 2463 (2024).
202. Swinscow, T. Correlation and regression. in *Statistics at Square One* (BMJ Publishing Group, 1997).
203. Kofler, J. & Wiley, C. A. Microglia: Key Innate Immune Cells of the Brain. *Toxicol Pathol* **39**, 103–114 (2011).
204. Thorsdottir, S., Henriques-Normark, B. & Iovino, F. The role of microglia in bacterial meningitis: Inflammatory response, experimental models and new neuroprotective therapeutic strategies. *Front Microbiol* **10**, 1–8 (2019).
205. Louveau, A. *et al.* Structural and functional features of central nervous system lymphatic vessels. *Nature* **523**, 337–341 (2015).
206. Mendes, M. S. & Majewska, A. K. An overview of microglia ontogeny and maturation in the homeostatic and pathological brain. *European Journal of Neuroscience* **53**, 3525–3547 (2021).
207. Sargeant, T. J. & Fourrier, C. Human monocyte-derived microglia-like cell models: A review of the benefits, limitations and recommendations. *Brain Behav Immun* **107**, 98–109 (2023).
208. Michell-Robinson, M. A. *et al.* Roles of microglia in brain development, tissue maintenance and repair. *Brain* **138**, 1138–1159 (2015).
209. Gogoleva, V. S., Drutskaya, M. S. & Atretkhany, K. S. N. The Role of Microglia in the Homeostasis of the Central Nervous System and Neuroinflammation. *Mol Biol* **53**, 696–703 (2019).
210. Rock, R. B. *et al.* Role of microglia in central nervous system infections. *Clin Microbiol Rev* **17**, 942–964 (2004).
211. Djukic, M. *et al.* Circulating monocytes engraft in the brain, differentiate into microglia and contribute to the pathology following meningitis in mice. *Brain* **129**, 2394–2403 (2006).
212. Mockus, T. E., Ren, H. M. & Lukacher, A. E. To Go or Stay: The Development, Benefit, and Detriment of Tissue-Resident Memory CD8 T Cells during Central Nervous System Viral Infections. *Viruses* **11**, (2019).

213. Ní Chasaide, C. & Lynch, M. A. The role of the immune system in driving neuroinflammation. *Brain Neurosci Adv* **4**, 239821281990108 (2020).
214. Filiano, A. J., Gadani, S. P. & Kipnis, J. How and why do T cells and their derived cytokines affect the injured and healthy brain? *Nat Rev Neurosci* **18**, 375–384 (2017).
215. Lane, T. E. *et al.* A Central Role for CD4 T Cells and RANTES in Virus-Induced Central Nervous System Inflammation and Demyelination. *J Virol* **74**, 1415–1424 (2000).
216. Maizels, R. M. & Smith, K. A. Regulatory T Cells in Infection. in *Advances in Immunology* vol. 112 73–136 (Academic Press Inc., 2011).
217. Mills, K. H. G. Regulatory T cells: friend or foe in immunity to infection? *Nat Rev Immunol* **4**, 841–855 (2004).
218. Askenasy, N., Kaminitz, A. & Yarkoni, S. Mechanisms of T regulatory cell function. *Autoimmun Rev* **7**, 370–375 (2008).
219. Joosten, S. A. & Ottenhoff, T. H. M. Human CD4 and CD8 regulatory T cells in infectious diseases and vaccination. *Hum Immunol* **69**, 760–770 (2008).
220. Yu, Y. *et al.* Recent advances in CD8+ regulatory T cell research (Review). *Oncol Lett* **15**, 8187–8194 (2018).
221. Welte, T. *et al.* Role of two distinct γδ T cell subsets during West Nile virus infection. *FEMS Immunol Med Microbiol* **53**, 275–283 (2008).
222. Shiromizu, C. M. & Jancic, C. C. γδ T lymphocytes: An effector cell in autoimmunity and infection. *Front Immunol* **9**, 1–8 (2018).
223. Laidlaw, B. J., Craft, J. E. & Kaech, S. M. The multifaceted role of CD4+ T cells in CD8+ T cell memory. *Nat Rev Immunol* **16**, 102–111 (2016).
224. Sonar, S. A. & Lal, G. Differentiation and transmigration of CD4 T cells in neuroinflammation and autoimmunity. *Front Immunol* **8**, 1–9 (2017).
225. Ożańska, A., Szymczak, D. & Rybka, J. Pattern of human monocyte subpopulations in health and disease. *Scand J Immunol* **92**, (2020).
226. Garré, J. M. & Yang, G. Contributions of monocytes to nervous system disorders. *J Mol Med* **96**, 873–883 (2018).
227. Ashhurst, T. M., Vreden, C. van, Niewold, P. & King, N. J. C. The plasticity of inflammatory monocyte responses to the inflamed central nervous system. *Cell Immunol* **291**, 49–57 (2014).
228. Marais, S. *et al.* Neutrophil-associated central nervous system inflammation in tuberculous meningitis immune reconstitution inflammatory syndrome. *Clinical infectious diseases* **59**, 1638–1647 (2014).
229. Loxton, N. W. *et al.* A pilot study of inflammatory mediators in brain extracellular fluid in paediatric TBM. *PLoS One* **16**, (2021).
230. Akalin, H., Mistik, R., Helvaci, S. & Kiliçturgay, K. Cerebrospinal Fluid Interleukin-1 β/InterLeukin-1 Receptor Antagonist Balance and Tumor Necrosis Factor-α Concentrations in Tuberculous, Viral and Acute Bacterial Meningitis. *Scand J Infect Dis* **26**, 667–674 (1994).
231. Helmy, A., De Simoni, M. G., Guilfoyle, M. R., Carpenter, K. L. H. & Hutchinson, P. J. Cytokines and innate inflammation in the pathogenesis of human traumatic brain injury. *Prog Neurobiol* **95**, 352–372 (2011).
232. Donald, P. R. *et al.* Pediatric meningitis in the Western cape province of South Africa. *J Trop Pediatr* **42**, 256–261 (1996).

233. Singh, G. & Rohlwink, U. The influence of fixation and cryopreservation of cerebrospinal fluid on antigen expression and cell percentages by flow cytometric analysis. (University of Cape Town, 2021).
234. Pekny, M. & Pekna, M. Astrocyte reactivity and reactive astrogliosis: costs and benefits. *Physiol Rev* **94**, 1077–1098 (2014).
235. Ma, Q. *et al.* Interactions between CNS and immune cells in tuberculous meningitis. *Front Immunol* **15**, 1–10 (2024).
236. Jarvis, J. N. *et al.* Adult meningitis in a setting of high HIV and TB prevalence: findings from 4961 suspected cases. *BMC Infect Dis* **10**, (2010).
237. Soeters, H. M. *et al.* Bacterial Meningitis Epidemiology in Five Countries in the Meningitis Belt of Sub-Saharan Africa, 2015-2017. *Journal of Infectious Diseases* **220**, S165–S174 (2019).
238. Wolzak, N. K., Cooke, M. L., Orth, H. & Van Toorn, R. The changing profile of pediatric meningitis at a referral centre in Cape Town, South Africa. *J Trop Pediatr* **58**, 491–495 (2012).
239. Bartanusz, V., Jezova, D., Alajajian, B. & Digicaylioglu, M. The blood-spinal cord barrier: Morphology and clinical implications. *Ann Neurol* **70**, 194–206 (2011).
240. Reiber, H. Proteins in cerebrospinal fluid and blood: barriers, CSF flow rate and source-related dynamics. *Restor Neurol Neurosci* **21**, 79–96 (2003).
241. Loxton, N. W. *et al.* A pilot study of inflammatory mediators in brain extracellular fluid in paediatric TBM. *PLoS One* **16**, (2021).